UNIVERSITY OF CALIFORNIA,
IRVINE

Probing the Tropospheric Oxidation Capacity in Pristine to Polluted Environments

DISSERTATION

submitted in partial satisfaction of the requirements
for the degree of

DOCTOR OF PHILOSOPHY

in Earth System Science

by

Daun Jeong

Dissertation Committee:
Associate Professor Saewung Kim, Chair
Professor Alex B. Guenther
Associate Professor Craig Murray

2019

DEDICATION

To my husband, Jooseok Lee, for his unconditional support.

TABLE OF CONTENTS

LIST OF FIGURES

LIST OF TABLES

ACKNOWLEDGMENTS

I would like to express my sincere gratitude to my advisor Saewung Kim for his support. He has given me so many opportunities to travel to different parts of the world and do measurements and provided me with so many academic and career related opportunities with great guidance. His door was always open to any of the questions I had. He always encouraged me whenever I was in doubt of myself and was not only my academic advisor but a life mentor and a good friend.

I would also like to thank all of our BAI group members, for supporting each other and cultivating an enjoyable working environment. I always enjoyed working as a team with the group members both in the lab and field. Thanks to Gracie Wong for inspiring me to live the best of my life, Sanjeevi Nagalingam, for taking care of the lab even in weekends and holidays, Anne Mielnik, for being our sunshine living the dream, Jesus Campos, for always being thoughtful and helping others, and Dasa Gu, for spreading the cheerfulness in the basement lab. Special thanks to Roger Seco, who survived with me through more than a month of research cruise to Antarctica and Youngro Lee and Dianne Sanchez, for being with me on our first field campaign at the Taehwa mountains.

Cyril McCormick and David Tanner, with patience, always helped me with any instrument related issues with their insightful knowledge. I would like to thank the whole KORUS-AQ team for providing a great field work experience. My research was a collaborative work of so many people from the KORUS-AQ, who helped me while I progressed through my project. Especially, Benjamin Nault, for the scientific discussions and advise he shared, and Louisa Emmons, for the discussions on modeling and giving me such a wonderful experience at NCAR.

I appreciate the time and support from the committee members Alex Guenther and Craig Murray. They gave me insightful guidance throughout my dissertation work. I would like to thank Prof. Youngpyo Kim for being my academic mentor since undergrad and Hwajin Kim for being my role model as a proud female scientist.

I would like to thanks my best friends, Debapriya Chakraborty, Lilian Goldberg, and Youngmin Choi. They have made my experience in Irvine so wonderful and exciting.

Last but not least, I would like to express my warmest appreciation to my family. I would like to thank my mom and dad for being patient with me through all those years in school. Thanks to my biggest supporter and husband, Jooseok Lee. I was able be a strong person and continue to pursue my passion because of him.

CURRICULUM VITAE

Daun Jeong

EDUCATION:

2011	B.A. in Environmental Science and Engineering, Ewha Womans University
2013	M.S. in Environmental Science and Engineering, Pohang University of Science and Technology
2019	Ph.D. in Earth System Science, University of California, Irvine

FIELD OF STUDY:

Earth System Science, Atmospheric Chemistry in Field Observation

TEACHING:

Teaching Assistant for ESS15, Climate Change (Winter 2019)
Teaching Assistant for ESS114, Field Methods (Fall 2018)
Teaching Assistant for ESS23, Air Pollution (Winter 2017 and 2018)
Teaching Assistant for ESS1, Introduction to Earth System Science (Fall 2015 and 2017)
Teaching Assistant for ESS7, Physical Geology (Winter 2016)

AWARDS:

NASA Group Achievement Award for KORUS-AQ (2017)
Jenkins Family Graduate Fellowship (2014)
POSTECH Best Paper Award (2013)
EWHA Honor Scholarship (2010)

PUBLICATIONS:

Sullivan, J. T.; McGee, T. J.; Stauffer, R. M.; Thompson, A. M.; Weinheimer, A.; Knote, C.; Janz, S.; Wisthaler, A.; Long, R.; Szykman, J.; Park, J.; Lee, Y.; Kim, S.; **Jeong, D.**; Sanchez, D.; Twigg, L.; Sumnicht, G.; Knepp, T.; Schroeder, J. R. Taehwa Research Forest: A receptor site for severe domestic pollution events in Korea during 2016. *Atmospheric Chemistry and Physics* (2019), 19, 5051-5067

Jeong, D.; Seco, R.; Gu, D.; Lee, Y.; Nault, B. A.; Knote, C. J.; Mcgee, T.; Sullivan, J. T.; Jimenez, J. L.; Campuzano-Jost P.; Blake, D. R.; Sanchez, D.; Guenther, A. B.; Tanner, D.; Huey, L. G.; Long, R.; Anderson, B. E.; Hall, S. R.; Ullmann, K.; Shin, H.; Herndon, S. C.; Lee, Y.; Kim, D.; Ahn, J.; Kim, S. Integration of Airborne and Ground Observations of Nitryl Chloride in the Seoul

Metropolitan Area and the Implications on Regional Oxidation Capacity During KORUS-AQ 2016. *Atmospheric Chemistry and Physics Discussions* (2018)

Kim, S.; **Jeong, D.**; Sanchez, D.; Wang, M.; Seco, R.; Blake, D.; Meinardi, S.; Barletta, B.; Hughes, S.; Jung, J.; Kim, D.; Lee, G.; Lee, M.; Ahn, J.; Lee, S.; Cho, G.; Sung, M.; Lee, Y.; Park, R. The controlling factors of photochemical ozone production in Seoul, South Korea. *Aerosol and Air Quality Research* (2018), 18, 2253 – 2261

Sanchez, D.; **Jeong, D.**; Seco, R.; Wrangham, I.; Park, J.; Brune, W. H.; Koss, A.; Gilman, J.; Gouw, J.; Misztal, P.; Goldstein, A.; Baumann, K.; Wennberg, P. O.; Keutsch, F. N.; Guenther, A.; Kim, S. Intercomparison of OH and OH reactivity measurements in a high isoprene and low NO environment during the Southern Oxidant and Aerosol Study (SOAS). *Atmospheric Environment* (2018), 174, 227-236.

Kim, S.; Sanchez, D.; Wang, M.; Seco, R.; **Jeong, D.**; Hughes, S.; Barletta, B.; Blake, D. R.; Jung, J.; Kim, D.; Lee, G.; Lee, M.; Ahn, J.; Lee, S.-D.; Cho, G.; Sung, M.-Y.; Lee, Y.-H.; Kim, D. B.; Kim, Y.; Woo, J.-H.; Jo, D.; Park, R.; Park, J.-H.; Hong, Y.-D.; Hong, J.-H. OH reactivity in urban and suburban regions in Seoul, South Korea - an East Asian megacity in a rapid transition. *Faraday Discussions* (2016), *189*, 231-251.

Jeong, D.; Kim, K.; Min, D. W.; Choi, W. Freezing-Enhanced Dissolution of Iron Oxides: Effects of Inorganic Acid Anions, *Environmental Science & Technology* (2015), 49, 12816-12822.

Jeong, D.; Kim, K.; and Choi, W. Accelerated Dissolution of Iron Oxides in Ice, *Atmospheric Chemistry and Physics* (2012), 12, 11125-11133

ABSTRACT OF THE DISSERTATION

Probing the Tropospheric Oxidation Capacity in Pristine to Polluted Environments

By

Daun Jeong

Doctor of Philosophy in Earth System Science

University of California, Irvine, 2019

Associate Professor Saewung Kim, Chair

This study presents ground observation of hydroxyl radicals (OH) during GoAmazon2014/5, ground and airborne observations of nitryl chloride ($ClNO_2$) during KORUS-AQ2016, and ship-borne observation of molecular iodine (I_2) during ARAON2018. Measurements were made with a Chemical Ionization Mass Spectrometer (CIMS). Observation data sets of the radicals and radical precursors are compared with observation constrained box model simulations in order to understand the oxidation capacity of the troposphere from polluted to pristine environments.

During the GoAmazon2014/5 campaign, OH was measured in February-March of 2016 during the wet season at the T3 site, ~ 60 km west of Manaus, Brazil. Measurements are compared to box model simulations embedded with the near-explicit Master Chemical Mechanism (MCM v3.3.1) and other mechanisms used in global models. The model was highly constrained with measured meteorology and other trace gas observations. The results show that the simulations agree well with the OH observations. This confirms the HO_x-NO_x-VOC chemistry in this high

biogenic volatile organic compound (BVOC) and low NO_X environment is well understood contrary to the recent studies of higher than expected OH in isoprene dominant forested regions.

$ClNO_2$ measurements were carried out in May to early June in the Seoul Metropolitan Area (SMA) during the KORUS-AQ 2016 campaign. Ground observations were conducted at the Olympic Park site and Taehwa Research Forest, each representing a polluted site near the city center and a forested region downwind. Airborne observations were made on the NASA DC-8, which made measurements over the Korean peninsula and the yellow sea during the campaign period. Significant levels of daytime $ClNO_2$ were measured at both ground sites with a positive correlation to Cl_2, which was suppressed at low O_3. Box model simulations show that this is likely due to the heterogeneous reaction of HOCl and $ClONO_2$ on aerosols and the autocatalytic production of Cl_2. In the early morning, a second $ClNO_2$ peak was observed when there were predominant westerlies. Based on airborne observations, box model simulations, and backtrajectories, this morning peak is possibly due to a mix of vertical and horizontal transport from the west coast. Box model runs show that chlorine chemistry can enhance up to 25 % of net chemical production of O_3 in the SMA.

Gas phase I_2 and HOI were measured with a CIMS, on-board the Korean ice breaker R/V ARAON from late March to early May. Up to ~ 15 ppt of I_2 was measured near the Antarctic Peninsula, which corresponds to previous studies that reported high IO levels in West Antarctica. Short O_3 depletion events were observed simultaneous to enhanced levels of Br_2 and I_2. Sources of iodine precursors can be both from inorganic, like accelerated reactions within the ice matrix, and organic sources, like sea ice diatoms. Correlation between I_2 and biological tracers like DMS and isoprene was observed.

CHAPTER 1

INTRODUCTION

1.1 Overview

Tropospheric oxidation capacity is controlled by highly reactive radicals and reactive trace gases. Radicals control the lifetime of trace gases like methane (Prather and Spivakovsky, 1990), which is a greenhouse gas, and affect the level of photochemical products like ozone (Chameides and Walker, 1973; Crutzen, 1971) and secondary organic aerosols (Jimenez et al., 2009; Kroll and Seinfeld, 2008; Lim and Ziemann, 2005). The most dominant radical in the troposphere is the hydroxyl radical (OH) (Levy, 1971). The level of OH is governed through primary production mainly from O_3 photolysis and recycling processes from hydroperoxy radical (HO_x) - organic peroxy radical (RO_x) - NO_x reactions that are non-linear (Chameides and Walker, 1973; Crutzen, 1971; Levy, 1971). Therefore, depending on the chemical regime of the environment, level of OH can be suppressed or enhanced. Recent studies in forests with high biogenic volatile organic compounds (BVOC) and low NO_x, reported OH observations that are up to 10-fold higher than expected than model simulations indicating remaining uncertainties in our current understanding (Kubistin et al., 2010; Lelieveld et al., 2008; Rohrer et al., 2014).

More recently, growing number of studies have shown that halogen radicals like chlorine (Cl), iodine (I), and bromine (Br) also have significant impacts in the tropospheric oxidation capacity in the boundary layer. Reactive halogen species go through gas-phase and multi-phase reactions among halogen containing compounds like halogen oxides, dihalogens, halides, and hypohalous acids to catalytically produce halogen radicals. Once produced, they rapidly react with O_3 (Barrie et al., 1988; Bottenheim and Gallant, 1986; Oltmans and Komhyr, 1986), hydrocarbons

like CH_4 (Jobson et al., 1994; Platt et al., 2004), dimethyl sulfide (DMS) (Charlson et al., 1987), and long-lived pollutants like elemental mercury (Lindberg et al., 2002; Schroeder et al., 1998). Reactive iodine species have also been reported to contribute to new particle formation (Allan et al., 2015; Davison et al., 1996) that has implications for radiative forcing of the atmosphere. Depending on the chemical regime, reactive halogens can trigger ozone depletion events, like in the polar regions (Barrie et al., 1988; Oltmans and Komhyr, 1986), or enhance O_3 in more polluted environments (Osthoff et al., 2008; Riedel et al., 2012). Field observations are still very limited in various chemical environments and the sources and chemistries of reactive halogens are poorly constrained in global models inhibiting our ability to fully understand the photochemistry and its resulting impact in the quality of air.

1.2 Motivation and Approach

The main goal of my Ph.D research is to examine the uncertainties of tropospheric oxidation capacity through observation constrained box model simulations and field studies of hydroxyl radicals and halogen radical precursors measured by a Chemical Ionization Mass Spectrometer (CIMS). Significant developments on chemical ionization mass spectrometry techniques in the past decades has allowed the detection of radicals with high sensitivity and selectivity (Huey, 2007). The CIMS has been used in previous airborne and ground field observations due to its fast response time and low detection limit. Box model simulations of radicals and radical precursors, embedded with a near-explicit chemical mechanism, is a good test-bed of our current understanding of the chemistry. Moreover, it is a great tool for sensitivity tests of different trace gas and other parameters. Discrepancies between model simulations and observations can be an indication of a missing chemistry, measurement, or possible artifacts of the

obtained data. Chemical transport models are used for examining the regional to global air quality. These 3D models use different type of chemical mechanisms that are often outdated and can affect the model results. A box model is a great tool for comparing discrepancies resulting from the choice of different mechanisms. The overall approach used in this study is: 1) Measure radicals and radical precursors with the CIMS, 2) Use box model simulations to compare to observations, 3) Carry out sensitivity tests with box model runs to study the implications on the regional photochemistry. Three field observation data sets from a tropical rain forest (GoAmazon2014/5, Chapter 3), an Asian mega-city (KORUS-AQ2016, Chapter 4), and the Antarctic peninsula (ARAON2018, Chapter 5) are presented.

1.3 Background

1.3.1 HO_x-NO_x-VOC chemistry

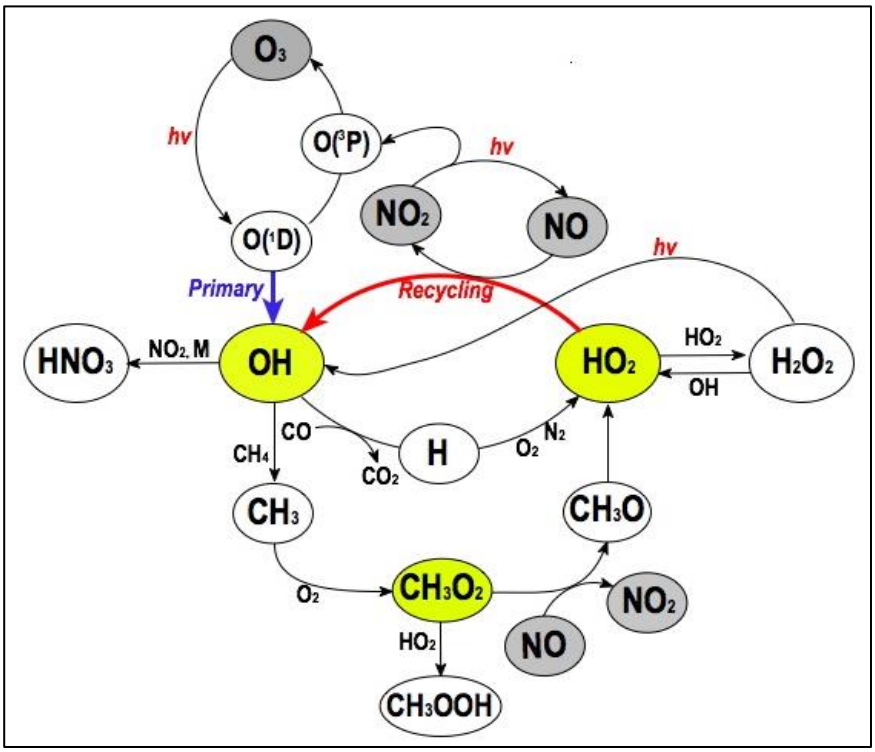

Figure 1.1 HO_x-NO_x-VOC photochemistry in the troposphere.

Various radicals control the tropospheric oxidation capacity in the atmosphere. OH was suggested as a main tropospheric oxidant by Levy (1971). Although OH exists at very low concentrations, with a global average of ~ 10^6 molecules cm^{-3} (Prather and Spivakovsky, 1990; Spivakovsky et al., 1990), it determines the chemical lifetime of most trace gases due to its high reactivity. OH driven oxidation of both anthropogenic and natural reactive trace gases have significant implications towards regional and global air quality (Chameides et al., 1988; Goldstein and Galbally, 2007; Guenther et al., 2012). In the presence of nitrogen oxide (NO), OH driven volatile organic compound (VOC) oxidation produces ozone (O_3) (Chameides and Walker, 1973; Crutzen, 1971) (Fig. 1.1), which is both a greenhouse gas (GHG) and an air pollutant. VOC oxidation may also generate products with lower vapor pressure than the reactants which tends to participate into particle phase contributing towards aerosol growth (Jimenez et al., 2009; Poschl et al., 2010). This aspect is important in terms of understanding the direct and indirect (i.e., as cloud condensation nuclei) effects of aerosol as a climate forcing agent which has been reported to be highly uncertain (IPCC, 2013). In addition, atmospheric lifetime of methane (CH_4) is solely determined by the global average OH concentration (IPCC, 2013; Levy, 1971; Prather and Spivakovsky, 1990).

Figure 1.1 shows photochemical reactions of HO_X-NO_X-VOC in the troposphere. OH is primarily generated by O_3 photolysis followed by a reaction with water vapor. Once it reacts with VOCs, peroxy radicals are generated. In the presence of NO peroxy radicals can regenerate OH (Levy, 1971). This has been the primary understanding in how tropospheric oxidation capacity is maintained. This notion of understanding illustrates that OH production is restricted in high VOCs and low NO environments such as remote forest environments as OH recycling is suppressed. However, OH observations using laser induced fluorescence (LIF) techniques consistently report

higher than expected OH especially in high isoprene (C_5H_8) and low NO environments (Table 1.1). Figure 1.2 summarizes OH observations as a function of NO_x taken in 10 field measurements ranging from polluted urban areas to pristine regions with high C_5H_8 and low NO environments. As notated in the blue solid line in Figure 1.2 (b), conventional understanding predicts low OH levels in low NO_x conditions due to the suppressed recycling processes. Contrary to this, the measurements do not show inhibited OH levels over the low NO range. Rohrer et al. (2014) proposed that additional OH from "unrecognized recycling" processes, mediated by isoprene photo-oxidation reactions, were responsible for sustaining high tropospheric oxidation capacity in these NO_x-limited conditions.

Table 1. Comparison between modeled and measured OH taken in high BVOC and low NO_x environments

Field campaign name (year)	Location	Instrumental technique	Comparison between model and observation	Reference
AEROBIC(1997)	Indigenous forest, North West Greece	FAGE	50% under prediction by model	Carslaw et al. (2001) Creasey et al. (2001)
PROPHET-98(1998)	Deciduous forest, North Michigan, USA	FAGE	Observation ~2.7 times greater	Tan et al. (2001)
INTEX-A(2004)	North America	FAGE	Observed up to 5 times	Ren et al. (2008)
GABRIEL(2005)	Suriname, South America	FAGE	Observed up to 12.2 times	Butler et al. (2008) Lelieveld et al. (2008)
PRIDE-PRD(2006)	Rural, Southern China	FAGE	Observed up to 3-5times greater	Hofzumahaus et al. (2009) Lou et al. (2010)
BEARPEX07(2007)	Blodgett forest, California	FAGE	Model under prediction by a factor of 6	Wolfe et al. (2011)
OP3(2008)	Sabah, Borneo	FAGE	Model under prediction by a factor of 10	Pugh et al. (2010) Stone et al. (2011)

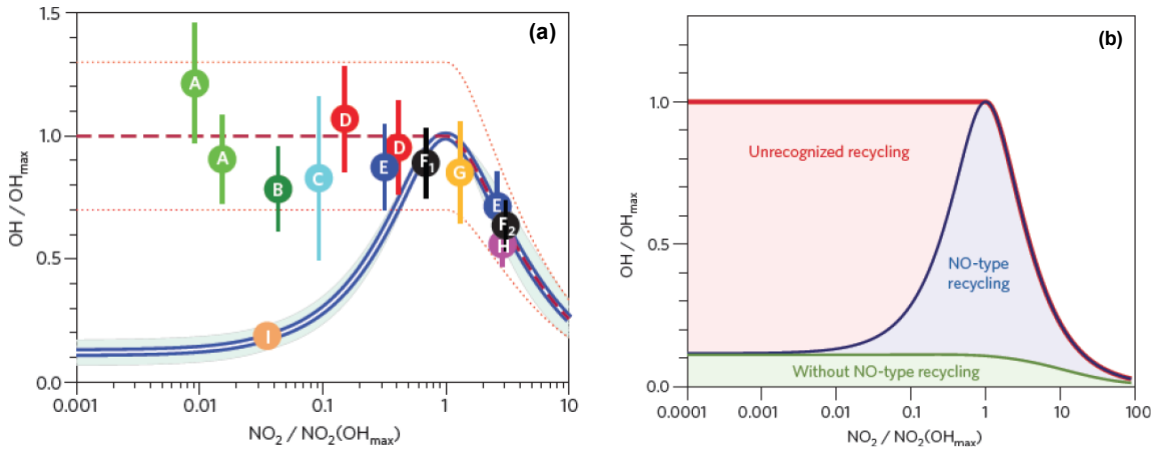

Figure 1.2 Comparison of modeled OH and observed OH taken from different field measurements in high BVOC and low NOx regions. The measurements were taken from ten campaigns: A, Suriname forest (Lelieveld et al., 2008)**; B, Borneo rainforest** (Whalley et al., 2011)**; C, US deciduous forest** (Tan et al., 2001)**; D, Pearl Delta River** (Hofzumahaus et al., 2009)**; E, Beijing** (Lu et al., 2013)**; F1, Mexico city** (Mao et al., 2010)**; F2, Mexico city** (Dusanter et al., 2009)**; G, Tokyo** (Kanaya et al., 2007)**; H, New York** (Ren et al., 2003)**; I, US ponderosa pineforest** (Mao et al., 2012)**. (Figure taken from Rohrer et al.** (2014)**)**

Chemical mechanisms have been proposed to account this higher than expected OH in high C_5H_8 and low NO environments. First is the OH production through reaction between organic peroxy radicals (RO_2) and peroxy radicals (HO_2). This has long been thought to be a chain terminating reaction by forming hydroperoxide products (ROOH) (Fig. 1.1). However, indirect laboratory experiments (Jenkin et al., 2007, 2010) show that the reaction could be a source of OH. In a field study in a pristine Amazonian forest, Lelieveld et al. (Lelieveld et al., 2008) demonstrated that by including isoprene-derived peroxy radical chemistry and an OH production efficiency of 40-80%, the model well predicted the observed OH level. Second is the existence of a hypothetical compound 'X', which has a chemical kinetic behavior identical to NO and therefore recycles OH through reaction with HO_2. Hofzumahaus et al. (2009) observed OH through LIF at a heavily populated (i.e., 57.15 million) Pearl River Delta region (~60 km from Guangzhou) with high emissions of natural BVOCs (i.e., 1-2 ppb of C_5H_8). The discrepancy between the modeled and observed OH was highest (3-5 times) at relatively lower NO conditions (< 1ppb) and matched

well at relatively higher NO conditions (> 1ppb). By adding 'X' equivalent to 0.85ppb of NO, the authors were able to reproduce both OH and HO_2. Lastly is the OH recycling processes through hydroxy peroxy isoprene radical isomerization. Peeters et al. (2009) first theoretically suggested that these hydroxy peroxy radicals can undergo 1,5-H-shift (i.e., β-hydroxy peroxy radicals) to directly form OH (along with methyl vinyl ketone or methacrolein and HCHO) or go through 1,6-H-shift (i.e., z isomers of the δ- hydroxy peroxy radicals) to form unsaturated C_5-hydroperoxyaldehydes (HPALDs) that further react to generate OH. Crounse et al. (2011) experimentally confirmed the generation of HPALDs from isoprene oxidation by OH in a chamber experiment. However, based on their calculation, the 1,6-H-shift and 1,5-H-shift reactions were slower than the original rates calculated by Peeters and Muller (2010) by a factor of 50 and 30 respectively. Laboratory experiments by Wolfe et al. (2012) have confirmed that once produced, C_5-HPALDs can photolyze with a quantum yield of 1 (300-400 nm) to produce OH (yield =1). Additional OH production from this isoprene radical isomerization reaction has been further supported by Fuchs et al. (2013) through an isoprene-oxidation chamber experiment with experimental conditions similar to the field sites in the borneo rainforest and Pearl River Delta. The conventional chemistry in the MCM v 3.2 (Master Chemical Mechanism) predicted OH a factor of 2 lower while the model embedded with the unimolecular isoprene isomerization (i.e., rate constant based on Crouse et al. (2011)) matched well. The authors concluded that more than half of the OH, that react with isoprene in high BVOC regions, are recycled back through this unimolecular isomerization. Peeters et al. (2014) later on extended their findings and updated their reactions (denoted as LIM1) that match better with the studies (Crounse et al., 2011; Da Silva et al., 2010) that followed since their first report and these have been included in the Master Chemical Mechanism (MCM 3.3.1) (Jenkin et al., 2015).

Mao et al. (2012) presented an observational evidence that the previously reported higher than expected OH could have been caused by instrumental artifacts associated with the background characterization processes. Hens et al. (2014) presented ambient OH measured in a boreal forest and compared between the results from the LIF instrumentation from the Max Planck Institute for Chemistry and AP-CIMS instrumentation from the University of Helsinki. The LIF consistently reported 30 % higher OH than the CIMS instrumentation. Sanchez et al. (2017) also presented an inter-comparison between the Penn State LIF and the CIMS identical to the one deployed in this study, at a C_5H_8 dominant rural southeastern US forest. The OH observational datasets measured by the CIMS and LIF generally agreed well within the analytical uncertainty with diel averages of 8.2×10^5 molecules cm^{-3} and 4.96×10^5 molecules cm^{-3} respectively. Both the LIF and CIMS used a chemical removal method for background characterization that eliminates potential chemical artifacts that were described in Mao et al. (2012). As substantial fraction of high C_5H_8 emission region can be categorized as low NO_x environments, these uncertainties of higher than expected OH should be addressed.

1.3.2 Halogen Chemistry in the Tropospheric Boundary Layer

It was not until the late 1980s that halogen species were recognized to be important in controlling the tropospheric oxidation capacity in polar regions during Springtime. Before, OH radicals were considered to be the most powerful oxidant in the troposphere while the roles of halogens were highly uncertain (Cicerone, 1981) and thought to be insignificant. Barrie and co-workers (Barrie et al., 1988, 1989) were the first to discover the anti-correlation between filtered bromine and ozone depletion events (ODEs) that were routinely observed during Arctic Spring (Bottenheim and Gallant, 1986; Oltmans and Komhyr, 1986). During ODEs, background O_3 levels

dropped to near zero and persisted for hours to days. Since then, studies have confirmed that the photochemistry of halogen gas species is more prevalent in the troposphere than previously thought influencing a wide range of environments including, polar, marine, coastal, and continental boundary layers.

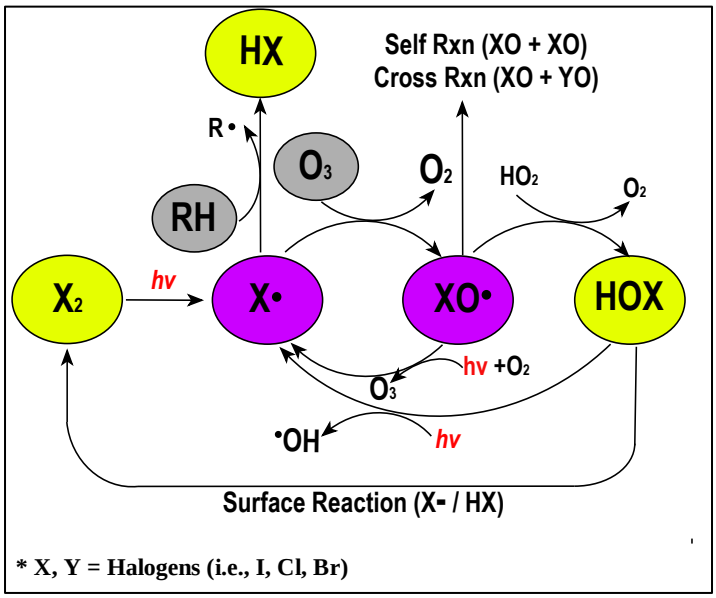

Figure 1.3 Simplified gas-phase and multi-phase catalytic cycle of halogen radicals

Reactive halogen species like halogen radicals (i.e., Cl, Br, I) and halogen oxides have high reactivity towards volatile organic compounds and inorganic gases like O_3. Through multiphase and gas-phase catalytic reactions, halogen species in the troposphere influence the lifetime of VOCs (e.g. CH_4), deplete or enhance O_3 levels (Barrie et al., 1988, 1989), oxidize elemental mercury (Schroeder et al., 1998; Steffen et al., 2007), DMS (Charlson et al., 1987), and influence nucleation and condensation of particles (Allan et al., 2015; Davison et al., 1996). Figure 1.3 shows a simplified catalytic cycle of the initiation, propagation, and termination steps of halogen radicals. The photolysis of gas-phase molecular halogens like I_2, Cl_2, and Br_2 is the

primary initiation step, in which they readily breakdown by the visible to near UV photons (peak absorption cross sections at 298 K, I_2 ~ 533 nm, Cl_2 ~330 nm, Br_2 ~420 nm (Atkinson et al., 2007; Saiz-Lopez et al., 2004)). The generated halogen atoms can compete to react with hydrocarbons (denoted 'RH' in Figure 1.3) or O_3, which is a radical propagation step where the total number of radicals are conserved. The relative reactivity towards hydrocarbons are in the order Cl, Br, and I. Chlorine radicals are reactive towards VOCs with up to two orders of magnitude higher reactivity than hydroxyl radicals (e.g., $k_{OH+CH4} = 0.6 \times 10^{-14}$ cm^3 molec^{-1}s^{-1}, $k_{Cl+CH4} = 1.0 \times 10^{-13}$ cm^3 molec^{-1}s^{-1} at 298 K) (Atkinson, 1997; Atkinson and Arey, 2003). Bromine and iodine radicals are much less reactive to VOCs and mostly react with O_3, which can lead to ODEs. IO and BrO ('XO' in Figure 1.3), produced from reaction between a halogen atom and O_3, rapidly photolyzes to reproduce I and Br and therefore results in a null cycle. Rather, ODEs are catalyzed through reactions between halogen oxides (R1.1 – R1.2) or multiphase reactions of hypohalous acids ('HOX' in Figure 1.3) and halide containing surfaces (R1.3). For reaction R1.2, cross reactions between different halogen oxides are faster than self-reactions (e.g., $k_{IO+IO} = 3.8 \times 10^{-11}$ cm^3 molec^{-1}s^{-1}, $k_{BrO+BrO} = 2.7 \times 10^{-12}$ cm^3 molec^{-1}s^{-1}, $k_{BrO+IO} = 6.8 \times 10^{-11}$ cm^3 molec^{-1}s^{-1}, at 298K) (Atkinson et al., 2007) accelerating depletion of O_3 in the presence of different types of halogens. Another important reaction for ODEs is the heterogeneous reaction of HOX on halide containing surfaces (R1.3), a reaction pathway well-known to cause "bromine explosion" events (Wennberg, 1999). Multi-phase chemistry is a key reaction in producing significant levels of reactive halogens to trigger ODEs. The properties of the reacting surfaces have been known to be the main factor controlling the efficiency. Uncertainties remain in the detailed mechanisms involved but studies show surface characteristics like the type of surface (e.g., ice, snow, aerosols) (Abbatt et al., 2012), abundance of inorganic ions, organic coating (McNeill et al., 2006; Thornton and Abbatt, 2005),

and pH (Abbatt et al., 2010; Huff and Abbatt, 2002; Sjostedt and Abbatt, 2008) may control the efficiency of the production of reactive halogens.

$$X + O_3 \rightarrow XO \quad (X=Br, I) \qquad R1.1$$

$$XO + XO \rightarrow X + X + O_2 \qquad R1.2$$

$$HOX\ (g) \xrightarrow{X-/HX\ (het),h\nu} X_2\ (g) + H_2O \qquad R1.3$$

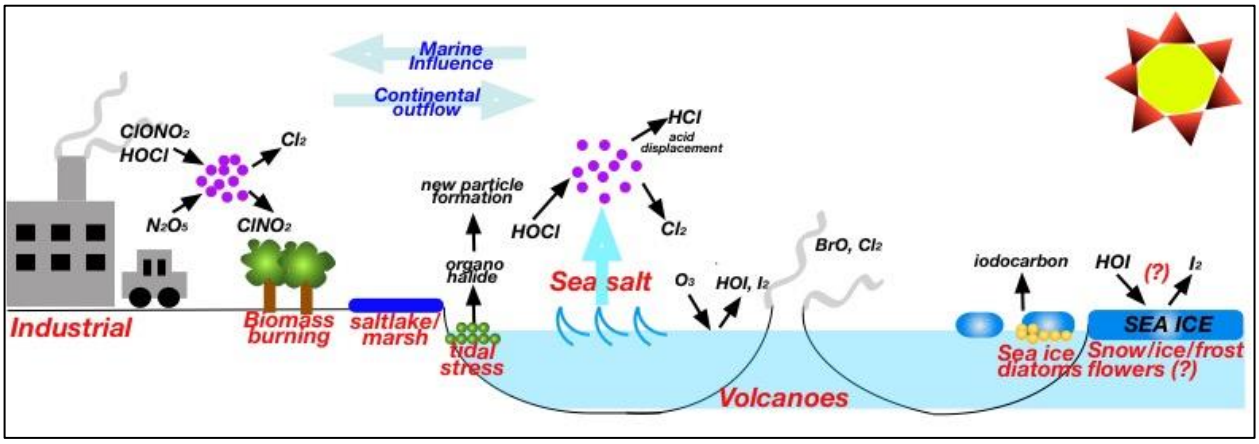

Figure 1.4 Schematic diagram of a summary of anthropogenic and natural sources of halogen radical precursors in continental, coastal, marine, and polar boundary layers.

Figure 1.4 shows examples of sources of gaseous reactive halogens in the boundary layer. Ocean is the most dominant natural source of halogens. In the marine boundary layer, wave breaking actions create sea salt aerosols (Blanchard, 1985; Woodcock, 1953), and through heterogeneous reactions release gas-phase halogens. Studies by Lawler et al. (2009, 2011), in the Cape Verde observatory in eastern tropical Atlantic, measured up to ~150 ppt of HOCl and ~ 35 ppt of Cl_2 with a CIMS from aged airmass influenced by continental outflow. When the airmass was mostly influenced from the open ocean, the levels were up to 60 and 10 ppt for HOCl and Cl_2, respectively. The authors concluded that acidification of aerosols in aged air-masses and its

resulting enhancement of autocatalytic production of Cl_2 from heterogeneous reaction of HOCl was the possible cause of the observed differences. On the other hand, lower levels of reactive gas-phase bromine have been observed in the marine boundary layer (Leser et al., 2003; Mahajan et al., 2010b; Martin et al., 2009; Read et al., 2008). In the Cape Verde, BrO was measured by long path differential optical absorption spectroscopy (LP-DOAS) with a max of 2.5 ppt (Read et al., 2008) and 5.6 ppt (Mahajan et al., 2010b). In the east North Atlantic, while BrO was observed up to ~10 ppt by Martin et al. (2009), Leser et al. (2003) reported that BrO was mostly below detection limit except for the 2 days when the ship was near the Canary Islands where they measured up to 2.4 ppt. Modeling studies (von Glasow et al., 2004; Long et al., 2014; Sommariva and Von Glasow, 2012) show that the measured BrO levels in the open ocean are lower than expected, which is surprising considering its abundance in the ocean, and bromide has been reported to be depleted in marine aerosols (Sander et al., 2003). Compared to bromide and chloride, iodide is depleted in the ocean due to the uptake by marine organisms as a nutrient. Therefore, the main sources of gas-phase iodine in the open ocean are from oxidation of iodocarbons and O_3 mediated heterogeneous processes that could lead to HOI and I_2 production (Garland et al., 1980; Garland and Curtis, 1981).

Tidal stress on macroalgae in the ocean, caused by routine drying and exposure to sun, has been known to trigger production of inorganic and organic Iodine in coastal areas (Carpenter, 2003; Carpenter et al., 1999; Saiz-Lopez and Plane, 2004). Snow and ice surfaces in polar regions provide a unique environment for enhanced production of reactive halogen species (Abbatt et al., 2012). Since the first report by Barrie et al. (1988) of the relationship between filtered bromine and ODEs, direct measurements of molecular and reactive gas-phase bromine (Buys et al., 2013; Foster et al., 2001; Hausmann and Platt, 1994; Liao et al., 2012; Pohler et al., 2010; Pratt et al., 2013; Saiz-lopez et al., 2007), chlorine (Liao et al., 2014; Pohler et al., 2010), and iodine (Atkinson

et al., 2012; Grilli et al., 2013; Mahajan et al., 2010a; Saiz-lopez et al., 2007) in the polar boundary layer have been carried out mostly using the DOAS and CIMS technique. While similar levels of bromine species have been detected in both the Arctic and Antarctic (i.e., Br_2: ~ 50 ppt, BrO: ~ 30 ppt), significant hemispheric differences have been reported for reactive iodine species, which gives uncertainty in the mechanisms driving the sources. In a polluted boundary layer, NO_x mediated reactions can lead to enhanced formation of O_3 through generation of organic peroxy radicals from the oxidation of VOC by halogen radicals (Figure 1.3). Until recently, impact of Cl on the oxidation capacity or O_3 production was considered to be marginal in continental boundaries and only limited to marine environments in some cases due to slow oxidation of HCl, low aerosol surface areas, and low NO_x levels in a typical marine boundary layer (Jacob, 2000; Knipping and Dabdub, 2003). Recent studies consistently show strong evidence that Cl could indeed have a large influence on the tropospheric oxidation capacity even in areas away from its largest natural source, the ocean. In this context, formation of nitryl chloride ($ClNO_2$) is of particular interest. Laboratory study by Finlayson-Pitts et al. (1989) first confirmed the production mechanism of $ClNO_2$. The first ambient measurement was carried out by Osthoff et al. (2008) where they measured 50ppt - 1ppb of $ClNO_2$ in a subtropical marine boundary layer influenced by urban air and ship plumes. In following studies, measurements in multiple field studies both including marine and continental boundary layers (Bannan et al., 2015; Faxon et al., 2015; Phillips et al., 2012; Riedel et al., 2012; Tham et al., 2016; Thornton et al., 2010; Wang et al., 2016; Young et al., 2012) have confirmed that $ClNO_2$ is ubiquitous in the polluted boundary layer.

1.4 References

Abbatt, J., Oldridge, N., Symington, A., Chukalovskiy, V., McWhinney, R. D., Sjostedt, S. and Cox, R. A.: Release of gas-phase halogens by photolytic generation of OH in frozen halide-nitrate solutions: An active halogen formation mechanism?, J. Phys. Chem. A, 114(23), 6527–6533, doi:10.1021/jp102072t, 2010.

Abbatt, J. P. D., Thomas, J. L., Abrahamsson, K., Boxe, C., Granfors, A., Jones, A. E., King, M. D., Saiz-Lopez, A., Shepson, P. B., Sodeau, J., Toohey, D. W., Toubin, C., Von Glasow, R., Wren, S. N. and Yang, X.: Halogen activation via interactions with environmental ice and snow in the polar lower troposphere and other regions, Atmos. Chem. Phys., 12(14), 6237–6271, doi:10.5194/acp-12-6237-2012, 2012.

Allan, J. D., Williams, P. I., Najera, J., Whitehead, J. D., Flynn, M. J., Taylor, J. W., Liu, D., Darbyshire, E., Carpenter, L. J., Chance, R., Andrews, S. J., Hackenberg, S. C. and McFiggans, G.: Iodine observed in new particle formation events in the Arctic atmosphere during ACCACIA, Atmos. Chem. Phys., 15(10), 5599–5609, doi:10.5194/acp-15-5599-2015, 2015.

Atkinson, H. M., Huang, R. J., Chance, R., Roscoe, H. K., Hughes, C., Davison, B., Schönhardt, A., Mahajan, A. S., Saiz-Lopez, A., Hoffmann, T. and Liss, P. S.: Iodine emissions from the sea ice of the Weddell Sea, Atmos. Chem. Phys., 12(22), 11229–11244, doi:10.5194/acp-12-11229-2012, 2012.

Atkinson, R.: Gas-Phase Tropospheric Chemistry of Volatile Organic Compounds: 1. Alkanes and Alkenes, J. Phys. Chem. Ref. Data, 26(2), 215–290, doi:10.1063/1.556012, 1997.

Atkinson, R. and Arey, J.: Gas-phase tropospheric chemistry of biogenic volatile organic compounds: A review, Atmos. Environ., 37(SUPPL. 2), doi:10.1016/S1352-2310(03)00391-1, 2003.

Atkinson, R., Baulch, D. L., Cox, R. A., Crowley, J. N., Hampson, R. F., Hynes, R. G., Jenkin, M. E., Rossi, M. J. and Troe, J.: Evaluated kinetic and photochemical data for atmospheric chemistry: Volume III - Gas phase reactions of inorganic halogens, Atmos. Chem. Phys., 7(4), 981–1191, doi:10.5194/acp-7-981-2007, 2007.

Bannan, T. J., Booth, a M., Bacak, A., Muller, J. B. a, Leather, K. E., Breton, M. Le, Jones, B., Young, D., Coe, H., Allan, J., Visser, S., Slowik, J. G., Furger, M., Prévôt, A. S. H., Lee, J., Dunmore, R. E., Hopkins, J. R., Hamilton, J. F., Lewis, A. C., Whalley, L. K., Sharp, T., Stone, D., Heard, D. E., Fleming, Z. L., Leigh, R., Shallcross, D. E. and Percival, C. J.: Journal of Geophysical Research : Atmospheres of the role of Cl atom oxidation, J. Geophys. Res. Atmos., 120, 5638-5657, doi:10.1002/2014JD022629, 2015.

Barrie, L. A., Bottenheim, J. W., Schnell, R. C., Crutzen, P. J. and Rasmussen, R. A.: Ozone destruction and photochemical reactions at polar sunrise in the lower Arctic atmosphere, Nature, 334(14), 6–9, 1988.

Barrie, L. A., den Hartog, G., Bottenheim, J. W. and Landsberger, S.: Anthropogenic aerosols and gases in the lower troposphere at Alert Canada in April 1986, J. Atmos. Chem., 9(1–3), 101–127, doi:10.1007/BF00052827, 1989.

Blanchard, D.: The oceanic production of atmospheric sea salt, J. Geophys. Res., 90(C1), 961–963, doi:10.1029/JC090iC01p00961, 1985.

Bottenheim, J. W. and Gallant, A. G.: Measurements of NO_y species and O_3 at 82°N Latitude, Geophys. Res. Lett., 13(1), 113–116, 1986.

Butler, T. M., Taraborrelli, D., Brühl, C., Fischer, H., Harder, H., Martinez, M., Williams, J., Lawrence, M. G. and Lelieveld, J.: Improved simulation of isoprene oxidation chemistry with the ECHAM5/MESSy chemistry-climate model: lessons from the GABRIEL airborne field campaign, Atmos. Chem. Phys. Discuss., 8(2), 6273–6312, doi:10.5194/acpd-8-6273-2008, 2008.

Buys, Z., Brough, N., Huey, L. G., Tanner, D. J., Von Glasow, R. and Jones, A. E.: High temporal resolution Br_2, BrCl and BrO observations in coastal Antarctica, Atmos. Chem. Phys., doi:10.5194/acp-13-1329-2013, 2013.

Carpenter, L. J.: Iodine in the Marine Boundary Layer, Chem. Rev., 103(12), 4953–4962, doi:10.1021/cr0206465, 2003.

Carpenter, L. J., Sturges, W. T., Penkett, S. A. and Liss, P. S.: Short-lived alkyl iodides and bromides at Mace Head, Ireland: Links to biogenic sources and halogen oxide production, J. Geophys. Res. Atmos., 104(D1), 1679–1689, doi:10.1029/98JD02746, 1999.

Carslaw, N., Creasey, D. J., Harrison, D., Heard, D. E., Hunter, M. C., Jacobs, P. J., Jenkin, M. E., Lee, J. D., Lewis, A. C., Pilling, M. J., Saunders, S. M. and Seakins, P. W.: OH and HO_2 radical chemistry in a forested region of north-western Greece, Atmos. Environ., 35(27), 4725–4737, doi:10.1016/S1352-2310(01)00089-9, 2001.

Chameides, W. and Walker, J. C. G.: A photochemical theory of tropospheric ozone, J. Geophys. Res., 78(36), 8751–8760, doi:10.1029/jc078i036p08751, 1973.

Chameides, W. L., Lindsay, R. W., Richardson, J. and Kiang, C. S.: The role of biogenic hydrocarbons in urban photochemical smog: Atlanta as a case study, Science, 241(4872), 1473–1475, 1988.

Charlson, R. J., Lovelock, J. E., Andreae, M. O. and Warren, S. G.: Oceanic phytoplankton, atmospheric sulphur, cloud albedo and climate, Nature, 330, 1987.

Cicerone, J.: Halogens in the Atmosphere of the stratosphere, Rev. Geophys. Space phys., 19(1), 123–139, 1981.

Creasey, D. J., Heard, D. E. and Lee, J. D.: OH and HO_2 measurements in a forested region of north-western Greece, Atmos. Environ., 35(27), 4713–4724, doi:10.1016/S1352-2310(01)00090-5, 2001.

Crounse, J. D., Paulot, F., Kjaergaard, H. G. and Wennberg, P. O.: Peroxy radical isomerization in the oxidation of isoprene, Phys. Chem. Chem. Phys., 13(30), 13607, doi:10.1039/c1cp21330j, 2011.

Crutzen, P. J.: Ozone production rates in an oxygen-hydrogen-nitrogen oxide atmosphere, J. Geophys. Res., 76, 7311–7327, 1971.

Davison, B., Hewitt, C. N., O'Dowd, C. D., Lowe, J. A., Smith, M. H., Schwikowski, M., Baltensperger, U. and Harrison, R. M.: Dimethyl sulfide, methane sulfonic acid and physicochemical aerosol properties in Atlantic air from the United Kingdom to Halley Bay, J. Geophys. Res. Atmos., 101(D17), 22855–22867, doi:10.1029/96jd01166, 1996.

Dusanter, S., Vimal, D., Stevens, P. S., Volkamer, R. and Molina, L. T.: Measurements of OH and HO_2 concentrations during the MCMA-2006 field campaign – Part 1: Deployment of the Indiana University laser-induced fluorescence instrument, Atmos. Chem. Phys., 9(5), 1665–1685, doi:10.5194/acp-9-1665-2009, 2009.

Faxon, C., Bean, J. and Ruiz, L.: Inland Concentrations of Cl_2 and $ClNO_2$ in Southeast Texas Suggest Chlorine Chemistry Significantly Contributes to Atmospheric Reactivity, Atmosphere (Basel)., 6(10), 1487–1506, doi:10.3390/atmos6101487, 2015.

Finlayson-Pitts, B. J., Ezell, M. J. and Pitts Jr, J. N. : Formation of chemically active chlorine compounds by reactions of atmospheric NaCl particles with gaseous N_2O_5 and $ClONO_2$, Nature, 337(19), 241-244, 1989.

Foster, K. L., Plastridge, R. A., Bottenheim, J. W., Shepson, P. B., Finlayson-Pitts, B. J. and Spicer, C. W.: The role of Br_2 and BrCl in surface ozone destruction at polar sunrise, Science, 291(5503), 471–474, doi:10.1126/science.291.5503.471, 2001.

Fuchs, H., Hofzumahaus, A., Rohrer, F., Bohn, B., Brauers, T., Dorn, H.-P., Häseler, R., Holland, F., Kaminski, M., Li, X., Lu, K., Nehr, S., Tillmann, R., Wegener, R. and Wahner, A.: Experimental evidence for efficient hydroxyl radical regeneration in isoprene oxidation, Nat. Geosci., 6(12), 1023–1026, doi:10.1038/ngeo1964, 2013.

Garland, J. A. and Curtis, H.: Emission of iodine from the sea surface in the presence of ozone, J. Geophys. Res., 86(C4), 3183, doi:10.1029/jc086ic04p03183, 1981.

Garland, J. A., Elzerman, A. W. and Penkett, S. A.: The mechanism for dry deposition of ozone to seawater surfaces, J. Geophys. Res., 85, 7488–7492, 1980.

von Glasow, R., von Kuhlmann, R., Lawrence, M. G., Platt, U. and Crutzen, P. J.: Impact of reactive bromine chemistry in the troposphere, Atmos. Chem. Phys., 4(4), 2481-2497, doi:10.5194/acp-4-2481-2004, 2004.

Goldstein, A. H. and Galbally, I. E.: Known and unexplored organic constituents in the earth's atmosphere, Environ. Sci. Technol., 41(5), 1514–1521, doi:10.1021/es072476p, 2007.

Grilli, R., Legrand, M., Kukui, A., Méjean, G., Preunkert, S. and Romanini, D.: First investigations of IO, BrO, and NO_2 summer atmospheric levels at a coastal East Antarctic site using mode-locked cavity enhanced absorption spectroscopy, Geophys. Res. Lett., 40(4), 791–796, doi:10.1002/grl.50154, 2013.

Guenther, A. B., Jiang, X., Heald, C. L., Sakulyanontvittaya, T., Duhl, T., Emmons, L. K. and Wang, X.: The model of emissions of gases and aerosols from nature version 2.1 (MEGAN2.1): An extended and updated framework for modeling biogenic emissions, Geosci. Model Dev., 5(6), 1471–1492, doi:10.5194/gmd-5-1471-2012, 2012.

Hausmann, M. and Platt, U.: Spectroscopic measurement of bromine oxide and ozone in the high Arctic during Polar Sunrise Experiment 1992, J. Geophys. Res., 99(D12), 25399, doi:10.1029/94jd01314, 1994.

Hens, K., Novelli, A., Martinez, M., Auld, J., Axinte, R., Bohn, B., Fischer, H., Keronen, P., Kubistin, D., Nölscher, A. C., Oswald, R., Paasonen, P., Petäjä, T., Regelin, E., Sander, R., Sinha, V., Sipilä, M., Taraborrelli, D., Tatum Ernest, C., Williams, J., Lelieveld, J. and Harder, H.: Observation and modelling of HO_x radicals in a boreal forest, Atmos. Chem. Phys., 14(16), 8723–8747, doi:10.5194/acp-14-8723-2014, 2014.

Hofzumahaus, A., Rohrer, F., Lu, K., Bohn, B., Brauers, T., Chang, C., Fuchs, H., Holland, F., Kita, K., Kondo, Y., Li, X., Lou, S., Shao, M., Zeng, L., Wahner, A. and Zhang, Y.: Amplified Trace Gas Removal in the Troposphere, Science , 324, 1702–1704, 2009.

Huey, L. G.: Measurement of trace atmospheric species by chemical ionization mass spectrometry: Speciation of reactive nitrogen and future directions, Mass Spectrom. Rev., 26(2), 166–184, doi:10.1002/mas.20118, 2007.

Huff, A. K. and Abbatt, J. P. D.: Kinetics and product yields in the heterogeneous reactions of HOBr with ice surfaces containing NaBr and NaCl, J. Phys. Chem. A, 106(21), 5279–5287, doi:10.1021/jp014296m, 2002.

IPCC: Climate Change 2013: The physical Science Basis. Contribution of Working Group I to the Fifth Assessment Report of the Intergovernmental Panel on Climate., 2013.

Jacob, D. J.: Heterogenous chemistry and tropospheric ozone, Atmos. Environ., 34, 2131–2159, 2000.

Jenkin, M. E., Hurley, M. D. and Wallington, T. J.: Investigation of the radical product channel of the CH3C(O)O_2 + HO_2 Reaction in the Gas Phase, Phys. Chem. Chem. Phys., 9(24), 3149–3162, doi:10.1039/b702757e, 2007.

Jenkin, M. E., Hurley, M. D. and Wallington, T. J.: Investigation of the radical product channel of the CH3OCH 2O2 + HO_2 Reaction in the Gas Phase, J. Phys. Chem. A, 114(1), 408–416, doi:10.1021/jp908158w, 2010.

Jenkin, M. E., Young, J. C. and Rickard, A. R.: The MCM v3.3.1 degradation scheme for isoprene, Atmos. Chem. Phys., 15(20), 11433–11459, doi:10.5194/acp-15-11433-2015, 2015.

Jimenez, J. L., Canagaratna, M. R., Donahue, N. M., Prevot, A. S. H., Zhang, Q., Kroll, J. H., DeCarlo, P. F., Allan, J. D., Coe, H., Ng, N. L., Aiken, A. C., Docherty, K. S., Ulbrich, I. M., Grieshop, A. P., Robinson, A. L., Duplissy, J., Smith, J. D., Wilson, K. R., Lanz, V. A., Hueglin, C., Sun, Y. L., Tian, J., Laaksonen, A., Raatikainen, T., Rautiainen, J., Vaattovaara, P., Ehn, M., Kulmala, M., Tomlinson, J. M., Collins, D. R., Cubison, M. J., Dunlea, J., Huffman, J. A., Onasch, T. B., Alfarra, M. R., Williams, P. I., Bower, K., Kondo, Y., Schneider, J., Drewnick, F., Borrmann, S., Weimer, S., Demerjian, K., Salcedo, D., Cottrell, L., Griffin, R., Takami, A., Miyoshi, T., Hatakeyama, S., Shimono, A., Sun, J. Y., Zhang, Y. M., Dzepina, K., Kimmel, J. R., Sueper, D., Jayne, J. T., Herndon, S. C., Trimborn, A. M., Williams, L. R., Wood, E. C., Middlebrook, A. M., Kolb, C. E., Baltensperger, U. and Worsnop, D. R.: Evolution of Organic Aerosols in the Atmosphere, Science, 326(5959), 1525–1529, doi:10.1126/science.1180353, 2009.

Jobson, B. T., Niki, H., Yokouchi, Y., Bottenheim, J., Hopper, F. and Leaitch, R.: Measurements of C2 -C6 hydrocarbons during the Polar Sunrise1992 Experiment: Evidence for Cl atom and Br atom chemistry , J. Geophys. Res., 99(D12), 25355, doi:10.1029/94jd01243, 1994.

Kanaya, Y., Cao, R., Akimoto, H., Fukuda, M., Komazaki, Y., Yokouchi, Y., Koike, M., Tanimoto, H., Takegawa, N. and Kondo, Y.: Urban photochemistry in central Tokyo: 1. Observed and modeled OH and HO_2 radical concentrations during the winter and summer of 2004, J. Geophys. Res. Atmos., 112(21), doi:10.1029/2007JD008670, 2007.

Knipping, E. M. and Dabdub, D.: Impact of chlorine emissions from sea-salt aerosol on coastal urban ozone, Environ. Sci. Technol., 37(2), 275–284, doi:10.1021/es025793z, 2003.

Kroll, J. H. and Seinfeld, J. H.: Chemistry of secondary organic aerosol: Formation and evolution of low-volatility organics in the atmosphere, Atmos. Environ., 42(16), 3593–3624, doi:10.1016/j.atmosenv.2008.01.003, 2008.

Kubistin, D., Harder, H., Martinez, M., Rudolf, M., Sander, R., Bozem, H., Eerdekens, G., Fischer, H., Gurk, C., Klüpfel, T., Königstedt, R., Parchatka, U., Schiller, C. L., Stickler, A., Taraborrelli, D., Williams, J. and Lelieveld, J.: Hydroxyl radicals in the tropical troposphere over the Suriname rainforest: Comparison of measurements with the box model MECCA, Atmos. Chem. Phys., 10(19), 9705–9728, doi:10.5194/acp-10-9705-2010, 2010.

Lawler, M. J., Finley, B. D., Keene, W. C., Pszenny, A. A. P., Read, K. A., Glasow, R. von and Saltzman, E. S.: Pollution-enhanced reactive chlorine chemistry in the eastern tropical Atlantic boundary layer, Geophys. Res. Lett., 36(L08810), doi:10.1029/2008GL036666, 2009.

Lawler, M. J., Sander, R., Carpenter, L. J., Lee, J. D., Von Glasow, R., Sommariva, R. and Saltzman, E. S.: HOCl and Cl2 observations in marine air, Atmos. Chem. Phys., 11(15), 7617–7628, doi:10.5194/acp-11-7617-2011, 2011.

Lelieveld, J., Butler, T. M., Crowley, J. N., Dillon, T. J., Fischer, H., Ganzeveld, L., Harder, H., Lawrence, M. G., Martinez, M., Taraborrelli, D. and Williams, J.: Atmospheric oxidation capacity sustained by a tropical forest, Nature, 452(7188), 737–740, doi:10.1038/nature06870, 2008.

Leser, H., Hönninger, G. and Platt, U.: MAX-DOAS measurements of BrO and NO_2 in the marine boundary layer , Geophys. Res. Lett., 30(10), doi:10.1029/2002gl015811, 2003.

Levy, H.: Normal Atmosphere: Large Radical and Formaldehyde Concentrations Predicted, Science, 173(3992), 141–143, doi:10.1126/science.173.3992.141, 1971.

Liao, J., Huey, L. G., Tanner, D. J., Flocke, F. M., Orlando, J. J., Neuman, J. A., Nowak, J. B., Weinheimer, A. J., Hall, S. R., Smith, J. N., Fried, A., Staebler, R. M., Wang, Y., Koo, J. H., Cantrell, C. A., Weibring, P., Walega, J., Knapp, D. J., Shepson, P. B. and Stephens, C. R.: Observations of inorganic bromine (HOBr, BrO, and Br_2) speciation at Barrow, Alaska, in spring 2009, J. Geophys. Res. Atmos., 117(6), 1–11, doi:10.1029/2011JD016641, 2012.

Liao, J., Huey, L. G., Liu, Z., Tanner, D. J., Cantrell, C. A., Orlando, J. J., Flocke, F. M., Shepson, P. B., Weinheimer, A. J., Hall, S. R., Ullmann, K., Beine, H. J., Wang, Y., Ingall, E. D., Stephens, C. R., Hornbrook, R. S., Apel, E. C., Riemer, D., Fried, A., Mauldin, R. L., Smith, J. N., Staebler, R. M., Neuman, J. A. and Nowak, J. B.: High levels of molecular chlorine in the Arctic atmosphere, Nat. Geosci., 7(2), 91–94, doi:10.1038/ngeo2046, 2014.

Lim, Y. Bin and Ziemann, P. J.: Products and mechanism of secondary organic aerosol formation from reactions of n-alkanes with OH radicals in the presence of NO_x, Environ. Sci. Technol., 39(23), 9229–9236, doi:10.1021/es051447g, 2005.

Lindberg, S. E., Brooks, S., Lin, C. J., Scott, K. J., Landis, M. S., Stevens, R. K., Goodsite, M. and Richter, A.: Dynamic oxidation of gaseous mercury in the arctic troposphere at polar sunrise, Environ. Sci. Technol., 36(6), 1245–1256, doi:10.1021/es0111941, 2002.

Long, M. S., Keene, W. C., Easter, R. C., Sander, R., Liu, X., Kerkweg, A. and Erickson, D.: Sensitivity of tropospheric chemical composition to halogen-radical chemistry using a fully coupled size-resolved multiphase chemistry-global climate system: Halogen distributions, aerosol composition, and sensitivity of climate-relevant gases, Atmos. Chem. Phys., 14(7), 3397–3425, doi:10.5194/acp-14-3397-2014, 2014.

Lou, S., Holland, F., Rohrer, F., Lu, K., Bohn, B., Brauers, T., Chang, C. C., Fuchs, H., Häseler, R., Kita, K., Kondo, Y., Li, X., Shao, M., Zeng, L., Wahner, A., Zhang, Y., Wang, W. and Hofzumahaus, A.: Atmospheric OH reactivities in the Pearl River Delta - China in summer 2006: Measurement and model results, Atmos. Chem. Phys., 10(22), 11243–11260, doi:10.5194/acp-10-11243-2010, 2010.

Lu, K. D., Hofzumahaus, A., Holland, F., Bohn, B., Brauers, T., Fuchs, H., Hu, M., Häseler, R., Kita, K., Kondo, Y., Li, X., Lou, S. R., Oebel, A., Shao, M., Zeng, L. M., Wahner, A., Zhu, T., Zhang, Y. H. and Rohrer, F.: Missing OH source in a suburban environment near Beijing: Observed and modelled OH and HO_2 concentrations in summer 2006, Atmos. Chem. Phys., 13(2), 1057–1080, doi:10.5194/acp-13-1057-2013, 2013.

Mahajan, A. S., Shaw, M., Oetjen, H., Hornsby, K. E., Carpenter, L. J., Kaleschke, L., Tian-Kunze, X., Lee, J. D., Moller, S. J., Edwards, P., Commane, R., Ingham, T., Heard, D. E. and

Plane, J. M. C.: Evidence of reactive iodine chemistry in the Arctic boundary layer, J. Geophys. Res. Atmos., 115(20), 1–11, doi:10.1029/2009JD013665, 2010a.

Mahajan, A. S., Plane, J. M. C., Oetjen, H., Mendes, L., Saunders, R. W., Saiz-Lopez, A., Jones, C. E., Carpenter, L. J. and McFiggans, G. B.: Measurement and modelling of tropospheric reactive halogen species over the tropical Atlantic Ocean, Atmos. Chem. Phys., 10(10), 4611–4624, doi:10.5194/acp-10-4611-2010, 2010b.

Mao, J., Ren, X., Chen, S., Brune, W. H., Chen, Z., Martinez, M., Harder, H., Lefer, B., Rappenglück, B., Flynn, J. and Leuchner, M.: Atmospheric oxidation capacity in the summer of Houston 2006: Comparison with summer measurements in other metropolitan studies, Atmos. Environ., 44(33), 4107–4115, doi:10.1016/j.atmosenv.2009.01.013, 2010.

Mao, J., Ren, X., Zhang, L., Van Duin, D. M., Cohen, R. C., Park, J. H., Goldstein, A. H., Paulot, F., Beaver, M. R., Crounse, J. D., Wennberg, P. O., Digangi, J. P., Henry, S. B., Keutsch, F. N., Park, C., Schade, G. W., Wolfe, G. M., Thornton, J. A. and Brune, W. H.: Insights into hydroxyl measurements and atmospheric oxidation in a California forest, Atmos. Chem. Phys., 12(17), 8009–8020, doi:10.5194/acp-12-8009-2012, 2012.

Martin, M., Pöhler, D., Seitz, K., Sinreich, R. and Platt, U.: BrO measurements over the Eastern North-Atlantic, Atmos. Chem. Phys., 9(24), 9545–9554, doi:10.5194/acp-9-9545-2009, 2009.

McNeill, V. F., Patterson, J., Wolfe, G. M. and Thornton, J. A.: The effect of varying levels of surfactant on the reactive uptake of N2O5 to aqueous aerosol, Atmos. Chem. Phys., 6(6), 1635–1644, doi:10.5194/acp-6-1635-2006, 2006.

Oltmans, S. J. and Komhyr, W. D.: Surface ozone distributions and variations from 1973-1984 measurements at the NOAA geophysical monitoring for climatic change baseline observatories., J. Geophys. Res., 91(6), 5229–5236, doi:10.1029/JD091iD04p05229, 1986.

Osthoff, H. D., Roberts, J. M., Ravishankara, A. R., Williams, E. J., Lerner, B. M., Sommariva, R., Bates, T. S., Coffman, D., Quinn, P. K., Dibb, J. E., Stark, H., Burkholder, J. B., Talukdar, R. K., Meagher, J., Fehsenfeld, F. C. and Brown, S. S.: High levels of nitryl chloride in the polluted subtropical marine boundary layer, Nat. Geosci., 1(5), 324–328, doi:10.1038/ngeo177, 2008.

Peeters, J. and Müller, J.-F.: HO_x radical regeneration in isoprene oxidation via peroxy radical isomerisations. II: experimental evidence and global impact, Phys. Chem. Chem. Phys., 12(42), 14227, doi:10.1039/c0cp00811g, 2010.

Peeters, J., Nguyen, T. L. and Vereecken, L.: HO_x radical regeneration in the oxidation of isoprene, Phys. Chem. Chem. Phys., 11(28), 5935, doi:10.1039/b908511d, 2009.

Peeters, J., Müller, J. F., Stavrakou, T. and Nguyen, V. S.: Hydroxyl radical recycling in isoprene oxidation driven by hydrogen bonding and hydrogen tunneling: The upgraded LIM1 mechanism, J. Phys. Chem. A, 118(38), 8625–8643, doi:10.1021/jp5033146, 2014.

Phillips, G. J., Tang, M. J., Thieser, J., Brickwedde, B., Schuster, G., Bohn, B., Lelieveld, J. and Crowley, J. N.: Significant concentrations of nitryl chloride observed in rural continental Europe associated with the influence of sea salt chloride and anthropogenic emissions, Geophys. Res. Lett., 39(10), 1–5, doi:10.1029/2012GL051912, 2012.

Platt, U., Allan, W. and Lowe, D.: Hemispheric average Cl atom concentration from 13C/12C ratios in atmospheric methane, Atmos. Chem. Phys., 4(9/10), 2393–2399, doi:10.5194/acp-4-2393-2004, 2004.

Pohler, D., Vogel, L., Friess, U. and Platt, U.: Observation of halogen species in the Amundsen Gulf, Arctic, by active long-path differential optical absorption spectroscopy, Proc. Natl. Acad. Sci., 107(15), 6582–6587, doi:10.1073/pnas.0912231107, 2010.

Poschl, U., Martin, S. T., Sinha, B., Chen, Q., Gunthe, S. S., Huffman, J. A., Borrmann, S., Farmer, D. K., Garland, R. M., Helas, G., Jimenez, J. L., King, S. M., Manzi, A., Mikhailov, E., Pauliquevis, T., Petters, M. D., Prenni, A. J., Roldin, P., Rose, D., Schneider, J., Su, H., Zorn, S. R., Artaxo, P. and Andreae, M. O.: Rainforest Aerosols as Biogenic Nuclei of Clouds and Precipitation in the Amazon, Science, 329, 1513–1517, 2010.

Prather, M. and Spivakovsky, C. M.: Tropospheric OH and the Lifetimes of Hydrochlorofluorocarbons, J. Geophys. Res., 95(Dll), 18723–18729, 1990.

Pratt, K. A., Custard, K. D., Shepson, P. B., Douglas, T. A., Pöhler, D., General, S., Zielcke, J., Simpson, W. R., Platt, U., Tanner, D. J., Gregory Huey, L., Carlsen, M. and Stirm, B. H.: Photochemical production of molecular bromine in Arctic surface snowpacks, Nat. Geosci., 6(5), 351–356, doi:10.1038/ngeo1779, 2013.

Pugh, T. A. M., MacKenzie, A. R., Hewitt, C. N., Langford, B., Edwards, P. M., Furneaux, K. L., Heard, D. E., Hopkins, J. R., Jones, C. E., Karunaharan, A., Lee, J., Mills, G., Misztal, P., Moller, S., Monks, P. S. and Whalley, L. K.: Simulating atmospheric composition over a South-East Asian tropical rainforest: Performance of a chemistry box model, Atmos. Chem. Phys., 10, 279–298, doi:10.5194/acpd-9-19243-2009, 2010.

Read, K. A., Mahajan, A. S., Carpenter, L. J., Evans, M. J., Faria, B. V. E., Heard, D. E., Hopkins, J. R., Lee, J. D., Moller, S. J., Lewis, A. C., Mendes, L., McQuaid, J. B., Oetjen, H., Saiz-Lopez, A., Pilling, M. J. and Plane, J. M. C.: Extensive halogen-mediated ozone destruction over the tropical Atlantic Ocean, Nature, 453(7199), 1232–1235, doi:10.1038/nature07035, 2008.

Ren, X., Harder, H., Martinez, M., Lesher, R. L., Oliger, A., Simpas, J. B., Brune, W. H., Schwab, J. J., Demerjian, K. L., He, Y., Zhou, X. and Gao, H.: OH and HO2 chemistry in the urban atmosphere of New York City, Atmos. Environ., 37(26), 3639–3651, doi:10.1016/S1352-2310(03)00459-X, 2003.

Ren, X., Olson, J. R., Crawford, J. H., Brune, W. H., Mao, J., Long, R. B., Chen, Z., Chen, G., Avery, M. A., Sachse, G. W., Barrick, J. D., Diskin, G. S., Huey, L. G., Fried, A., Cohen, R. C., Heikes, B., Wennberg, P. O., Singh, H. B., Blake, D. R. and Shetter, R. E.: HO_x chemistry during INTEX-A 2004: Observation, model calculation, and comparison with previous studies, J. Geophys. Res. Atmos., 113(5), 1–13, doi:10.1029/2007JD009166, 2008.

Riedel, T. P., Bertram, T. H., Crisp, T. A., Williams, E. J., Lerner, B. M., Vlasenko, A., Li, S. M., Gilman, J., De Gouw, J., Bon, D. M., Wagner, N. L., Brown, S. S. and Thornton, J. A.: Nitryl chloride and molecular chlorine in the coastal marine boundary layer, Environ. Sci. Technol., 46(19), 10463–10470, doi:10.1021/es204632r, 2012.

Rohrer, F., Lu, K., Hofzumahaus, A., Bohn, B., Brauers, T., Chang, C.-C., Fuchs, H., Häseler, R., Holland, F., Hu, M., Kita, K., Kondo, Y., Li, X., Lou, S., Oebel, A., Shao, M., Zeng, L., Zhu, T., Zhang, Y. and Wahner, A.: Maximum efficiency in the hydroxyl-radical-based self-cleansing of the troposphere, Nat. Geosci., 7(8), 559–563, doi:10.1038/ngeo2199, 2014.

Saiz-lopez, A., Mahajan, A. S., Salmon, R. A., Bauguitte, S. J., Jones, A. E., Roscoe, H. K. and Plane, J. M. C.: Boundary Layer Halogens in Coastal Antarctica, Science, 348(July), 348–352, doi:10.1126/science.1141408, 2007.

Saiz-Lopez, A. and Plane, J. M. C.: Novel iodine chemistry in the marine boundary layer, Geophys. Res. Lett., 31(4), 1999–2002, doi:10.1029/2003GL019215, 2004.

Saiz-Lopez, A., Saunders, R. W., Joseph, D. M., Ashworth, S. H. and Plane, J. M. C.: Absolute absorption cross-section and photolysis rate of I2, Atmos. Chem. Phys., 4(3), 1443-1450, doi:10.5194/acpd-4-1443-2004, 2004.

Sanchez, D., Jeong, D., Seco, R., Wrangham, I., Jeong-Hoo, P., Brune, W. H., Koss, A., Gilman, J., De Gouw, J., Misztal, P., Goldstein, A. H., Baumann, K., Wennberg, P. O., Keutsch, F. N., Guenther, A. and Kim, S.: Intercomparison of OH concentrations and OH reactivity measurements in a high isoprene and moderate NO environment during the Southern Oxidants and Aerosol Study (SOAS), Atmos. Environ., 174, 227-236, 2018

Sander, R., Keene, W. C., Pszenny, A. A. P., Arimoto, R., Ayers, G. P., Baboukas, E., Cainey, J. M., Crutzen, P. J., Duce, R. A., Hönninger, G., Huebert, B. J., Maenhaut, W., Mihalopoulos, N., Turekian, V. C. and Van Dingenen, R.: Atmospheric Chemistry and Physics Inorganic bromine in the marine boundary layer: a critical review, Ger. Now Meteorol. Serv. Canada, 3, 1301–1336, 2003.

Schroeder, W. H., Anlauf, K. G., Barrie, L. A., Steffen, A., Schneeberger, D. R. and Berg, T.: Arctic sprintime depletion of mercury, Nature, 394, 331–332, doi:10.1111/j.1365-2990.2009.01039.x, 1998.

Da Silva, G., Graham, C. and Wang, Z. F.: Unimolecular β-hydroxyperoxy radical decomposition with OH recycling in the photochemical oxidation of isoprene, Environ. Sci. Technol., 44(1), 250–256, doi:10.1021/es900924d, 2010.

Sjostedt, S. J. and Abbatt, J. P. D.: Release of gas-phase halogens from sodium halide substrates: Heterogeneous oxidation of frozen solutions and desiccated salts by hydroxyl radicals, Environ. Res. Lett., 3(4), doi:10.1088/1748-9326/3/4/045007, 2008.

Sommariva, R. and Von Glasow, R.: Multiphase halogen chemistry in the tropical atlantic ocean, Environ. Sci. Technol., 46(19), 10429–10437, doi:10.1021/es300209f, 2012.

Spivakovsky, C. M., Yevich, R., Logan, J. A., Wofsy, S. C., McElroy, M. B. and Prather, M. J.: Tropospheric OH in a three-dimensional chemical tracer model: An assessment based on observations of CH_3CCl_3, J. Geophys. Res., 95(D11), 18441, doi:10.1029/jd095id11p18441, 1990.

Steffen, A., Douglas, T., Amyot, M., Ariya, P., Aspmo, K., Berg, T., Bottenheim, J., Brooks, S., Cobbett, F., Dastoor, A., Dommergue, A., Ebinghaus, R., Ferrari, C., Gardfeldt, K., Goodsite, M. E., Lean, D., Poulain, A., Scherz, C., Skov, H., Sommar, J. and Temme, C.: A synthesis of atmospheric mercury depletion event chemistry linking atmosphere, snow and water, Atmos. Chem. Phys., 8, 1445-1482, doi:10.5194/acp-8-1445-2008, 2008.

Stone, D., Evans, M. J., Edwards, P. M., Commane, R., Ingham, T., Rickard, A. R., Brookes, D. M., Hopkins, J., Leigh, R. J., Lewis, A. C., Monks, P. S., Oram, D., Reeves, C. E., Stewart, D. and Heard, D. E.: Isoprene oxidation mechanisms: Measurements and modelling of OH and HO_2 over a South-East Asian tropical rainforest during the OP3 field campaign, Atmos. Chem. Phys., 11(13), 6749–6771, doi:10.5194/acp-11-6749-2011, 2011.

Tan, D., Faloona, I., Simpas, J. B., Brune, W., Shepson, P. B., Couch, T. L., Sumner, a. L., Carroll, M. a., Thornberry, T., Apel, E., Riemer, D. and Stockwell, W.: HOx budgets in a deciduous forest: Results from the PROPHET summer 1998 campaign, J. Geophys. Res. Atmos., 106(D20), 24407–24427, doi:10.1029/2001JD900016, 2001.

Tham, Y. J., Wang, Z., Li, Q., Yun, H., Wang, W., Wang, X., Xue, L., Lu, K., Ma, N., Bohn, B., Li, X., Kecorius, S., Größ, J., Shao, M., Wiedensohler, A., Zhang, Y. and Wang, T.:

Significant concentrations of nitryl chloride sustained in the morning: Investigations of the causes and impacts on ozone production in a polluted region of northern China, Atmos. Chem. Phys., 16(23), 14959–14977, doi:10.5194/acp-16-14959-2016, 2016.

Thornton, J. A. and Abbatt, J. P. D.: N_2O_5 reaction on submicron sea salt aerosol: Kinetics, products, and the effect of surface active organics, J. Phys. Chem. A, 109(44), 10004–10012, doi:10.1021/jp054183t, 2005.

Thornton, J. A., Kercher, J. P., Riedel, T. P., Wagner, N. L., Cozic, J., Holloway, J. S., Dubé, W. P., Wolfe, G. M., Quinn, P. K., Middlebrook, A. M., Alexander, B. and Brown, S. S.: A large atomic chlorine source inferred from mid-continental reactive nitrogen chemistry, Nature, 464(7286), 271–274, doi:10.1038/nature08905, 2010.

Wang, T., Tham, Y. J., Xue, L., Li, Q., Zha, Q., Wang, Z., Poon, S. C. N., Dubé, W. P., Blake, D. R., Louie, P. K. K., Luk, C. W. Y., Tsui, W. and Brown, S. S.: Observations of nitryl chloride and modeling its source and effect on ozone in the planetary boundary layer of southern China, J. Geophys. Res. Atmos., (2), 2476–2489, doi:10.1002/2015JD024556, 2016.

Wennberg, P.: Bromine explosion, Nature, 397, 1999.

Whalley, L. K., Edwards, P. M., Furneaux, K. L., Goddard, A., Ingham, T., Evans, M. J., Stone, D., Hopkins, J. R., Jones, C. E., Karunaharan, A., Lee, J. D., Lewis, A. C., Monks, P. S., Moller, S. J. and Heard, D. E.: Quantifying the magnitude of a missing hydroxyl radical source in a tropical rainforest, Atmos. Chem. Phys., 11(14), 7223–7233, doi:10.5194/acp-11-7223-2011, 2011.

Wolfe, G. M., Thornton, J. A., Bouvier-Brown, N. C., Goldstein, A. H., Park, J. H., McKay, M., Matross, D. M., Mao, J., Brune, W. H., LaFranchi, B. W., Browne, E. C., Min, K. E., Wooldridge, P. J., Cohen, R. C., Crounse, J. D., Faloona, I. C., Gilman, J. B., Kuster, W. C., De Gouw, J. A., Huisman, A. and Keutsch, F. N.: The chemistry of atmosphere-forest exchange (CAFE) model-part 2: Application to BEARPEX-2007 observations, Atmos. Chem. Phys., 11(3), 1269–1294, doi:10.5194/acp-11-1269-2011, 2011.

Wolfe, G. M., Crounse, J. D., Parrish, J. D., St. Clair, J. M., Beaver, M. R., Paulot, F., Yoon, T. P., Wennberg, P. O. and Keutsch, F. N.: Photolysis, OH reactivity and ozone reactivity of a proxy for isoprene-derived hydroperoxyenals (HPALDs), Phys. Chem. Chem. Phys., 14(20), 7276–7286, doi:10.1039/c2cp40388a, 2012.

Woodcock, A. H.: Salt Nuclei in Marine Air As a Function of Altitude and Wind Force, J. Meteorol.,10(5), 362–371, doi:10.1175/1520-0469(1953)010<0366:SNIMAA>2.0.CO;2, 1953.

Young, C. J., Washenfelder, R. A., Roberts, J. M., Mielke, L. H., Osthoff, H. D., Tsai, C., Pikelnaya, O., Stutz, J., Veres, P. R., Cochran, A. K., Vandenboer, T. C., Flynn, J., Grossberg, N., Haman, C. L., Lefer, B., Stark, H., Graus, M., De Gouw, J., Gilman, J. B., Kuster, W. C. and Brown, S. S.: Vertically resolved measurements of nighttime radical reservoirs in los angeles and their contribution to the urban radical budget, Environ. Sci. Technol., 46(20), 10965–10973, doi:10.1021/es302206a, 2012.

CHAPTER 2

METHODS

2.1 Chemical Ionization Mass Spectrometer

2.1.1 OH Measurement using NO_3^- Ion Chemistry

A THS Instruments LLC Atmospheric Pressure Chemical Ionization Mass Spectrometer (AP-CIMS) was used to quantify ambient OH with an identical instrument configuration deployed for the Southern Oxidant and Aerosol Study (SOAS) in 2013 (Sanchez et al., 2017). The analytical method was developed by Tanner et al. (1997) and had mostly been used in low relative humidity environments such as the free troposphere (Kim et al., 2007), polar (Liao et al., 2011b, 2012, 2014; Mauldin et al., 2010; Raso et al., 2017; Sjostedt et al., 2007), and non-urban regions (Kim et al., 2015b; Sanchez et al., 2017). During the past few years, the AP-CIMS has been deployed in high BVOC environments and compared with ambient OH concentration reported by using the LIF instrumentation (Hens et al., 2014; Sanchez et al., 2017).

$$^{34}SO_2 + OH + M \rightarrow H^{34}SO_3 + M \qquad \text{R2.1}$$

$$H^{34}SO_3 + O_2 \rightarrow {}^{34}SO_3 + HO_2 \qquad \text{R2.2}$$

$$^{34}SO_3 + H_2O + M \rightarrow H_2{}^{34}SO_4 + M \qquad \text{R2.3}$$

$$H_2{}^{34}SO_4 + NO_3^- \rightarrow H^{34}SO_4^- + HNO_3 \qquad \text{R2.4}$$

As thoroughly described in Tanner et al. (1997), the AP-CIMS technique for OH quantification draws bulk air flow into the inlet (1/2” OD metal tube) with a blower. From the center of the inlet flow, a sample flow of 5 standard liters per minute (slpm) is introduced to an

injector system which consists of a pair of front and rear injectors. This allows injection of a mixture of gases to convert the sampled OH into H_2SO_4. Background is characterized by adding excess C_3F_6 or C_3H_8 for chemical removal of OH. In an ion reaction chamber, H_2SO_4 is ionized by NO_3^- reagent ion to produce HSO_4^-. NO_3^- is generated by a corona discharge ion source unit described in Kurten et al. (2011) as a HNO_3 doped zero air stream passes over the ion source. The generated analyte ion (HSO_4^-) is introduced to a collision dissociation chamber (CDC), an octopole ion focus unit, and a quadrupole-channeltron ion detection unit, a typical configuration for mass spectrometry applications in atmospheric chemistry (Huey, 2007). A multi-point calibration was carried out as described in Sanchez et al. (2017). Briefly, OH was generated from photolysis (184.9 nm) of water in a ~ 30 slpm N_2 flow. The humidity in the calibration system was known and controlled by adjusting the fraction of N_2 flow being introduced to the water bubbler. The calibration was conducted on a weekly basis. The assessed limit of detection was 1 x 10^5 molecules cm^{-3} and the uncertainty was 40 % in 5 minutes 2σ.

2.1.2 $ClNO_2$ and I_2 Measurement using I^- Ion Chemistry

During KORUS-AQ 2016, a CIMS using iodide (I^-) as the reagent ion was used for measuring Cl_2 and $ClNO_2$ at the Taehwa Research Forest (TRF), Olympic Park (OP) and on the NASA DC-8. The system was similar to what is described in Slusher et al. (2004) and Liao et al. (2011a), and the inlet configuration during the campaign is shown in Figure 2.1. Ambient air was sampled through a stainless steel donut shaped inlet at TRF and a Polytetrafluoroethylene (PTFE) tube inlet at OP. The stainless steel donut inlet has been shown to effectively avoid wall loss of reactive halogens during previous campaigns (Liao et al., 2011a). The lengths of the three CIMS systems were 20-30 cm. The PTFE inlet line at the TRF site was washed on a weekly basis and

the ones at the OP and DC-8 were not washed routinely during the campaign due to difficulties on detaching the inlet. The potential bias on interactions of Cl_2 and $ClNO_2$ inside the inlet were not tested but the artifacts have been shown to be negligible in various field conditions (Liao et al., 2014; Riedel et al., 2012; Thornton et al., 2010). Therefore, the use of different types of inlets (e.g., the use of the donut), described above, at the two ground sites and on the DC-8 is not expected to be an issue for the quantitative comparisons in this study. The sampled air went through the first 3-way valves to be delivered to an ambient or charcoal scrubber mode for background, alternating every 5 minutes. The second 3-way valve was for heated (150 ^oC) and unheated cycles. $ClNO_2$ and Cl_2 were only quantified during the unheated cycles to avoid any potential artifacts as described in Liu et al. (2017). A total of 3000 standard liters per minute (slpm) was drawn in with a blower with an additional flow of 4 slpm drawn at the end of the inlet to reduce the residence time and 1 slpm was sampled into the CIMS. All the inlet parts, after the blower, including the fittings and tubings, were made of PTFE.

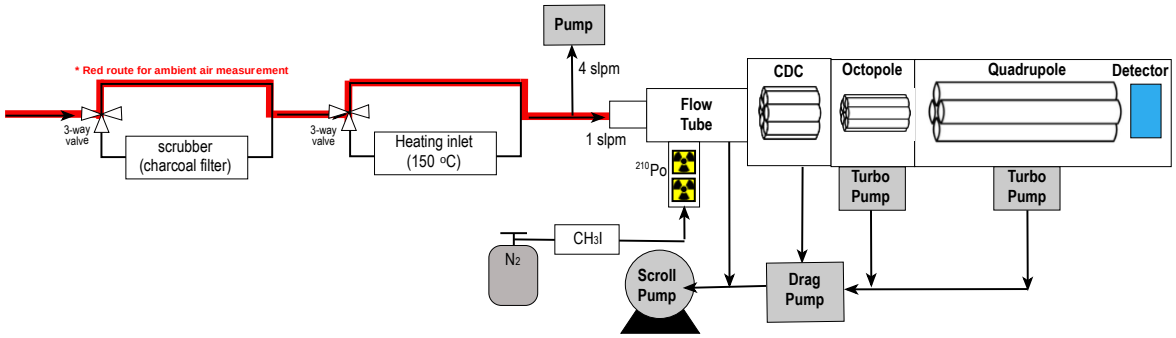

Figure 2.1 Inlet configuration during KORUS-AQ

In the flow tube, the target compounds form clusters with I^- (R2.5-R2.6) (Huey, 2007; Huey et al., 1995), which were generated by flowing 1 slpm N_2 through a methyl iodide (CH_3I) permtube

oven maintained at 50 °C. Polonium (NRD LLC, Static Master, Model:2U500, Activity: 20 mCi) was used as the radioactive source for ionization. Clusters of Cl_2 isotopes were detected at the mass to charge ratio (m/z) of 197 and 199, and $ClNO_2$ was measured at 208 and 210. The natural abundance of Cl_2 and $ClNO_2$ isotopes are approximately 9:6:1 ($^{35}Cl^{35}Cl$: $^{35}Cl^{37}Cl$: $^{37}Cl^{37}Cl$) and 3:1 ($^{35}ClNO_2$: $^{37}ClNO_2$) respectively. Mass 201 ($^{37}Cl^{37}Cl$) was not considered in the data processing due to artifacts.

$$ClNO_2(g) + I^- \rightarrow ICl NO_2^-(g) \qquad R2.5$$

$$Cl_2(g) + I^- \rightarrow ICl_2^-(g) \qquad R2.6$$

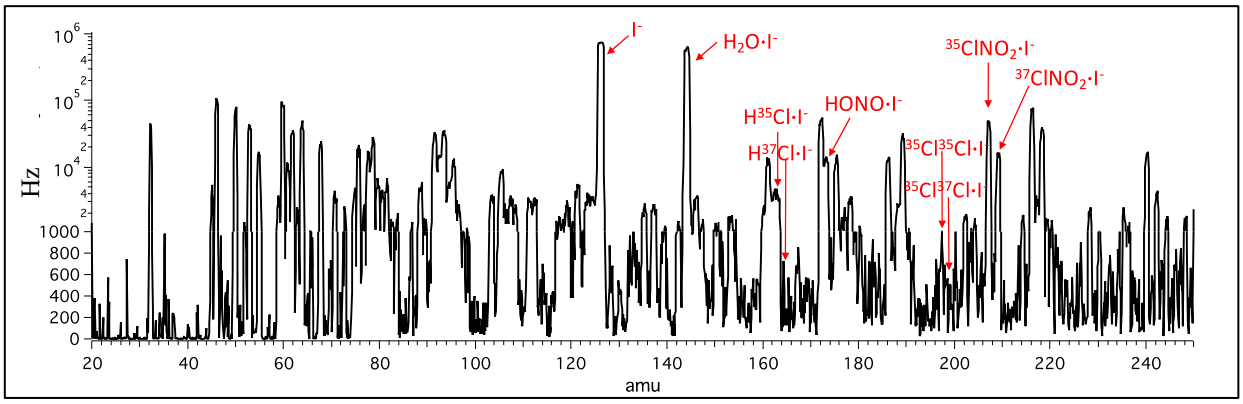

Figure 2.2 CIMS mass spectrum taken at the Taehwa Research site on May 4th 6:35 local standard Time

Calibrations of Cl_2 and $ClNO_2$ were carried out during and after the campaign. Cl_2 in a cylinder (Airgas, 10 ppm in N_2) was diluted with zero air to be sampled in either ambient or scrubber (charcoal) mode (Figure 2.1). The Cl_2 in the cylinder was quantified through the method described by Liao et al. (2012) and was 8.84 ± 0.43 ppm. $ClNO_2$ was synthesized, based on Thaler et al. (2011). Briefly, Cl_2 gas in N_2 was passed through a pyrex reservoir (diameter = 1.3 cm, length

= 5.5 cm) containing a bed of NaCl (MACRON) and $NaNO_2$ (Sigma Aldrich) with a molar ratio of 10 to 1. This slurry mixture contains NO_2^- that reacts with the flowing Cl_2 to generate $ClNO_2$. The output flow was further diluted with 4 $Lmin^{-1}$ of zero air in order to sufficiently provide gas flow. The flow containing synthesized $ClNO_2$ was then analyzed at m/z of 208 and 210 with the CIMS. NO_2 and NO-NO_y were simultaneously measured with a Cavity Ring Down Spectroscopy (CRDS, Los Gatos Research, detection limit: 10 pptv, precision: 50 pptv at 1σ, model: 907-0009-0002) and chemiluminescence (CL, Thermo Scientific, detection limit: 50 pptv, model: 42 i) respectively. $ClNO_2$ is detected as NO_y in the CL through conversion to NO on the heated (325 ^oC) molybdenum catalytic converter (Williams et al., 1998). The efficiency of the conversion was assumed to be unity. Therefore, $ClNO_2$ could be determined by comparing the three instruments and subtracting the byproducts (HONO and NO_2) from the total NO_y. The averaged sensitivity of Cl_2 was 31.5 ± 11.2 Hz/ppt and $ClNO_2$ was 19.7 ± 1.5 Hz/ppt. The 2 sigma detection limits of Cl_2 and $ClNO_2$ were 2.9 and 1.5 ppt, respectively, over 30 min.

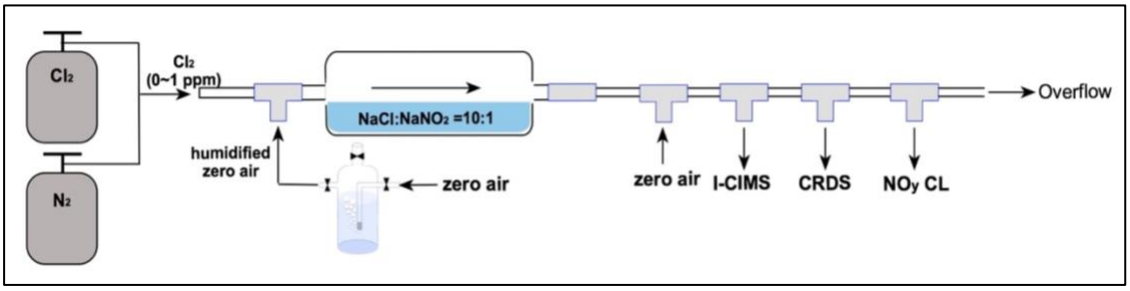

Figure 2.3 Diagram of $ClNO_2$ synthesis process.

During ARAON2018, iodine and bromine reservoir compounds were measured with a CIMS using I^- as a reagent ion. Gas-phase I_2 was detected from charge transfer or clusters in m/z of 254 and 381, respectively (Figure 2.4). The configuration of the inlet was similar to that at the

TRF during the KORUS-AQ campaign, except for the heating of the inlet. A donut shaped aluminum inlet used to avoid wall loss of halogen species (Liao et al., 2011a; Raso et al., 2017). A blower was connected to the stainless steel donut part to draw in ~ 3000 slpm of air. Background was measured every 15 min for 15 min using a glass wool and charcoal scrubber. The CIMS inlet was facing the front of the ship, on the 3rd deck of the R/V ARAON, with a height of ~ 13 meters from sea level. Sampling part was temperature controlled to 25 ºC. Calibration was carried out with permtube as described in Raso et al. (2017). The limit of detection was 0.6 ppt (2σ) over 1 min average.

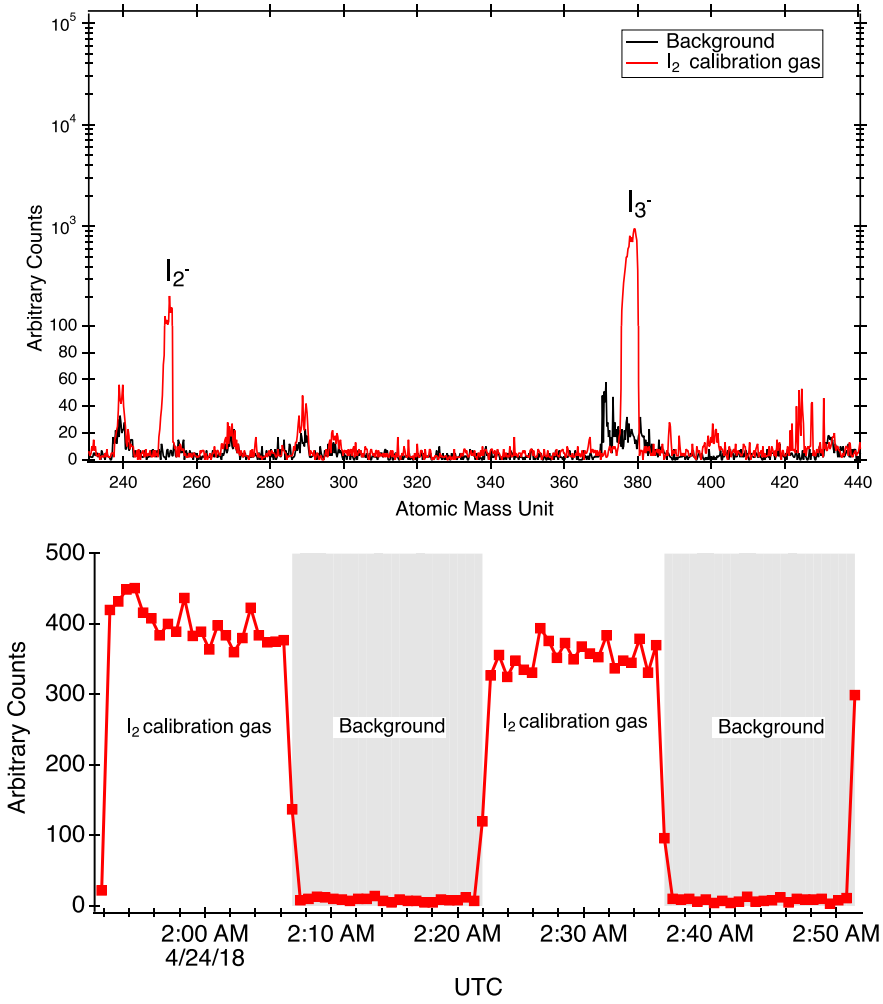

Figure 2.4 CIMS mass spectrum during background and calibration of I_2.

2.2 Box Model Simulations

2.2.1 OH Simulations during GoAmazon2014/5

The Framework for 0-D Atmospheric Modeling (F0AM v3.2) chemical box model was used to evaluate various chemical mechanisms on reproducing OH levels during GoAmazon2014/5. F0AM is a MATLAB (Mathworks®) based zero-dimensional model framework (Wolfe et al., 2016) and has been used in many field studies to explore the oxidation chemistry in the troposphere and compare it to observations (Feiner et al., 2016; Kaiser et al., 2016; Kim et al., 2015a, 2016b). The box model was constrained with a comprehensive set of trace gas and meteorology measurements collected during GoAmazon2014/5 and the analytical techniques used are in Table #. A total of 16 days (i.e., Feb 12-14, 16-19, Mar 5, 9-11, 13-16, 18) were chosen during the campaign based on the availability of data. A full cycle of the model was for 24 hours and each step of the model was constrained with observations of inorganics (i.e., O_3, NO_2, CO), organics (i.e., CH_4, biogenic and anthropogenic non-methane hydrocarbons), and meteorology measured at that time of day with a data frequency of 5 minutes. These constrained parameters were kept constant throughout each step. Interpolation was carried out for missing data or measurements with lower time frequency. Each step of the model was integrated for 5 minutes to give a 24-hour diel cycle of OH. This cycle was repeated to allow for buildup of unmeasured species and the results from the second cycle is reported in this study. Hybrid method was used for calculation of photolysis rate constants (J values) in the model. This method in the F0AM model uses solar spectra from the Tropospheric Ultraviolet Visible radiation model (TUV v5.2) (Madronich and Flocke, 1998) with cross sections and quantum yields from literature. More information on the comparisons on different J deriving methods are described in Wolfe et al. (2016). The J values were scaled to the solar radiation measured during the study. Heterogenous

reactions were all switched off in order to separate the differences in gas chemistry between the mechanisms on simulating OH. Emission, transport, deposition were not considered in the model except for dilution, which were assumed to be 4 day^{-1} as in Kaiser et al., (2016). Background concentration of all the species were assumed to be zero.

Table 2.1 Chemical mechanisms used for box model simulations in the GoAmazon2014/5 study.

Mechanism	Number of Species / Reactions	3D model	Reference
MCM v3.3.1	[a]5832 / 17224		Jenkin et al. (2015)
MOZART_T1	159 / 328	[c]CAM-Chem	[h]Knote et al. (2015)
RCIM	[b]148 / 412	[d]GEOS-Chem	Bates and Jacob (2019)
RACM2	124 / 363	e.g, [e]CMAQ, [f]WRF	Goliff et al. (2013)
CB05	53 /156	e.g, CMAQ, WRF	Yarwood et al. (2005)
CB6r2	77 / 363	[g]CAMx	Ruiz and Yarwood (2013)

[a] Full mechanism. For the subset used in this study, 5254 reactions and 1694 species
[b] Isoprene oxidation mechanism
[c] Community Atmosphere Model with Chemistry (CAM-chem), which is part of the NCAR CESM.
[d] Goddard Earth Observing System (GEOS-Chem)
[e] Community Multiscale Air Quality system (CMAQ)
[f] Weather Research and Forecasting Model (WRF)
[g] Comprehensive Air quality Model with extensions (CAMx)
[h] A preliminary version of the MOZART_T1, with updates from the MOZART-4, described in the study.

Six chemical mechanisms were tested in this study and these are the Master Chemical Mechanism (MCM v3.3.1), Model for Ozone and Related Chemical Tracers (MOZART_T1), Reduced Caltech Isoprene Mechanism (RCIM), Carbon Bond Mechanism (CB05), Regional Atmospheric Chemistry Mechanism (RACM2), and Carbon Bond 6 Mechanism (CB6r2). The total number of species and reactions of each mechanism and their implementation in 3-D model frameworks are summarized in Table 2.1. The box model runs were set up the same for each

mechanism and were constrained with identical trace gas and meteorology parameters. The MCM v3.3.1 is the most explicit mechanism and other mechanisms have relatively less explicit isoprene oxidation scheme with varying degrees and lumping of VOCs for simplification. Appropriate lumping of VOCs were assigned in each mechanism as in Table 2.2. For MOZART_T1 runs, the Box Model Extensions to Kinetic PreProcessor (BOXMOX) was used since the mechanism was not included in the F0AM. BOXMOX is an extension to the Kinetic PreProcessor (Knote et al., 2015) that uses the Rosenbrock solver. Differences from different solvers not tested in this study. The original BOXMOX was modified to emulate the F0AM setup, so that the model can diurnally constrain measured trace gases with constant values throughout each step. The photolysis rate constants and concentration of water vapor (H_2O) were taken from the F0AM results. Comparison between the two box models embedded with the identical MCM 3.3.1 mechanisms showed good agreement, which verifies that they were set up properly (Figure 2.5).

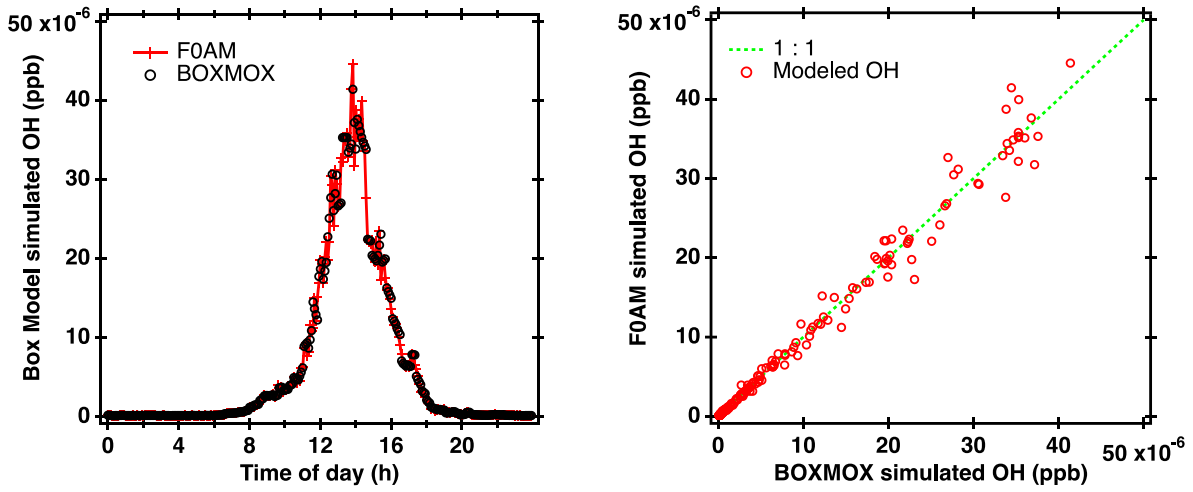

Figure 2.5 Comparison of box model simulated OH between F0AM and BOXMOX. Both model frameworks were constrained with the same meteorology and trace gas measurements from Mar 18th 2014 during the GoAmazon2014/5. For the purpose of comparing the two box models, only O_3, CO, NO_2, CH_4, isoprene, and methanol were constrained in both of the models.

Table 2.2. Summary of the trace gases constrained in the box models and their lumping in each mechanism

Trace Gases Constrained In the Box Model	Nomenclature and Lumping of each Mechanism					
	MCM	**RCIM**	**MOZART_T1**	**RACM2**	**CB05**	**CB6r2**
Ozone	O_3	O_3	O_3	O_3	O_3	O_3
Carbon Monoxide	CO	CO	CO	CO	CO	CO
Nitrogen Dioxide	NO_2	NO_2	NO_2	NO_2	NO_2	NO_2
Methane	CH_4		CH_4	CH_4	CH_4	CH_4
Methyl Vinyl Ketone	MVK	MVK	MVK	MVK	ISPD	ISPD
Methacrolein	MACR	MACR	MACR	MACR	ISPD	ISPD
Isoprene	C_5H_8	ISOP	ISOP	ISO	ISOP	ISOP
Monoterpene	APINENE		APIN	API	TERP	TERP
Ethane	C_2H_6		C_2H_6	ETH	ETHA	ETHA
Propane	C_3H_8		C_3H_8	HC3	1.5 PAR, 1.5 NR	PRPA
n-Butane	NC4H10		BIGALK	HC3	4 PAR	4 PAR
iso-Butane	IC4H10		BIGALK	HC3	4 PAR	4 PAR
n-Pentane	NC5H12		BIGALK	HC5	5 PAR	5 PAR
Iso-Pentane	IC5H12		BIGALK	HC5	5 PAR	5 PAR
n-Hexane	NC6H14		BIGALK	HC5	6 PAR	6 PAR
n-Heptane	NC7H16		BIGALK	HC8	7 PAR	7 PAR
Ethene	C_2H_4		C_2H_4	ETE	ETH	ETH
Propene	C_3H_6		C_3H_6	HC8	1 PAR, 1 OLE	1 PAR, 1 OLE
Toluene	TOLUENE		TOLUENE	TOL	TOL	TOL
Benzene	BENZENE		BENZENE	BEN	1 Par, 5 NR	BENZ
Acetone	CH_3COCH_3		CH_3COCH_3	ACT	3 PAR	ACET
Methanol	CH_3OH	CH_3OH	CH_3OH	MOH	MEOH	MEOH
Acetaldehyde	CH_3CHO		CH_3CHO	ACD	ALD2	ALD2

2.2.2 $ClNO_2$ Simulations during KORUS-AQ 2016

We used F0AM v3.1 for simulating three types of simulations: 1) daytime Cl_2 production, 2) in-situ $ClNO_2$ production in the morning, and 3) testing the impact of measured $ClNO_2$ on the regional tropospheric chemistry. Each step of the model was constrained with the averaged meteorology parameters (e.g., pressure, temperature, relative humidity) and trace gases observed in the two ground sites during KORUS-AQ 2016. The constrained trace gases include $ClNO_2$, Cl_2, O_3, NO, NO_2, CO, CH_4, and 20 non-methane hydrocarbons including 8 alkanes (i.e., ethane, propane, iso-butane, n-butane, iso-pentane, n-pentane, n-hexane, and n-heptane), that have high reaction rate constants with Cl. For simulations presented in Figure 4.6 and 4.7, a constant meteorology and trace gas observation set, collected at the corresponding time point, were constrained throughout the 72-hour simulation. The Cl_2 concentrations at the end of the 72-hour simulation are compared to simultaneously observed mixing ratios of $ClNO_2$ in Figure 4.4. Simulations in Figure 4.12 were similarly constrained as those in Figure 4.6 but allow $ClNO_2$ concentrations to vary with time in order to assess $ClNO_2$ production predicted by the model. For Figure 4.12, the model was constrained with a diurnal variation of the parameters. A full diurnal cycle of the model was for 24 hours consisting a total of 864 steps and each step was integrated for 100 seconds. Each step of the model was constrained with observations measured at that time of day. To assess the impact of $ClNO_2$ chemistry on net O_3 production, all species were constrained except for NO_2 and O_3, which were initialized with observed values and allowed to vary in time. Photolysis rate constants were derived through the hybrid method (Wolfe et al., 2016) in the F0AM box model. This method uses clear sky solar spectra from the tropospheric ultraviolet and visible radiation model (TUV v 5.2) and cross sections and quantum yields complied by the International Union of Pure and Applied Chemistry (IUPAC). To capture the effects of local environments such

as pollution on photolysis rates, the ratio of the measured J_{NO2} to the F0AM modeled J_{NO2} was calculated. This ratio was then applied to other photolysis rate constants calculated in the model. Measured J_{NO2} was taken from the DC-8 actinic flux measurements (Charged-couple device Actinic Flux Spectroradiometer; CAFS) when flying near SMA at altitudes under 1 km. A diurnal cycle was applied to the DC-8 measurement to determine j-values at other times of day. Photolysis rate constants of $ClNO_2$, Cl_2, and $ClONO_2$ were not present in the F0AM model and therefore taken directly from the DC-8 measurements to be used in the model runs in this study. Boundary layer height, emissions, and depositions were not considered in the model.

The Master Chemical Mechanism v3.3.1 (MCM) was taken from http://mcm.leeds.ac.uk/MCM and embedded in the box model. MCM v3.3.1 has a detailed gas photochemistry (i.e., 5832 species and 17224 reactions), including the oxidation of CH_4 and 142 non-methane primary emitted VOCs (Jenkin et al., 2015). Since MCM v3.3.1 only includes Cl reactions with alkane species, additional chlorine chemistry was embedded in the model, similar to what Riedel et al. (2014) reported. This was done by including multiple Cl precursors (e.g., Cl_2, $ClNO_2$, HCl, $ClONO_2$, HOCl) and Cl reactions with non-alkane VOCs, such as alkene, alcohol, aromatics, alkynes, ketones, organic acids and nitrates. All the reactions embedded in the model can be found in the supplementary of Riedel et al. (2014) and Wolfe et al. (2016). Heterogeneous reactions of gas-phase N_2O_5 (i.e., $N_2O_5(g) + Cl^-(aq) \rightarrow ClNO_2(g)$), $ClONO_2$ (i.e., $ClONO_2(g) + Cl^-(aq) + H^+(aq) \rightarrow Cl_2(g) + HNO_3$), and HOCl (i.e., $HOCl(g) + Cl^-(aq) + H^+(aq) \rightarrow Cl_2(g) + H_2O$), a simple first-order reaction was assumed by accounting from γ, ϕ, molecular speed of the gases, and surface area of aerosols. Hygroscopic growth factor was not considered in the model. γ_{N2O5} was calculated from the Bertram and Thornton (2009) study using measured inorganic aerosol composition, temperature, and relative humidity and water content derived from the

thermodynamic model Extended Aerosol Inorganics Model (E-AIMS, (Clegg et al., 1998; Friese and Ebel, 2010)). The average and median γ_{N2O5} values during the whole campaign were both 0.017. This is in the lower range of what has been derived from previous field observations in Asia that ranges from a campaign average of 0.004 to 0.072 (Brown et al., 2016; Tham et al., 2016; Wang et al., 2017a, 2017c; Yun et al., 2018b). γ values of $ClONO_2$ and HOCl were set to 0.06 (Deiber et al., 2004; Hanson and Ravishankara, 1994). The yields (ϕ) of the three heterogeneous reactions were assumed to be 1, therefore the steady state simulations would be an upper-limit of Cl_2 or $ClNO_2$ production. Since we did not have any aerosol size distribution data collected at the ground sites, aerosol surface area was taken from airborne measurements. An averaged value was used from data retrieved below 1 km over the SMA. The airborne data did not show a significant vertical dependence within the daytime boundary layer. Based on this, an average of 78 ± 41 m^2cm^{-3} were estimated from particle sized between 10 nm and 5 μm.

The FLEXible PARTicle dispersion model (FLEXPART v9.1, https://www.flexpart.eu) was used for the air mass source contribution (Figure 4.3) and backward trajectory analysis (Figure 4.14 and 4.16). The backward trajectories reported in our study were initialized 9:00 LST at TRF, following it 24 hours back in time. Only the center of the mass-weighted particles are shown in Figure 4.14 and clusters are included in Figure 4.16. These clusters represent fraction contributions of air masses (Figure 4.16). The trajectories were driven by the National Centers for Environmental Prediction (NCEP) Global Forecast System (GFS) with a 0.25 degree resolution. Influence of air mass originating from the ocean at TRF and OP was calculated every 6 hours following an air mass 5 days back in time. Meteorology was driven by WRF with a 5 km horizontal resolution. Since emissions of CO are very low in the ocean, and assumed to be inert in the model, it was used

as a tracer for contribution of air originating from the ocean within a given air mass at each ground site.

2.3 References

Bates, K. H. and Jacob, D. J.: A new model mechanism for atmospheric oxidation of isoprene: global effects on oxidants, nitrogen oxides, organic products, and secondary organic aerosol, Atmos. Chem. Phys. Discuss., 1–46, doi:10.5194/acp-2019-328, 2019.

Bertram, T. H. and Thornton, J. A.: Toward a general parameterization of N_2O_5 reactivity on aqueous particles: the competing effects of particle liquid water, nitrate and chloride, Atmos. Chem. Phys., 9(21), 8351–8363, doi:10.5194/acp-9-8351-2009, 2009.

Brown, S. S., Dubé, W. P., Tham, Y. J., Zha, Q., Xue, L., Poon, S., Wang, Z., Blake, D. R., Tsui, W., Parrish, D. D. and Wang, T.: Nighttime chemistry at a high altitude site above Hong Kong, J. Geophys. Res. Atmos., (3), 2457–2475, doi:10.1002/2015JD024566, 2016.

Clegg, S. L., Brimblecombe, P. and Wexler, A. S.: Thermodynamic Model of the System H^+–NH_4^+ –SO_4^{2-}–NO_3^-–H_2O at Tropospheric Temperatures, J. Phys. Chem. A, 102(12), 2137–2154, doi:10.1021/jp973042r, 1998.

Deiber, G., George, C., Le Calvé, S., Schweitzer, F. and Mirabel, P.: Uptake study of $ClONO_2$ and $BrONO_2$ by Halide containing droplets, Atmos. Chem. Phys., 4(5), 1291–1299, doi:10.5194/acp-4-1291-2004, 2004.

Feiner, P. A., Brune, W. H., Miller, D. O., Zhang, L., Cohen, R. C., Romer, P. S., Goldstein, A. H., Keutsch, F. N., Skog, K. M., Wennberg, P. O., Nguyen, T. B., Teng, A. P., DeGouw, J., Koss, A., Wild, R. J., Brown, S. S., Guenther, A., Edgerton, E., Baumann, K., Fry, J. L., Feiner, P. A., Brune, W. H., Miller, D. O., Zhang, L., Cohen, R. C., Romer, P. S., Goldstein, A. H., Keutsch, F. N., Skog, K. M., Wennberg, P. O., Nguyen, T. B., Teng, A. P., DeGouw, J., Koss, A., Wild, R. J., Brown, S. S., Guenther, A., Edgerton, E., Baumann, K. and Fry, J. L.: Testing Atmospheric Oxidation in an Alabama Forest, J. Atmos. Sci., 73(12), 4699–4710, doi:10.1175/JAS-D-16-0044.1, 2016.

Friese, E. and Ebel, A.: Temperature Dependent Thermodynamic Model of the System H^+–NH_4^+ –Na^+–SO_4^{2-}–NO_3^-–Cl^-–H_2O., J. Phys. Chem. A, 114, 11595-11631, 2010.

Goliff, W. S., Stockwell, W. R. and Lawson, C. V.: The regional atmospheric chemistry mechanism,version2,Atmos. Environ., 68, 174–185, doi:10.1016/j.atmosenv.2012.11.038, 2013.

Hanson, D. R. and Ravishankara, A. R.: Reactive Uptake of $ClONO_2$ onto Sulfuric Acid Due to Reaction with HCl and H_2O, J. Phy. Chem., 98(22), 5728–5735, doi:10.1021/j100073a026, 1994.

Huey, L. G.: Measurement of trace atmospheric species by chemical ionization mass spectrometry: Speciation of reactive nitrogen and future directions, Mass Spectrom. Rev., 26(2), 166–184, doi:10.1002/mas.20118, 2007.

Huey, L. G., Hanson, D. R. and Howard, C. J.: Reactions of SF_6^- and I^- with atmospheric trace gases, J. Phys. Chem., 99(14), 5001–5008, doi:10.1021/j100014a021, 1995.

Jenkin, M. E., Young, J. C. and Rickard, A. R.: The MCM v3.3.1 degradation scheme for isoprene, Atmos. Chem. Phys., 15(20), 11433–11459, doi:10.5194/acp-15-11433-2015, 2015.

Kaiser, J., Skog, K. M., Baumann, K., Bertman, S. B., Brown, S. B., Brune, W. H., Crounse, J. D., De Gouw, J. A., Edgerton, E. S., Feiner, P. A., Goldstein, A. H., Koss, A., Misztal, P. K., Nguyen, T. B., Olson, K. F., St Clair, J. M., Teng, A. P., Toma, S., Wennberg, P. O., Wild, R. J., Zhang, L. and Keutsch, F. N.: Speciation of OH reactivity above the canopy of an isoprene-dominated forest, Atmos. Chem. Phys., 16(14), 9349–9359, doi:10.5194/acp-16-9349-2016, 2016.

Kim, S., Huey, L. G., Stickel, R. E., Tanner, D. J., Crawford, J. H., Olson, J. R., Chen, G., Brune, W. H., Ren, X., Lesher, R., Wooldridge, P. J., Bertram, T. H., Perring, A., Cohen, R. C., Lefer, B. L., Shetter, R. E., Avery, M., Diskin, G. and Sokolik, I.: Measurement of HO2NO2 in the free troposphere during the Intercontinental Chemical Transport Experiment - North America 2004, J. Geophys. Res. Atmos., 112(12), 1–10, doi:10.1029/2006JD007676, 2007.

Kim, S., Kim, S. Y., Lee, M., Shim, H., Wolfe, G. M., Guenther, A. B., He, A., Hong, Y. and Han, J.: Impact of isoprene and HONO chemistry on ozone and OVOC formation in a semirural South Korean forest, Atmos. Chem. Phys., 15(8), 4357–4371, doi:10.5194/acp-15-4357-2015, 2015a.

Kim, S., Guenther, A., Lefer, B., Flynn, J., Griffin, R., Rutter, A. P., Gong, L. and Cevik, B. K.: Potential role of stabilized criegee radicals in sulfuric acid production in a high biogenic VOC environment, Environ. Sci. Technol., 49(6), 3383–3391, doi:10.1021/es505793t, 2015b.

Kim, S., Sanchez, D., Wang, M., Seco, R., Jeong, D., Hughes, S., Barletta, B., Blake, D. R., Jung, J., Kim, D., Lee, G., Lee, M., Ahn, J., Lee, S. D., Cho, G., Sung, M. Y., Lee, Y. H., Kim, D. B., Kim, Y., Woo, J. H., Jo, D., Park, R., Park, J. H., Hong, Y. D. and Hong, J. H.: OH reactivity in urban and suburban regions in Seoul, South Korea-an East Asian megacity in a rapid transition, Faraday Discuss., 189, 231–251, doi:10.1039/c5fd00230c, 2016.

Knote, C., Tuccella, P., Curci, G., Emmons, L., Orlando, J. J., Madronich, S., Baró, R., Jiménez-Guerrero, P., Luecken, D., Hogrefe, C., Forkel, R., Werhahn, J., Hirtl, M., Pérez, J. L., San José, R., Giordano, L., Brunner, D., Yahya, K. and Zhang, Y.: Influence of the choice of gas-phase mechanism on predictions of key gaseous pollutants during the AQMEII phase-2 intercomparison, Atmos. Environ., 115, 553–568, doi:10.1016/j.atmosenv.2014.11.066, 2015.

Kürten, A., Rondo, L., Ehrhart, S. and Curtius, J.: Performance of a corona ion source for measurement of sulfuric acid by chemical ionization mass spectrometry, Atmos. Meas. Tech., 4(3), 437–443, doi:10.5194/amt-4-437-2011, 2011.

Liao, J., Sihler, H., Huey, L. G., Neuman, J. A., Tanner, D. J., Friess, U., Platt, U., Flocke, F. M., Orlando, J. J., Shepson, P. B., Beine, H. J., Weinheimer, A. J., Sjostedt, S. J., Nowak, J. B., Knapp, D. J., Staebler, R. M., Zheng, W., Sander, R., Hall, S. R. and Ullmann, K.: A comparison of Arctic BrO measurements by chemical ionization mass spectrometry and long path-differential optical absorption spectroscopy, J. Geophys. Res. Atmos., 116(1), 1–14, doi:10.1029/2010JD014788, 2011a.

Liao, J., Huey, L. G., Tanner, D. J., Brough, N., Brooks, S., Dibb, J. E., Stutz, J., Thomas, J. L., Lefer, B., Haman, C. and Gorham, K.: Observations of hydroxyl and peroxy radicals and the impact of BrO at Summit, Greenland in 2007 and 2008, Atmos. Chem. Phys., 11(16), 8577–8591, doi:10.5194/acp-11-8577-2011, 2011b.

Liao, J., Huey, L. G., Tanner, D. J., Flocke, F. M., Orlando, J. J., Neuman, J. A., Nowak, J. B., Weinheimer, A. J., Hall, S. R., Smith, J. N., Fried, A., Staebler, R. M., Wang, Y., Koo, J.

H., Cantrell, C. A., Weibring, P., Walega, J., Knapp, D. J., Shepson, P. B. and Stephens, C. R.: Observations of inorganic bromine (HOBr, BrO, and Br_2) speciation at Barrow, Alaska, in spring 2009, J. Geophys. Res. Atmos., 117(6), 1–11, doi:10.1029/2011JD016641, 2012.

Liao, J., Huey, L. G., Liu, Z., Tanner, D. J., Cantrell, C. A., Orlando, J. J., Flocke, F. M., Shepson, P. B., Weinheimer, A. J., Hall, S. R., Ullmann, K., Beine, H. J., Wang, Y., Ingall, E. D., Stephens, C. R., Hornbrook, R. S., Apel, E. C., Riemer, D., Fried, A., Mauldin, R. L., Smith, J. N., Staebler, R. M., Neuman, J. A. and Nowak, J. B.: High levels of molecular chlorine in the Arctic atmosphere, Nat. Geosci., 7(2), 91–94, doi:10.1038/ngeo2046, 2014.

Liu, X., Qu, H., Huey, L. G., Wang, Y., Sjostedt, S., Zeng, L., Lu, K., Wu, Y., Hu, M., Shao, M., Zhu, T. and Zhang, Y.: High Levels of Daytime Molecular Chlorine and Nitryl Chloride at a Rural Site on the North China Plain, Environ. Sci. Technol., 51(17), 9588–9595, doi:10.1021/acs.est.7b03039, 2017.

Madronich, S. and Flocke, S.: Handbook of Environmental Chemistry, in Handbook of Environmental Chemistry, pp. 1–26, Springer_Verlag, Heidelberg., 1998.

Mauldin, R. L., Kosciuch, E., Henry, B., Eisele, F. L., Shetter, R., Lefer, B., Chen, G., Davis, D., Huey, L. G. and Tanner, D.: Measurements of OH, HO_2+RO_2,H_2SO_4, and MSA at the South Pole during ISCAT 2000, Adv. Hortic. Sci., 24(1), 43–52, doi:10.1016/j.atmosenv.2004.06.031, 2010.

Raso, A. R. W., Custard, K. D., May, N. W., Tanner, D., Newburn, M. K., Walker, L., Moore, R. J., Huey, L. G., Alexander, L., Shepson, P. B. and Pratt, K. A.: Active molecular iodine photochemistry in the Arctic, Proc. Natl. Acad. Sci., 114(38), 10053–10058, doi:10.1073/pnas.1702803114, 2017.

Riedel, T. P., Bertram, T. H., Crisp, T. A., Williams, E. J., Lerner, B. M., Vlasenko, A., Li, S. M., Gilman, J., De Gouw, J., Bon, D. M., Wagner, N. L., Brown, S. S. and Thornton, J. A.: Nitryl chloride and molecular chlorine in the coastal marine boundary layer, Environ. Sci. Technol., 46(19), 10463–10470, doi:10.1021/es204632r, 2012.

Riedel, T. P., Wolfe, G. M., Danas, K. T., Gilman, J. B., Kuster, W. C., Bon, D. M., Vlasenko, A., Williams, E. J., Lerner, B. M., Veres, P. R., Roberts, J. M., Holloway, J. S., Lefer, B., Brown, S. S. and Thornton, J. A.: An mcm modeling study of nitryl chloride ($ClNO_2$) impacts on oxidation, ozone production and nitrogen oxide partitioning in polluted continental outflow, Atmos. Chem. Phys., 14(8), 3789–3800, doi:10.5194/acp-14-3789-2014, 2014.

Ruiz, L. H. and Yarwood, G.: Interactions between Organic Aerosol and NO_y : Influence on Oxidant Production. Prepared for the Texas AQRP (Project 12-012)., 1–58, 2013.

Sanchez, D., Jeong, D., Seco, R., Wrangham, I., Jeong-Hoo, P., Brune, W. H., Koss, A., Gilman, J., De Gouw, J., Misztal, P., Goldstein, A. H., Baumann, K., Wennberg, P. O., Keutsch, F. N., Guenther, A. and Kim, S.: Intercomparison of OH concentrations and OH reactivity measurements in a high isoprene and moderate NO environment during the Southern Oxidants and Aerosol Study (SOAS), Atmos. Environ., 174, 227-236, 2018.

Sjostedt, S. J., Huey, L. G., Tanner, D. J., Peischl, J., Chen, G., Dibb, J. E., Lefer, B., Hutterli, M. A., Beyersdorf, A. J., Blake, N. J., Blake, D. R., Sueper, D., Ryerson, T., Burkhart, J. and Stohl, A.: Observations of hydroxyl and the sum of peroxy radicals at Summit, Greenland during summer 2003, Atmos. Environ., 41(24), 5122–5137, doi:10.1016/j.atmosenv.2006.06.065, 2007.

Slusher, D. L., Huey, L. G., Tanner, D. J., Flocke, F. M. and Roberts, J. M.: A thermal dissociation - Chemical ionization mass spectrometry (TD-CIMS) technique for the simultaneous measurement of peroxyacyl nitrates and dinitrogen pentoxide, J. Geophys. Res. D Atmos., 109(19), 1–13, doi:10.1029/2004JD004670, 2004.

Tanner, D. J., Jefferson, A. and Eisele, F. L.: Selected Ion Chemical Ionization Mass Spectrometric Measurement of OH, J. Geophys. Res., 102(D5), 6415–6425, doi:Doi 10.1029/96jd03919, 1997.

Thaler, R. D., Mielke, L. H. and Osthoff, H. D.: Quantification of nitryl chloride at part per trillion mixing ratios by thermal dissociation cavity ring-down spectroscopy, Anal. Chem., 83(7), 2761–2766, doi:10.1021/ac200055z, 2011.

Tham, Y. J., Wang, Z., Li, Q., Yun, H., Wang, W., Wang, X., Xue, L., Lu, K., Ma, N., Bohn, B., Li, X., Kecorius, S., Größ, J., Shao, M., Wiedensohler, A., Zhang, Y. and Wang, T.: Significant concentrations of nitryl chloride sustained in the morning: Investigations of the causes and impacts on ozone production in a polluted region of northern China, Atmos. Chem. Phys., 16(23), 14959–14977, doi:10.5194/acp-16-14959-2016, 2016.

Thornton, J. A., Kercher, J. P., Riedel, T. P., Wagner, N. L., Cozic, J., Holloway, J. S., Dubé, W. P., Wolfe, G. M., Quinn, P. K., Middlebrook, A. M., Alexander, B. and Brown, S. S.: A large atomic chlorine source inferred from mid-continental reactive nitrogen chemistry, Nature, 464(7286), 271–274, doi:10.1038/nature08905, 2010.

Wang, H., Lu, K., Chen, X., Zhu, Q., Chen, Q., Guo, S., Jiang, M., Li, X., Shang, D., Tan, Z., Wu, Y., Wu, Z., Zou, Q., Zheng, Y., Zeng, L., Zhu, T., Hu, M. and Zhang, Y.: High N2O5Concentrations Observed in Urban Beijing: Implications of a Large Nitrate Formation Pathway, Environ. Sci. Technol. Lett., 4(10), 416–420, doi:10.1021/acs.estlett.7b00341, 2017a.

Wang, Z., Wang, W., Tham, Y. J., Li, Q., Wang, H., Wen, L., Wang, X. and Wang, T.: Fast heterogeneous N_2O_5 uptake and $ClNO_2$ production in power plant and industrial plumes observed in the nocturnal residual layer over the North China Plain, Atmos. Chem. Phys, 175194(3), 12361–12378, doi:10.5194/acp-17-12361-2017, 2017b.

Williams, E. ., Baumann, K., Roberts, J. M., Bertman, S. B., Norton, R. B., Fehsenfeld, C., Springston, S. R., Nunnermacker, L. J., Newman, L., Olszyna, K., Meagher, J., Hartsell, B., Edgerton, E., Pearson, J. R. and Rodgers, M. O.: Intercomparison of ground-based NO_y measurement techniques, J. Geophys. Res., 103(D17), 22261–22280, 1998.

Wolfe, G. M., Marvin, M. R., Roberts, S. J., Travis, K. R. and Liao, J.: The framework for 0-D atmospheric modeling (F0AM) v3.1, Geosci. Model Dev., 9(9), 3309–3319, doi:10.5194/gmd-9-3309-2016, 2016.

Yarwood, G., Whitten, G. and Rao, S.: Updates to the Carbon Bond 4 photochemical mechanism, Environ. Int. Corp [online] Available from: http://www.ladco.org/reports/rpo/modeling/camx_cb4.pdf, 2005.

Yun, H., Wang, W., Wang, T., Xia, M., Yu, C., Wang, Z., Poon, S. C. N., Yue, D. and Zhou, Y.: Nitrate formation from heterogeneous uptake of dinitrogen pentoxide during a severe winter haze in southern China, Atmos. Chem. Phys. Discuss., (2), 1–23, doi:10.5194/acp-2018-698, 2018.

CHAPTER 3

OH OBSERVATIONS DURING GOAMAZON2014/5

3.1 Introduction

Since Levy (1971) first postulated the importance of hydroxyl radicals (OH) in driving the photochemistry of the troposphere, numerous modeling, laboratory, and field studies have explored its roles in determining the chemical lifetimes of reactive trace gases and producing photochemical byproducts such as ozone (O_3) and secondary organic aerosols (SOA). Tropospheric OH is primarily produced through O_3 photolysis and the following reaction of O (^1D) and water vapor (H_2O). The OH level is sustained by recycling processes through NO oxidation to NO_2 by organic peroxy (RO_2) and hydroperoxy (HO_2) radicals generated from the oxidation of volatile organic compounds (VOCs) (R 3.1 - 3.3). Cross ($HO_2 + RO_2$) or self-reactions ($HO_2 + HO_2$ or $RO_2 + RO_2$) between peroxy radicals compete with R3.2 and R3.3 to produce more stable compounds like organic hydroxy peroxides. At low NO_x and high VOC environments, re-production of OH can be suppressed by these chain terminating reactions. Therefore early studies of conventional chemistry speculated OH levels to be depleted in remote tropical rain forests (Jacob and Wofsy, 1988; Logan et al., 1981).

$$RH + OH + O_2 \rightarrow RO_2 + H_2O \qquad \text{R3.1}$$

$$RO_2 + NO + O_2 \rightarrow HO_2 + RCHO + NO_2 \qquad \text{R3.2}$$

$$HO_2 + NO \rightarrow OH + NO_2 \qquad \text{R3.3}$$

However, field observations in forested regions have reported higher than expected OH concentrations, contrary to the expected levels from conventional chemistry (Carslaw et al., 2001; Hofzumahaus et al., 2009; Lelieveld et al., 2008; Pugh et al., 2010; Ren et al., 2008; Stone et al., 2010; Tan et al., 2001; Thornton et al., 2002; Whalley et al., 2011). In an airborne study in the tropical forests in Suriname, Lelieveld et al. (2008) measured up to ~ 10 times higher than expected OH in the boundary layer. During the Photochemistry, Emissions, and Transport (PROPHET) campaign in a deciduous forest in Michigan, observed OH was ~ 3 times higher than model simulations while HO_2 showed reasonable agreement (Tan et al., 2001). At an isoprene dominated rural region in Pearl River Delta, China, measured OH overestimated the conventional chemistry by ~ 5 times while HO_2 agreed within uncertainty (Hofzumahaus et al., 2009).

Early studies proposed hypothetical OH recycling pathways to reconcile the observed OH levels (Archibald et al., 2010; Butler et al., 2008; Hofzumahaus et al., 2009; Kubistin et al., 2010; Taraborrelli et al., 2009). For example, Hofzumahaus et al. (2009) were able to reconcile the measured OH levels by forcing a hypothetical compound 'X' that is equivalent to 0.85 of NO in their model simulations. Later on, noble chemical reaction mechanisms such as isoprene radical isomerization processes that lead to series of reactions reproducing OH (Asatryan et al., 2010; Crounse et al., 2011; Peeters et al., 2009, 2014; Peeters and Müller, 2010; Wolfe et al., 2012) were proposed. At the same time, potential artifacts have been explored of the OH background determining method used in some of the previous OH observation studies in high BVOC regions, with the laser induced fluorescence (LIF) (Feiner et al., 2016; Hens et al., 2014; Mao et al., 2012; Novelli et al., 2014). During the Biosphere Effects on Aerosols and Photochemistry Experiment II (BEARPEX09), Mao et al. (2012) compared the conventional procedure, which shifts the wavelength of the laser for background OH quantification, with the modified one that adds

hexafluoropropylene (C_3F_6) or propane in the inlet to chemically remove OH. In the conventional method, background OH is quantified by comparing the fluorescence at 308 nm to another wavelength at which OH absorption is negligible. However, this can result in interference from additional OH generation within the detection cell. The level of interferences from using the LIF method vary depending on the configuration of the inlet. On the other hand, the chemical removal method adds propane or hexafluoropropylene in the inlet, and therefore scrubs any externally generated OH. According to Mao et al. (2012) this chemical OH removal technique resulted in up to four-fold lower observed OH concentrations than the original method. By applying this chemical removal method, the authors were able to account for the OH levels measured at the Blodgett Forest Research Station in the California Sierra Nevada Mountains, using box model calculations embedded with the Regional Atmospheric Chemistry Mechanism (RACM2) updated with additional isoprene hydroxyperoxy radical isomerizations suggested in previous studies (Crounse et al., 2011; Peeters et al., 2009). Novelli et al. (2014) also implemented this chemical scavenging method in their LIF-FAGE system in three different forested areas in Spain, Finland, and Germany. The authors assigned 30 – 80 % of additional OH can be produced within the instrument from recycling processes. In the same study, intercomparisons of measured OH between the modified LIF and the Chemical Ionization Mass Spectrometer (CIMS), which also uses propane as a scavenger, showed good agreement between the different techniques. During the Southern Oxidant and Aerosol Study (SOAS), Feiner et al., (2016) conducted HO_x measurements with their Penn State's Ground-based Tropospheric Hydrogen Oxides Sensor (GTHOS) system using LIF, at a forested region near Brent, Alabama. Compared to the non-scavenging method, their LIF system using C_3F_6 measured ~3 times less OH during the campaign.

Recognizing the need to update the existing chemical mechanisms, extensive improvements have been made (Bates and Jacob, 2019; Jenkin et al., 2015; Knote et al., 2014; Saunders et al., 2003; Wennberg et al., 2018). Near-explicit chemical mechanisms like the Master Chemical Mechanism (MCM) (Jenkin et al., 2015; Saunders et al., 1997, 2003) and the recently reported mechanism by Wennberg et al. (2018) include the most recent laboratory results of detailed isoprene oxidation and the subsequent reaction of hydroxy peroxy radicals (i.e., ISOPOO) with other oxidants (NO, HO_2, RO_2) and its isomerization reactions. Feiner et al. (2016) showed that box model simulations embedded with the most recent MCM v3.3.1 were able to reproduce OH observations measured with the LIF with the chemical background method in an Alabama forest. However, for practical purposes, chemical mechanisms need to be more condensed to be used in global chemical transport models so that the host model framework can run efficiently (Goliff et al., 2013). These are done by lumping organic compounds with comparable structure or reactivity. The simplifications need to be carried out to the extent that it is still representative the environment of interest. For example, Bates and Jacob (2019) reduced the number of reactions and species from the initial explicit mechanism reported by Wennberg et al (2018). Simplification was made of the mechanism from 810 reactions with 385 species to 345 reactions and 108 species by lumping isoprene oxidation products (i.e., ISOPOO) and its consecutive reactions. Their Reduced Caltech Isoprene Mechanism (RCIM), agreed well with the MCM v3.3.1. However, the choice of the type of these condensed photochemical mechanism in a model should be taken cautiously since it can derive dissimilar results (Chen et al., 2010; Dodge, 2000; Gross and Stockwell, 2003; Jimenez et al., 2003; Knote et al., 2015; Kuhn et al., 1998). For example, Knote et al. (2015) compared gas-phase reactions of seven chemical mechanisms used in chemical transport models. The model was constrained with the same emission and meteorology parameters,

and the choice of different chemical mechanisms resulted up to 40% and 25 % of difference in simulated OH and HO_2 respectively. The authors concluded that the discrepancies were mainly coming from differences in oxidation reactions of BVOC and nighttime chemistry. In order to have a better understanding of the forested environment, it is crucial to test out both near-explicit and condensed mechanisms and examine whether they reproduce the radical levels reasonably.

Here, we present OH observation results measured by a CIMS at a site ~ 60 km to the west of Manaus, Brazil as part of the Green Ocean Amazon (GoAmazon2014/5) research initiative (Martin et al., 2017). This is the first OH dataset measured by a CIMS in a rain forest environment. A multi-platform field campaign was conducted in 2014 in two Intensive Operating Period (IOPs) – wet (I) and dry (II) seasons. The wet season (Feb 1 – Mar 30) represents a pristine condition with high wet deposition of aerosols while the dry season (Aug15 – Oct 15) is relatively polluted with increased biomass burning. Further description on different IOPs is described in Martin et al., (2016). We only present the data from the first IOP conducted. The T3 ground observation site served as a supersite to characterize trace gas and aerosol physical and chemical properties with frequent overpasses of the DOE G-1 research aircraft. The location of the T3 site was carefully selected to sample a wide spectrum of anthropogenic influences in the pristine background as Manaus, the largest city in the state of Amazonas, is ~ 60 km away and air pollution plumes were transported to the site at times during the field observation period. In order to test out our current understanding of the tropospheric photochemistry, measured OH levels are compared to observation constrained box model simulations embedded with the explicit MCM 3.3.1 and with gas-phase mechanisms used in global models.

3.2 Results and Discussion

3.2.1 Observation Results during GoAmazon2014/5

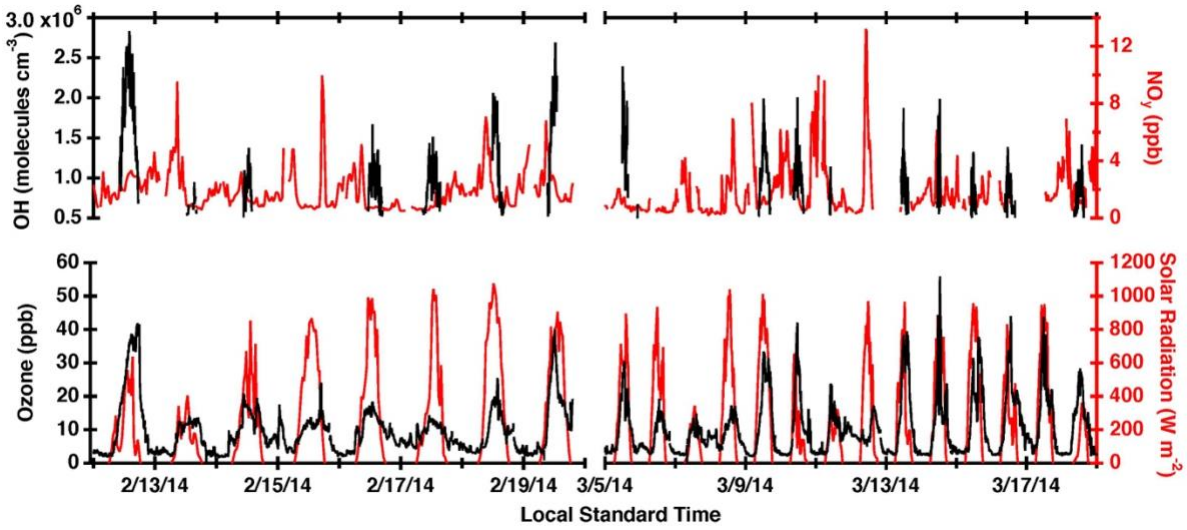

Figure 3.1 Temporal variation of OH, NO_y, O_3, and solar radiation during the GoAmazon2014/5. The frequency of the data is 5 min, 5 min, 30 min, and 30 min for OH, O_3, NO_y and solar radiation, respectively. Only the 16 days chosen for this study are presented for OH observations.

Data collected during the wet-season (IOP I) of the campaign was used and the days with complete overcast or precipitation were excluded from the discussion which left us with 16 days of dataset (February 12 – 14, 16 – 19, March 5, 9 – 11, 13 – 16, 18). A summary of the measured trace gases and meteorology parameters used in this study are in Table 3.1. For alkanes and alkenes, used in this study, the values were taken from Zimmerman et al. (1988), where they measured VOCs in a tropical forest near Manaus. Figure 3.1 shows temporal variations of measured OH, NO_y, O_3, and solar radiation. Averaged over the selected 16 days, the midday (11:00 – 15:00 local standard time) mean and standard deviation for OH, NO_y and O_3 were $1.2 \times 10^6 \pm 0.5\times 10^6$ molecules cm^{-3}, 1.5 ± 0.8 ppb, 21.9 ± 8.8 ppb, respectively. Bakwin et al. (1990) reported background conditions of NO_y in the Amazon rainforest during the wet season to be below 1 ppb based on the probability distribution of data collected from the whole observation period. As

shown in the variation of NO_y, enhanced levels of NO_y were frequently observed, possibly from the effect of plumes originating from Manaus. Diurnal averages and standard deviations for the 16 days of measured isoprene, total MVK and MACR, monoterpene, toluene, benzene, and CO are shown in Figure 3.2. BVOC levels show that the observation site was an isoprene dominant forest.

Table 3.1. Summary of trace gases and meteorological conditions used in this study measured during the GoAmazon2014/5 campaign and the analytical techniques used.

Trace Gas and Meteorology	Techniques	Manufacturer/Reference
Carbon monoxide (CO)	Cavity Ring Down Spectroscopy	Los Gatos Research, Inc
Nitrogen oxides (NO_x and NO_y)	Chemiluminescence	Thermo Scientific 42i-TL
Ozone (O_3)	UV photometry	Thermo Scientific 49i
Acetone (CH_3COCH_3) Benzene (C_6H_6) Toluene ($C_6H_5(CH_3)$) Isoprene (C_5H_8) Monoterpenes [a]Methyl vinyl ketone (MVK) [a]Methacrolein (MACR)	Proton Transfer Reaction-Time of Flight-Mass Spectrometer (PTR-TOF-MS)	Graus et al. (2010) Jordan et al. (2009)
Ethane (C_2H_6) Propane(C_3H_8) n-Butane (n-C_4H_{10}) i-Butane (i-C_4H_{10}) n-Hexane (n-C_6H_{14}) n-Heptane (C_7H_{16}) Propene(C_4H_6)	Gas Chromatography-Flame Ionization Detection (GC-FID)	Greenberg and Zimmerman (1984)
Radiation	Shortwave Array Spectroradiometer	Flynn (2016)
Ambient Temperature Relative Humidity	Aerosol Observing System Surface Meteorology (AOSMET)	Chen et al. (2015)

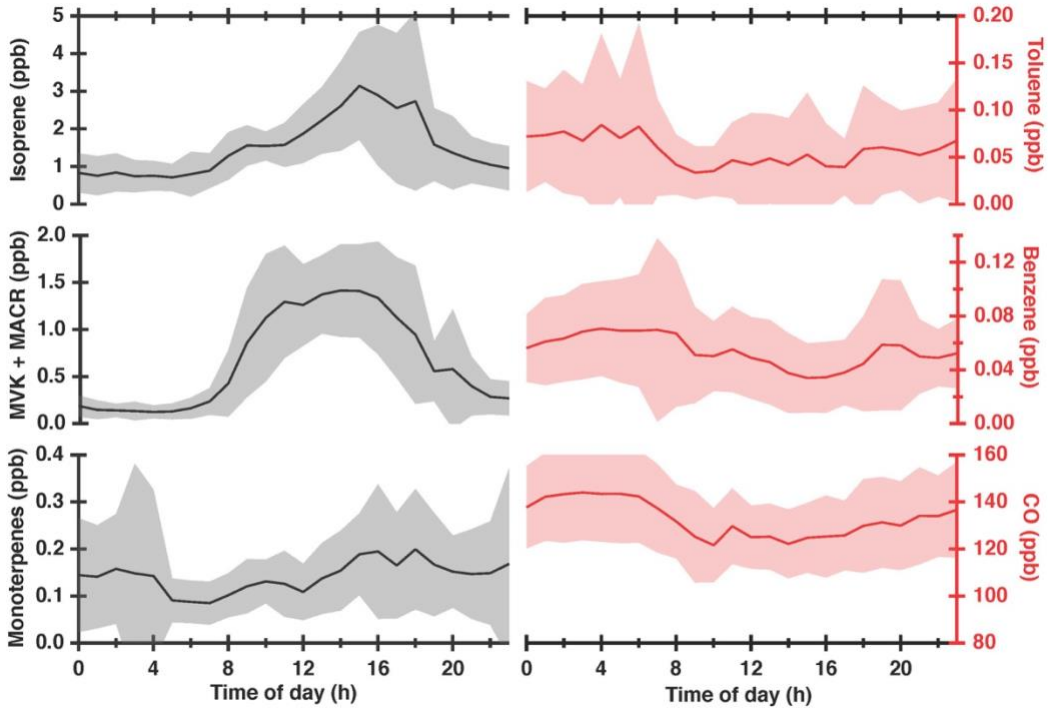

Figure 3.2 Diurnal variation of measured trace gases averaged over the 16 days selected for this study. Shaded areas are standard deviations of the averages.

The observed midday maximum OH level is significantly lower than most of the previous observations reported in high C_5H_8 and low NO_x environments. For comparison, the observed averages of OH and other trace gases from previous reports are shown in Table 3.2. The environmental characteristics of the measurement sites presented in Table 3.2 can be categorized into two. The campaigns shown in red font (GABRIEL, PROPHET, OP3) reported substantially higher OH than others indicated in blue (SOAS and BEARPEX09). For the GABRIEL, PROPHET, and OP3 campaign, LIF technique without the chemical removal method was used for OH quantification. Both BEARPEX 09 and SOAS campaigns were conducted by the Brune group at Pennsylvania State University, where they applied a OH chemical removal background characterization method in their LIF technique (Mao et al., 2012). Despite the substantial geographical distance among the field sites described in Table 3.2, there are two similarities. First,

C_5H_8 is the dominant OH sink among the quantified trace gases. Second, NO is below 100 ppt and close to 50 ppt, that can be categorized as low-to-moderate NO regime. For the BEARPEX 09 site, the local emissions were mostly 2-methyl-3-buten-2-ol (MBO) and monoterpenes but plumes of significant levels of isoprene were transported from an oak woodland area nearby in the afternoon (Mao et al., 2012). On the other hand, the extent of anthropogenic influence were different as can be seen in the level of CO. For example, the CO levels during the GoAmazon2014/5 were less than the BEARPEX09 and SOAS, which had similar photochemical environments in terms of the level of OH. During the SOAS campaign, the observation site was infrequently affected by nearby cities, powerplants and local transportation. The BEARPEX measurement site was influenced by anthropogenic plumes from the Sacramento area, ~75 km away from the site, in the late afternoon.

Table 3.2 A summary of OH and other trace gas measurements from various field campaigns conducted in high isoprene and low NO environments. The averaged dataset from GABRIEL, PROPHET, OP3, and BEARPEX09 are taken from Rohrer et al. (2014)**. The ones in red are observations that reported relatively high OH compared to the blue ones.**

	[a]GABRIEL (Oct. 2005)	[b]PROPHET (Aug. 1998)	[c]OP3 (Apr-May 2008)	[d]BEARPEX 09 (Jun-Jul 2009)	[e]SOAS (Jun-Jul 2013)	GoAmazon (Feb-Mar 2014)
Averaged Time (LST)	14:00 - 17:00	10:00 - 11:00	11:00 - 12:00	09:00 - 15:00	10:00 - 15:00	10:00 - 15:00
CO (ppb)	122	260	111	130	134	121
OH (molec cm^{-3})	4.4×10^6	3.6×10^6	2.2×10^6	1.3×10^6	1.2×10^6	9.8×10^5
Isoprene (ppb)	4.3	1.86	2	1.7	5.14	2.25
MVK+MACR (ppb)	1.6	0.34	0.21	0.79	1.41	1.34
NO (ppt)	13	80	40	74	42	N/A
NO_2 (ppt)		456	130	200	293	N/A
O_3 (ppb)	17	41	12.5	54	37	21
OH reactivity (s^{-1})	19	11	19.8	18.5	21.1	N/A

[a] Tropical forest in Suriname, Guyana and Guyane (Lelieveld et al., 2008)
[b] Deciduous forest in northern Michigan (Tan et al., 2001)
[c] Danum Valley in the Sabah region of a Borneo forest (Whalley et al., 2011)
[d] Ponderosa pine plantation in the California Sierra Nevada Mountains (Mao et al., 2012)
[e] Talladega National Forest in Brent, Alabama (Feiner et al., 2016)

3.2.2 Box model simulations of OH

With the observational dataset collected during GoAmazon2014/5, box model simulations were run for 6 different chemical mechanisms summarized in Table 2.1. The MCM v3.3.1 is a near explicit mechanism and others are condensed mechanisms that are used in chemical transport models. In these condensed mechanisms, reactions and VOCs are simplified through lumping of compounds with similar structure and reactivity defined by each mechanism. Box model simulations were constrained with observations and lumping of VOCs were carried out according to Table 2.2. The identical 16 days, used for averaging diurnal variations of trace gases in Figure 3.2, were selected for running the model simulations. Figure 3.3 shows the model simulation results along with the OH observation at the corresponding day. Mao et al. (2012) measured OH with the LIF using the chemical removal method at a ponderosa pine forest in Sierra Nevada. This site was dominated by local MBO emissions with isoprene influence from transport. The authors were able to reconcile the observed levels of OH through box model simulations embedded with the MCM chemistry. Another study, which used a similar method, showed good agreement between model and observations in the Talladega National Forest in Brent, Alabama (Feiner et al., 2016). Our study confirms that good agreement between modeled and observed OH was also achieved in a tropical rainforest environment during GoAmazon2014/5. In most of the days, all five chemical mechanisms (MCM v3.3.1, RACM2, CB05, CB6r2, and MOZART_T1) generally agreed well with the OH measurements. Among the total 16 days presented in this study, 12 days (February 12^{th}, 13^{th}, 14^{th}, 16^{th}, 17^{th}, 18^{th}, 19^{th}, March 5^{th}, 9^{th}, 11^{th}, 13^{th}, and 16^{th}) showed reasonable agreement to OH observations in most times of the day. The agreement between the model simulations and the observations were the highest in midday with more discrepancies during earlier or later in the day. For March 10^{th} and 18^{th}, the 5 model simulations underestimated the

observations up to 5-fold. For March 14th and 15th, all mechanisms overestimated the measurements up to 3-fold.

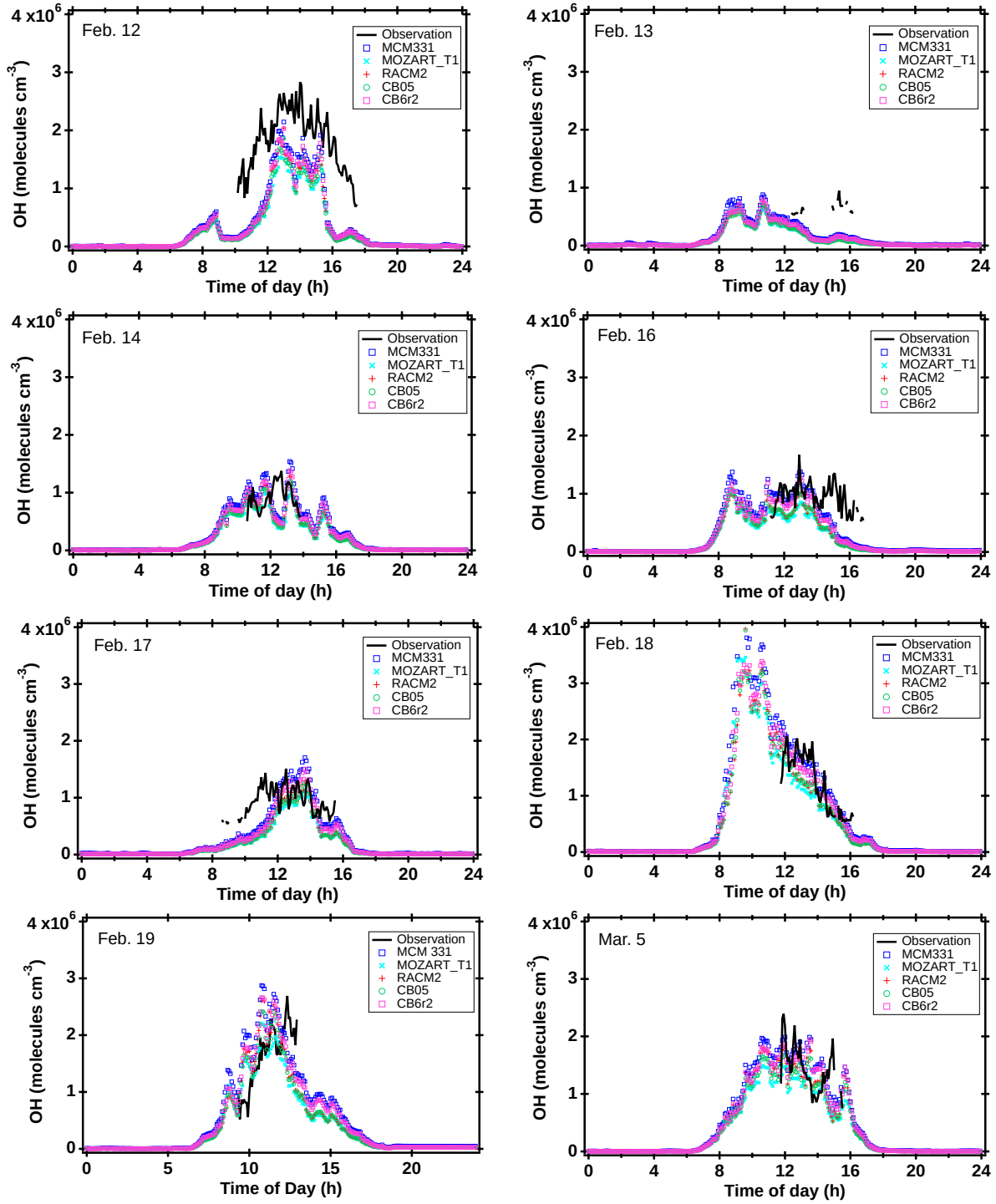

Figure 3.3 (continued on next page)

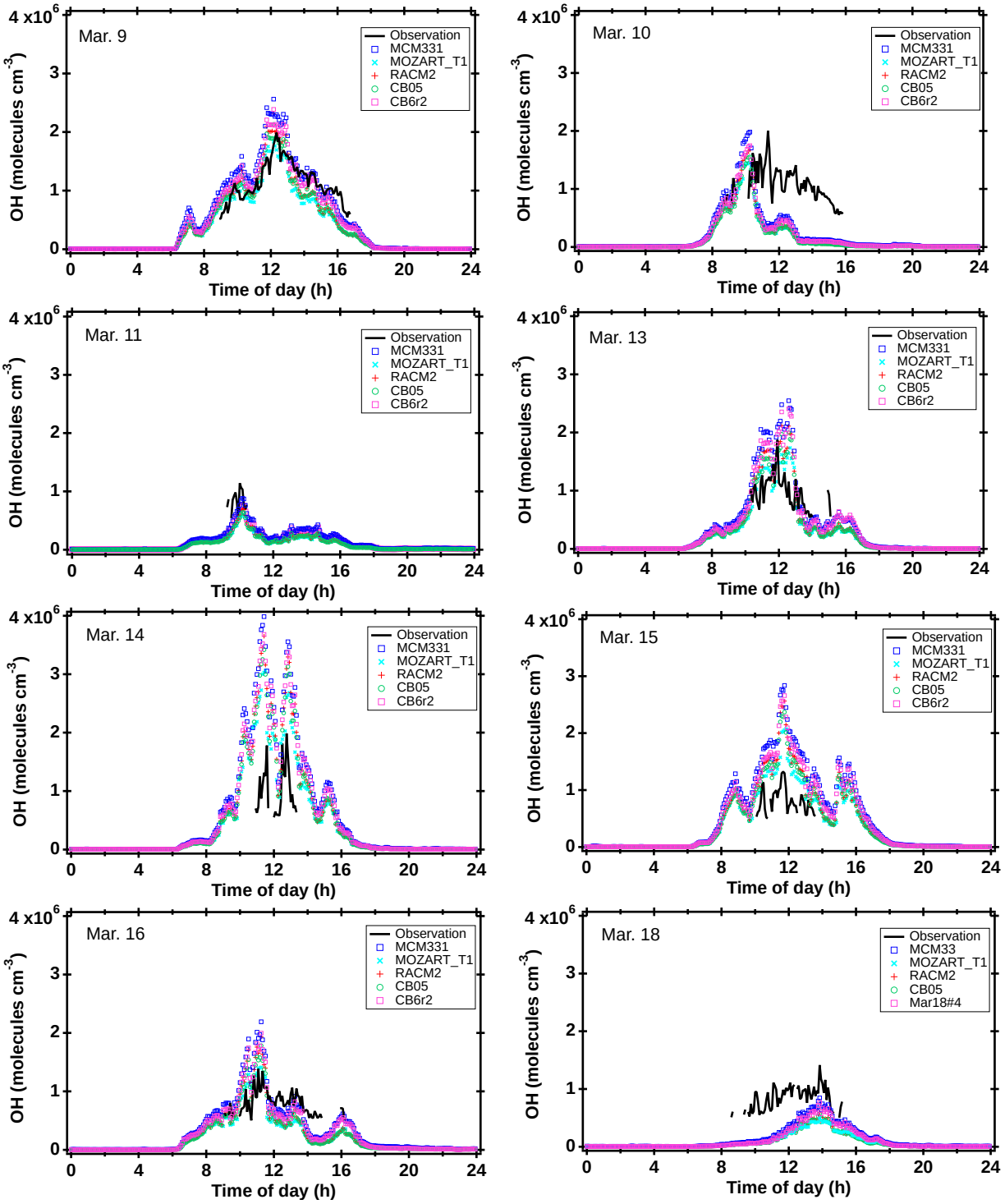

Figure 3.3 Comparison of OH observations by the CIMS during the GoAmazon2014/5 campaign to box model simulations of OH embedded with 6 different chemical mechanisms. The frequency of both OH observations and simulations is 5 min and grey shades are 40 % uncertainty of the CIMS measurement.

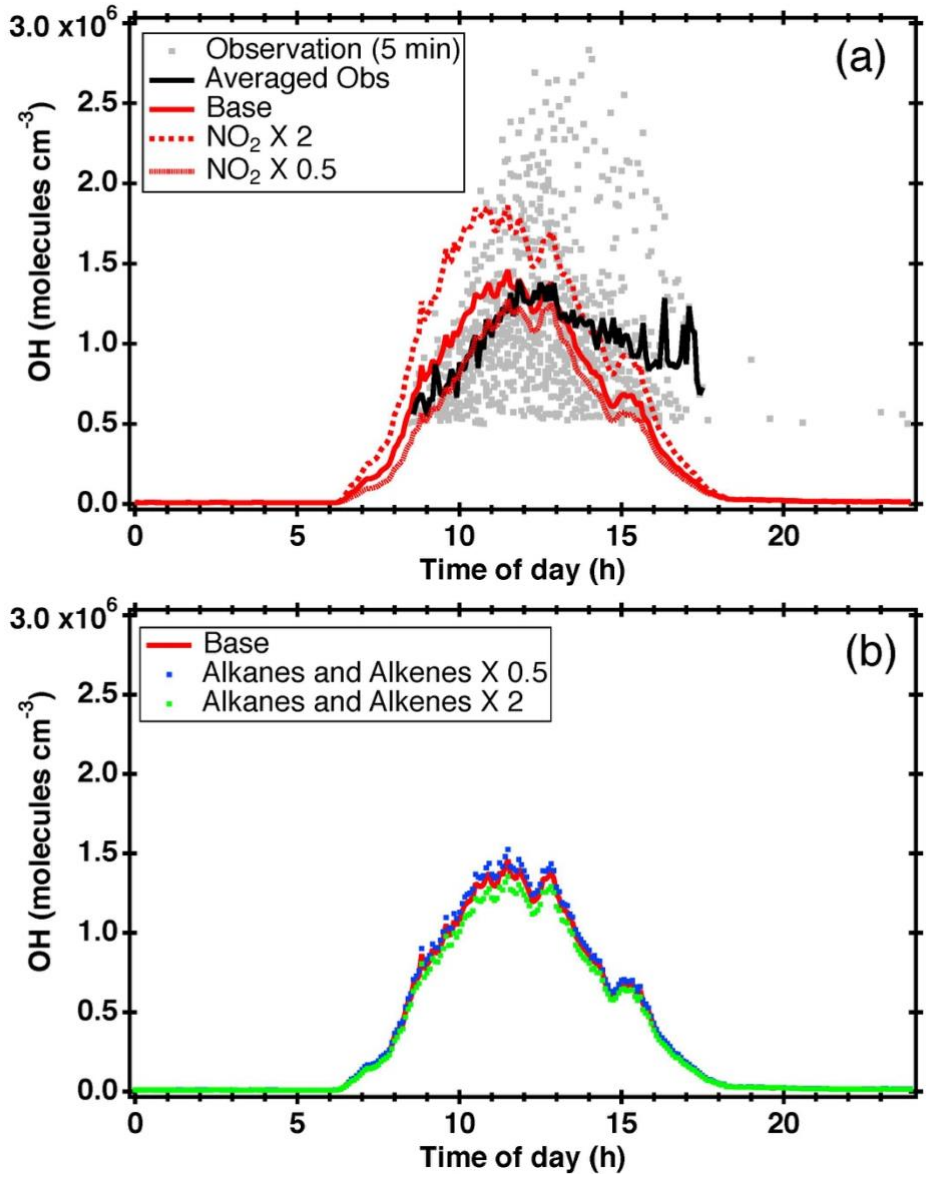

Figure 3.4 (a) NO_2 and (b) alkanes and alkenes sensitivity of modeled OH, simulated from F0AM v3.2 box model embedded with MCM v3.3.1 mechanism. 5 min averaged OH observations are in grey dots and diurnal average of this is in solid black line.

The discrepancies between OH model simulations and measurements could be driven by uncertainties in the assumptions made in the model setup. One possibility is how NO_x is treated in the model simulations. In this study, NO was deduced from NO_y observations as the instrument

deployed for NO_x quantification was not sensitive enough to accurately quantify low NO concentrations in the field environment. Liu et al. (2016) extensively discussed this issue using a box model and ground and aircraft NO_x datasets. In their study, NO concentrations were reasonably estimated for their purpose of interpreting ambient isoprene oxidation product distributions at the T3 site during the GoAmazon2014/5 campaign. The ratio (ξ) of hydroxyhydroperoxides (ISOPOOH) to methyl vinyl ketone (MVK) and methacrolein (MACR), both measured during the campaign, was used to deduce the ratio of the corresponding production rates of each (χ). The dependence of χ on NO was then simulated. Based on the analysis by Liu et al. (2016), we deduced a ratio of NO to NO_y as 0.03 for background conditions and used this factor for NO quantification. The estimated NO appeared to be in the range of the observed NO from previous observations from remote rain forests. NO_2 to NO ratio from airborne observations during the campaign was 2.3 ± 1 (for 1σ) when flying below 500 m. Therefore, we constrained the box model with NO_2 that was derived by doubling 3 % of measured NO_y. However, these assumptions are based on background conditions and the ratio of NO_2 to NO_y could vary, which could result in substantial changes in simulated OH level if the model is sensitive to constrained NO_2.

In order to examine the potential uncertainties in the model caused by the NO_x estimation method, sensitivity tests were carried out by constraining different NO_2 levels in the model embedded with MCM v 3.3.1. As in Figure 3.4 (a), doubling the constrained NO_2 resulted in, on average, ~ 40 % higher OH at midday. Although this is within the instrumental uncertainty, it illustrates that the simulated OH is sensitive to how NO_2 is constrained in the model runs. For March 14th and 15th, which the model simulations overestimated the observations, midday NO_y was in the range of 1 – 3 ppb. This is above the background levels and the airmasses are likely

affected by pollutions from Manaus as shown in the backtrajectories in Liu et al. (2016). Therefore, deriving NO as 3 % of measured NO_y might not be applicable in some observation periods selected for the model simulations in Figure 3.3. It should also be noticed that small alkane and alkene concentrations taken from Zimmerman et al. (1988) could be a factor of uncertainty. Based on the sensitivity runs in Figure 3.4 (b), doubling or halving the alkanes and alkenes in the model did not result in significant differences in the simulated OH. Another feature shown in about half of the simulated days (i.e., February 12th, 13th, 16th, 19th, March 9th, and 15th) is the early morning peak in the model results that occurred around 8:00 – 9:00 local standard time. These corresponded to a sudden peak in observed NO_y levels, which is most possibly from plume influence originating from Manaus. Therefore, NOx estimation method could be an uncertainty in the early morning.

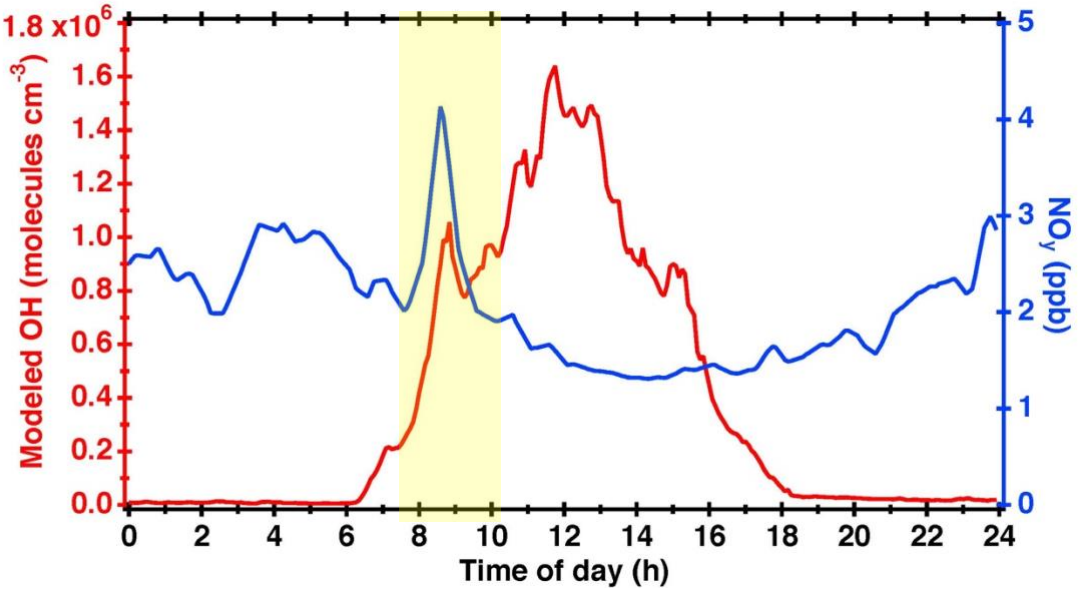

Figure 3.5 Modeled OH simulated from MCM v3.3.1 embedded box model and measured NO_y averaged over the selected days (i.e., February 12th, 13th, 16th, 19th, March 9th, and 15th) with OH peak in the early morning from model simulations.

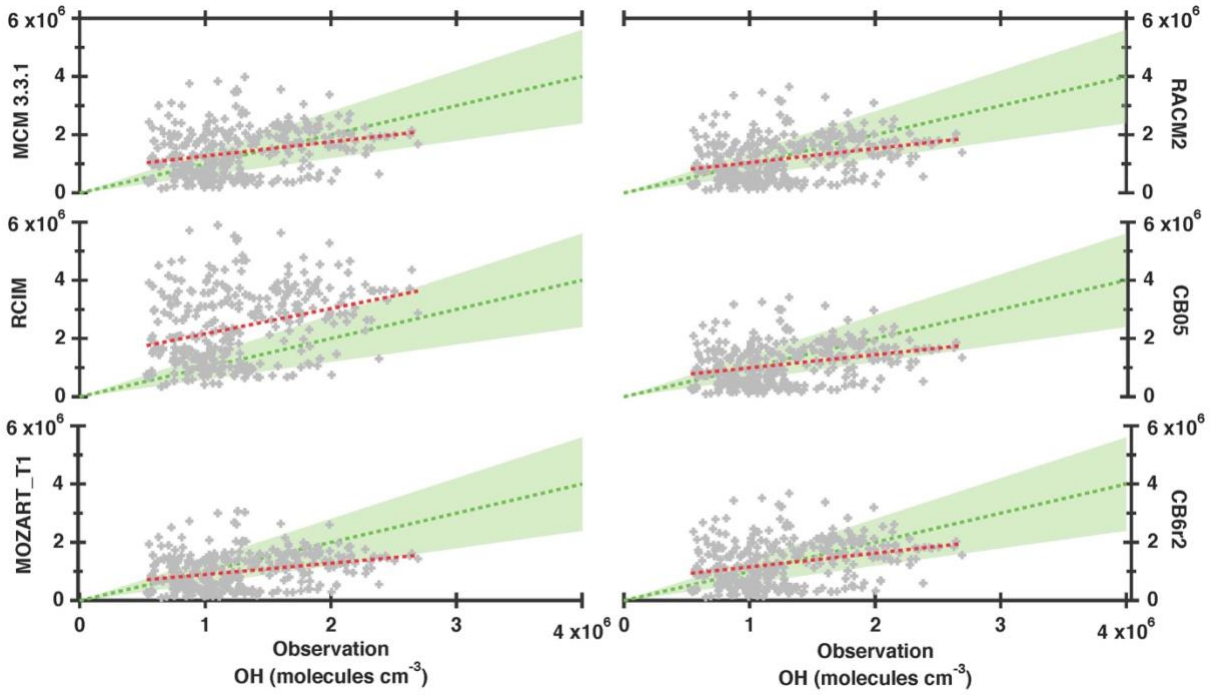

Figure 3.6 Correlation between midday (11:00 – 13:00, local standard time) observed OH to model simulation results for 6 different chemical mechanisms. The green dashed line is a 1 : 1 line and the green shade depicts the 40 % uncertainty. Each grey marker is a 5 min point and the red dashed lines are the linear trend lines of these.

Figure 3.6 shows correlation between OH observations to model results during midday, which is filtered from 11:00 to 15:00 local time. The model simulations from RCIM were only embedded with inorganic and isoprene initiated reactions but are included for the purpose of comparison. The red dashed lines are linear trend lines of the correlations between modeled and observed OH. The result illustrates that the correlation was within the 40 % uncertainty of the measurement throughout the midday OH range for the model runs with MCM 3.3.1, CB05, CB6r2, RACM2, and MOZART_T1 mechanisms. The simulated OH embedded with RCIM overestimated the observed OH by around 2-fold in the relatively lower OH concentration range. According to

Bates et al. (2019) box model simulations with isoprene constrained RCIM gave similar results to the one from MCM 3.3.1. Therefore, the overestimation of modeled OH, simulated with the RCIM in our study could be due to dampening of OH levels driven by additional alkanes and alkenes, which was not included in the RCIM runs.

Figure 3.7 illustrates midday modeled and observed OH as a function of other parameters such as JO^1D, NO_2, isoprene, and O_3. Each line is the averaged values of OH from observations and model runs of 5 different chemical mechanisms with respect to each parameter. The 5 min observation data is also presented in the figure for comparison. In relatively weaker solar radiation ($JO^1D < 1 \times 10^{-5}$ s^{-1}), all five mechanisms slightly underestimated the observation but were within the 40 % instrumental uncertainty above this radiation level. For other parameters, the averaged model results showed great agreement to the observation up until 0.25 ppb, 4 ppb, and 45 ppb of NO_2, isoprene, and O_3, respectively, where they started to diverge. The averaged points from when the divergence occurred are based on averages of 1-3 observation data points, and therefore would be difficult to conclude it as a trend. However, as shown in the sensitivity tests illustrated in Figure 3.4, model runs are sensitive to levels of NO_x and higher uncertainties are possible in relatively polluted conditions compared to background levels of NO_y. Model simulations of diurnal and midday HO_2 levels are compared between MCM 3.3.1 and other mechanisms in Figure 3.7. RACM2 resulted in about 25 % less HO_2 than other mechanism. This is consistent to what Wolfe et al. (2016) presented and is due to lower HO_2 production rates. Other mechanisms simulated HO2 similar to the MCM 3.3.1 and shows that the radical chemistry is comparable between these mechanisms embedded with the observation data set during GoAmazon2014/5.

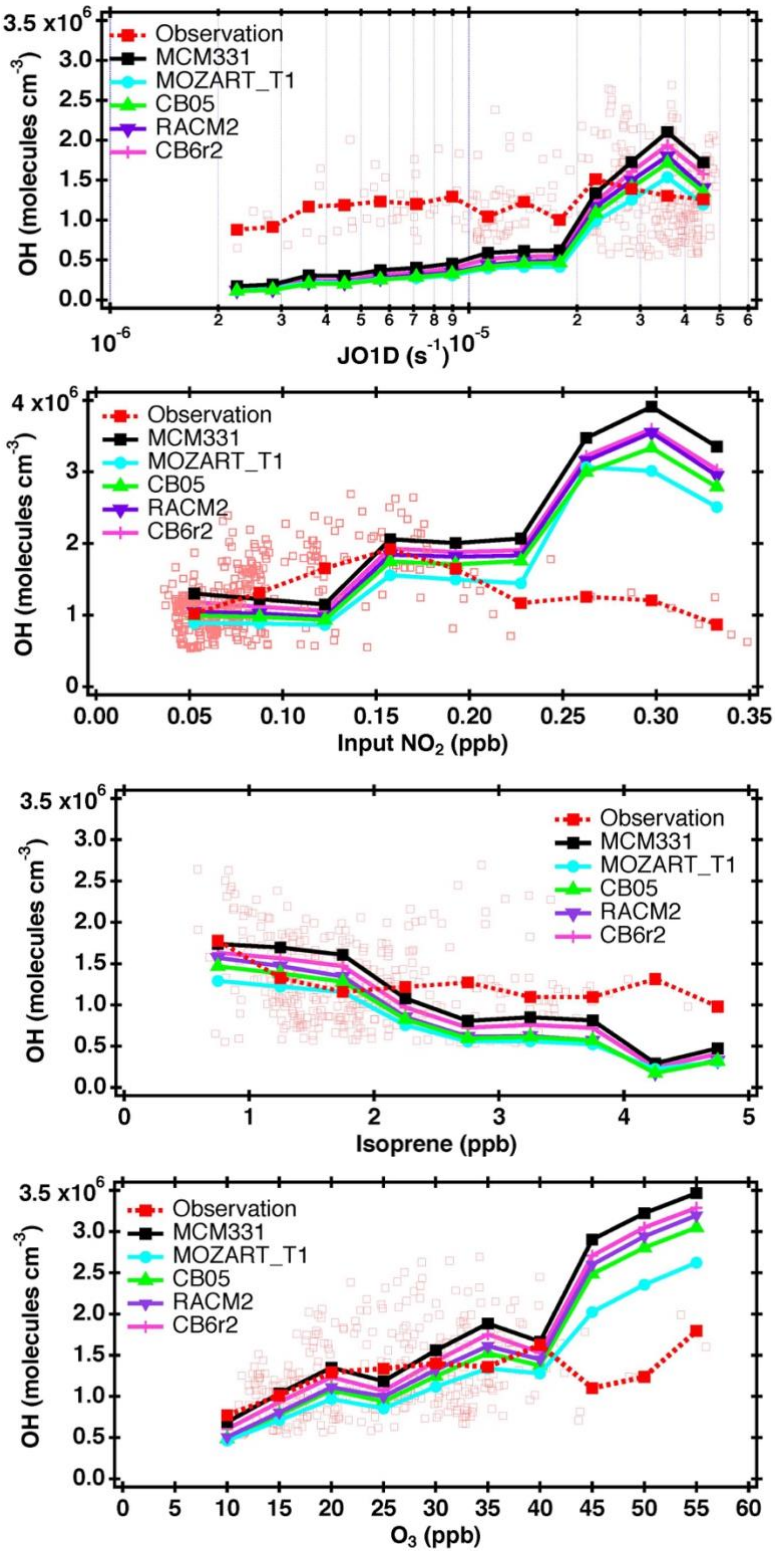

Figure 3.7 Observed and modeled midday averaged OH (11:00 – 13:00 local standard time) with respect to O_3 photolysis rate constant (JO^1D), input NO_2, isoprene, and O_3. Red square markers are 5 min averaged OH observation data.

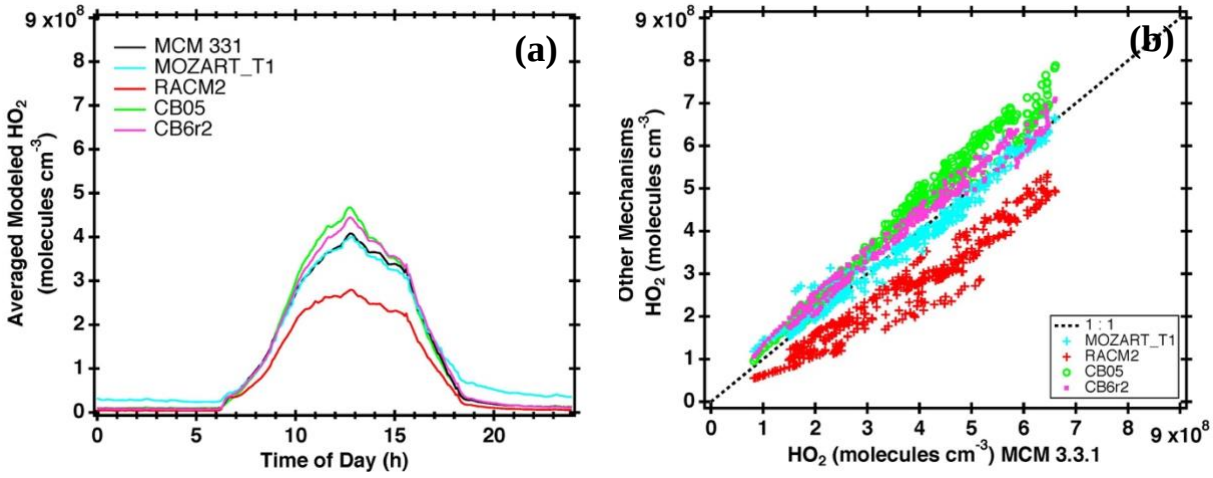

Figure 3.8 Box model simulated HO_2, embedded with different chemical mechanisms. (a) Diurnal variation of modeled HO_2 averaged over 16 days. (b) Comparison of simulated midday (11:00 – 13:00, local standard time) HO_2 between MCM v3.3.1 and other mechanisms.

3.3 Conclusion

In this study, we reported OH observation data measured with a CIMS in a rainforest during the GoAmazon2014/5. The levels observed were similar to previous field observations using the LIF technique with the chemical removal method. Great agreement was found between measured OH and box model simulations embedded with near-explicit and 4 other condensed mechanisms used in chemical transport models. This is contrary to previous studies that reported higher than expected OH levels in forested regions, but consistent to recent results by Mao et al. (2012)and Feiner et al. (2016), where they measured OH with the modified LIF technique during BEARPEX09 and SOAS campaigns. The observation and model results presented in this study, therefore, confirms that our current understanding in a low NO_x high BVOC rainforest is sufficient.

3.4 References

Archibald, A. T., Cooke, M. C., Utembe, S. R., Shallcross, D. E., Derwent, R. G. and Jenkin, M. E.: Impacts of mechanistic changes on HO_x formation and recycling in the oxidation of isoprene, Atmos. Chem. Phys., 10(17), 8097–8118, doi:10.5194/acp-10-8097-2010, 2010.

Asatryan, R., Da Silva, G. and Bozzelli, J. W.: Quantum chemical study of the acrolein (CH2CHCHO) + OH + O_2 reactions, J. Phys. Chem. A, 114(32), 8302–8311, doi:10.1021/jp104828a, 2010.

Bakwin, P. S., Wofsy, S. C. and Fan, S.: Measurements of Reactive Nitrogen Oxides (NO_y) Within and above a Tropical Forest Canopy in the Wet Season, J. Geophys. Res., 95(D10), 16765–16772, 1990.

Bates, K. H. and Jacob, D. J.: A new model mechanism for atmospheric oxidation of isoprene: global effects on oxidants, nitrogen oxides, organic products, and secondary organic aerosol, Atmos. Chem. Phys. Discuss., 1–46, doi:10.5194/acp-2019-328, 2019.

Butler, T. M., Taraborrelli, D., Brühl, C., Fischer, H., Harder, H., Martinez, M., Williams, J., Lawrence, M. G. and Lelieveld, J.: Improved simulation of isoprene oxidation chemistry with the ECHAM5/MESSy chemistry-climate model: lessons from the GABRIEL airborne field campaign, Atmos. Chem. Phys., 8(2), 4529-4546, doi:10.5194/acpd-8-6273-2008, 2008.

Carslaw, N., Creasey, D. J., Harrison, D., Heard, D. E., Hunter, M. C., Jacobs, P. J., Jenkin, M. E., Lee, J. D., Lewis, A. C., Pilling, M. J., Saunders, S. M. and Seakins, P. W.: OH and HO_2 radical chemistry in a forested region of north-western Greece, Atmos. Environ., 35(27), 4725–4737, doi:10.1016/S1352-2310(01)00089-9, 2001.

Chen, Q., Fan, J., Hagos, S., Gustafson, W. I. and Berg, L. K.: Roles of wind shear at different vertical levels: Cloud system organization and properties, J. Geophys. Res. Atmos., 120(13), 6551–6574, doi:10.1002/2015JD023253, 2015.

Chen, S., Ren, X., Mao, J., Chen, Z., Brune, W. H., Lefer, B., Rappenglück, B., Flynn, J., Olson, J. and Crawford, J. H.: A comparison of chemical mechanisms based on TRAMP-2006 field data, Atmos. Environ., 44(33), 4116–4125, doi:10.1016/j.atmosenv.2009.05.027, 2010.

Crounse, J. D., Paulot, F., Kjaergaard, H. G. and Wennberg, P. O.: Peroxy radical isomerization in the oxidation of isoprene, Phys. Chem. Chem. Phys., 13(30), 13607, doi:10.1039/c1cp21330j, 2011.

Dodge, M. C.: Chemical oxidant mechanisms for air quality modeling: Critical review, Atmos. Environ., 34(12–14), 2103–2130, doi:10.1016/S1352-2310(99)00461-6, 2000.

Feiner, P. A., Brune, W. H., Miller, D. O., Zhang, L., Cohen, R. C., Romer, P. S., Goldstein, A. H., Keutsch, F. N., Skog, K. M., Wennberg, P. O., Nguyen, T. B., Teng, A. P., DeGouw, J., Koss, A., Wild, R. J., Brown, S. S., Guenther, A., Edgerton, E., Baumann, K., Fry, J. L., Feiner, P. A., Brune, W. H., Miller, D. O., Zhang, L., Cohen, R. C., Romer, P. S., Goldstein, A. H., Keutsch, F. N., Skog, K. M., Wennberg, P. O., Nguyen, T. B., Teng, A. P., DeGouw, J., Koss, A., Wild, R. J., Brown, S. S., Guenther, A., Edgerton, E., Baumann, K. and Fry, J. L.: Testing Atmospheric Oxidation in an Alabama Forest, J. Atmos. Sci., 73(12), 4699–4710, doi:10.1175/JAS-D-16-0044.1, 2016.

Flynn, C. J.: Shortwave Array Spectroradiometer – Hemispheric Instrument Handbook., 2016.

Goliff, W. S., Stockwell, W. R. and Lawson, C. V.: The regional atmospheric chemistry mechanism,version2,Atmos. Environ., 68, 174–185, doi:10.1016/j.atmosenv.2012.11.038, 2013.

Graus, M., Muller, M. and Hansel, A.: High resolution PTR-TOF: Quantification and Formula Confirmation of VOC in Real Time, J. Am. Soc. Mass Spectrom., 21(6), 1037–1044, doi:10.1016/j.jasms.2010.02.006, 2010.

Greenberg, J. P. and Zimmerman, P. R.: Nonmethane hydrocarbons in remote tropical, continental, and marine atmospheres., J. Geophys. Res., 89(D3), 4767–4778, doi:10.1029/JD089iD03p04767, 1984.

Gross, A. and Stockwell, W. R.: Comparison of the EMEP, RADM2 and RACM mechanisms, J. Atmos. Chem., 44(2), 151–170, doi:10.1023/A:1022483412112, 2003.

Hens, K., Novelli, A., Martinez, M., Auld, J., Axinte, R., Bohn, B., Fischer, H., Keronen, P., Kubistin, D., Nölscher, A. C., Oswald, R., Paasonen, P., Petäjä, T., Regelin, E., Sander, R., Sinha, V., Sipilä, M., Taraborrelli, D., Tatum Ernest, C., Williams, J., Lelieveld, J. and Harder, H.: Observation and modelling of HOx radicals in a boreal forest, Atmos. Chem. Phys., 14(16), 8723–8747, doi:10.5194/acp-14-8723-2014, 2014.

Hofzumahaus, A., Rohrer, F., Lu, K., Bohn, B., Brauers, T., Chang, C., Fuchs, H., Holland, F., Kita, K., Kondo, Y., Li, X., Lou, S., Shao, M., Zeng, L., Wahner, A. and Zhang, Y.: Amplified Trace Gas Removal in the Troposphere, Science, 324, 1702–1704, 2009.

Jacob, J. and Wofsy, S. C.: Photochemistry of biogenic emissions over the Amazon Forest, J. Geophys. Res., 93(D2), 1477–1486, doi:10.1029/JD093iD02p01477, 1988.

Jenkin, M. E., Young, J. C. and Rickard, A. R.: The MCM v3.3.1 degradation scheme for isoprene, Atmos. Chem. Phys., 15(20), 11433–11459, doi:10.5194/acp-15-11433-2015, 2015.

Jimenez, P., Baldasano, J. M. and Dabdub, D.: Comparison of photochemical mechanisms for air quality modeling, Atmos. Environ., 37(30), 4179–4194, doi:10.1016/S1352-2310(03)00567-3, 2003.

Jordan, A., Haidacher, S., Hanel, G., Hartungen, E., Märk, L., Seehauser, H., Schottkowsky, R., Sulzer, P. and Märk, T. D.: A high resolution and high sensitivity proton-transfer-reaction time-of-flight mass spectrometer (PTR-TOF-MS), Int. J. Mass Spectrom., 286(2–3), 122–128, doi:10.1016/j.ijms.2009.07.005, 2009.

Knote, C., Hodzic, A., Jimenez, J. L., Volkamer, R., Orlando, J. J., Baidar, S., Brioude, J., Fast, J., Gentner, D. R., Goldstein, A. H., Hayes, P. L., Knighton, W. B., Oetjen, H., Setyan, A., Stark, H., Thalman, R., Tyndall, G., Washenfelder, R., Waxman, E. and Zhang, Q.: Simulation of semi-explicit mechanisms of SOA formation from glyoxal in aerosol in a 3-D model, Atmos. Chem. Phys., 14(12), 6213–6239, doi:10.5194/acp-14-6213-2014, 2014.

Knote, C., Tuccella, P., Curci, G., Emmons, L., Orlando, J. J., Madronich, S., Baró, R., Jiménez-Guerrero, P., Luecken, D., Hogrefe, C., Forkel, R., Werhahn, J., Hirtl, M., Pérez, J. L., San José, R., Giordano, L., Brunner, D., Yahya, K. and Zhang, Y.: Influence of the choice of gas-phase mechanism on predictions of key gaseous pollutants during the AQMEII phase-2 intercomparison, Atmos. Environ., 115, 553–568, doi:10.1016/j.atmosenv.2014.11.066, 2015.

Kubistin, D., Harder, H., Martinez, M., Rudolf, M., Sander, R., Bozem, H., Eerdekens, G., Fischer, H., Gurk, C., Klüpfel, T., Königstedt, R., Parchatka, U., Schiller, C. L., Stickler, A., Taraborrelli, D., Williams, J. and Lelieveld, J.: Hydroxyl radicals in the tropical troposphere over the Suriname rainforest: Comparison of measurements with the box model MECCA, Atmos. Chem. Phys., 10(19), 9705–9728, doi:10.5194/acp-10-9705-

2010, 2010.

Kuhn, M., Builtjes, P. J. H., Poppe, D., Simpson, D., Stockwell, W. R., Andersson-Sköld, Y., Baart, A., Das, M., Fiedler, F., Hov, Kirchner, F., Makar, P. A., Milford, J. B., Roemer, M. G. M., Ruhnke, R., Strand, A., Vogel, B. and Vogel, H.: Intercomparison of the gas-phase chemistry in several chemistry and transport models, Atmos. Environ., 32(4), 693–709, doi:10.1016/S1352-2310(97)00329-4, 1998.

Lelieveld, J., Butler, T. M., Crowley, J. N., Dillon, T. J., Fischer, H., Ganzeveld, L., Harder, H., Lawrence, M. G., Martinez, M., Taraborrelli, D. and Williams, J.: Atmospheric oxidation capacity sustained by a tropical forest, Nature, 452(7188), 737–740, doi:10.1038/nature06870, 2008.

Levy, H.: Normal Atmosphere: Large Radical and Formaldehyde Concentrations Predicted, Science (80-.)., 173(3992), 141–143, doi:10.1126/science.173.3992.141, 1971.

Liu, Y., Brito, J., Dorris, M. R., Rivera-Rios, J. C., Seco, R., Bates, K. H., Artaxo, P., Duvoisin, S., Keutsch, F. N., Kim, S., Goldstein, A. H., Guenther, A. B., Manzi, A. O., Souza, R. A. F., Springston, S. R., Watson, T. B., McKinney, K. A. and Martin, S. T.: Isoprene photochemistry over the Amazon rainforest, Proc. Natl. Acad. Sci., 113(22), 6125–6130, doi:10.1073/pnas.1524136113, 2016.

Logan, J. A., Prather, M. J., Wofsy, S. C. and Mc Elroy, M. B.: Tropospheric chemistry: A global perspective, J. Geophys. Res., 86(C9), 7210–7254, doi:10.1029/JC086iC08p07210, 1981.

Mao, J., Ren, X., Zhang, L., Van Duin, D. M., Cohen, R. C., Park, J. H., Goldstein, A. H., Paulot, F., Beaver, M. R., Crounse, J. D., Wennberg, P. O., Digangi, J. P., Henry, S. B., Keutsch, F. N., Park, C., Schade, G. W., Wolfe, G. M., Thornton, J. A. and Brune, W. H.: Insights into hydroxyl measurements and atmospheric oxidation in a California forest, Atmos. Chem. Phys., 12(17), 8009–8020, doi:10.5194/acp-12-8009-2012, 2012.

Novelli, A., Hens, K., Tatum Ernest, C., Kubistin, D., Regelin, E., Elste, T., Plass-Dülmer, C., Martinez, M., Lelieveld, J. and Harder, H.: Characterisation of an inlet pre-injector laser-induced fluorescence instrument for the measurement of atmospheric hydroxyl radicals, Atmos. Meas. Tech., 7(10), 3413–3430, doi:10.5194/amt-7-3413-2014, 2014.

Peeters, J. and Müller, J.-F.: HO_x radical regeneration in isoprene oxidation via peroxy radical isomerisations. II: experimental evidence and global impact, Phys. Chem. Chem. Phys., 12(42), 14227, doi:10.1039/c0cp00811g, 2010.

Peeters, J., Nguyen, T. L. and Vereecken, L.: HO_x radical regeneration in the oxidation of isoprene, Phys. Chem. Chem. Phys., 11(28), 5935, doi:10.1039/b908511d, 2009.

Peeters, J., Müller, J. F., Stavrakou, T. and Nguyen, V. S.: Hydroxyl radical recycling in isoprene oxidation driven by hydrogen bonding and hydrogen tunneling: The upgraded LIM1 mechanism, J. Phys. Chem. A, 118(38), 8625–8643, doi:10.1021/jp5033146, 2014.

Pugh, T. A. M., MacKenzie, A. R., Hewitt, C. N., Langford, B., Edwards, P. M., Furneaux, K. L., Heard, D. E., Hopkins, J. R., Jones, C. E., Karunaharan, A., Lee, J., Mills, G., Misztal, P., Moller, S., Monks, P. S. and Whalley, L. K.: Simulating atmospheric composition over a South-East Asian tropical rainforest: Performance of a chemistry box model, Atmos. Chem. Phys., 10, 279–298, doi:10.5194/acpd-9-19243-2009, 2010.

Ren, X., Olson, J. R., Crawford, J. H., Brune, W. H., Mao, J., Long, R. B., Chen, Z., Chen, G., Avery, M. A., Sachse, G. W., Barrick, J. D., Diskin, G. S., Huey, L. G., Fried, A., Cohen, R. C., Heikes, B., Wennberg, P. O., Singh, H. B., Blake, D. R. and Shetter, R. E.: HO_x chemistry during INTEX-A 2004: Observation, model calculation, and comparison with previous studies, J. Geophys. Res. Atmos., 113(5), 1–13, doi:10.1029/2007JD009166,

2008.

Rohrer, F., Lu, K., Hofzumahaus, A., Bohn, B., Brauers, T., Chang, C.-C., Fuchs, H., Häseler, R., Holland, F., Hu, M., Kita, K., Kondo, Y., Li, X., Lou, S., Oebel, A., Shao, M., Zeng, L., Zhu, T., Zhang, Y. and Wahner, A.: Maximum efficiency in the hydroxyl-radical-based self-cleansing of the troposphere, Nat. Geosci., 7(8), 559–563, doi:10.1038/ngeo2199, 2014.

Saunders, S. M., Jenkin, M. E., Derwent, R. G. and Pilling, M. J.: World Wide Web site of a master chemical mechanism (MCM) for use in tropospheric chemistry models, Atmos. Environ., 31(8), 1249, doi:10.1016/S1352-2310(97)85197-7, 1997.

Saunders, S. M., Jenkin, M. E., Derwent, R. G. and Pilling, M. J.: Protocol for the development of the Master Chemical Mechanism, MCM v3 (Part A): tropospheric degradation of non-aromatic volatile organic compounds, Atmos. Chem. Phys., 3(1), 161–180, doi:10.5194/acp-3-161-2003, 2003.

Stone, D., Evans, M. J., Commane, R., Ingham, T., Floquet, C. F. A., McQuaid, J. B., Brookes, D. M., Monks, P. S., Purvis, R., Hamilton, J. F., Hopkins, J., Lee, J., Lewis, A. C., Stewart, D., Murphy, J. G., Mills, G., Oram, D., Reeves, C. E. and Heard, D. E.: HO_x observations over West Africa during AMMA: Impact of isoprene and NO_x, Atmos. Chem. Phys., 10(19), 9415–9429, doi:10.5194/acp-10-9415-2010, 2010.

Tan, D., Faloona, I., Simpas, J. B., Brune, W., Shepson, P. B., Couch, T. L., Sumner, a. L., Carroll, M. a., Thornberry, T., Apel, E., Riemer, D. and Stockwell, W.: HO_x budgets in a deciduous forest: Results from the PROPHET summer 1998 campaign, J. Geophys. Res. Atmos., 106(D20), 24407–24427, doi:10.1029/2001JD900016, 2001.

Taraborrelli, D., Lawrence, M. G., Butler, T. M., Sander, R. and Lelieveld, J.: Mainz Isoprene Mechanism 2 (MIM2): An isoprene oxidation mechanism for regional and global atmospheric modelling, Atmos. Chem. Phys., 9(8), 2751–2777, doi:10.5194/acp-9-2751-2009, 2009.

Thornton, J. A.: Ozone production rates as a function of NO_x abundances and HO_x production rates in the Nashville urban plume, J. Geophys. Res., 107(D12), 4146, doi:10.1029/2001JD000932, 2002.

Wennberg, P. O., Bates, K. H., Crounse, J. D., Dodson, L. G., McVay, R. C., Mertens, L. A., Nguyen, T. B., Praske, E., Schwantes, R. H., Smarte, M. D., St Clair, J. M., Teng, A. P., Zhang, X. and Seinfeld, J. H.: Gas-Phase Reactions of Isoprene and Its Major Oxidation Products, Chem. Rev., 118(7), 3337–3390, doi:10.1021/acs.chemrev.7b00439, 2018.

Whalley, L. K., Edwards, P. M., Furneaux, K. L., Goddard, A., Ingham, T., Evans, M. J., Stone, D., Hopkins, J. R., Jones, C. E., Karunaharan, A., Lee, J. D., Lewis, A. C., Monks, P. S., Moller, S. J. and Heard, D. E.: Quantifying the magnitude of a missing hydroxyl radical source in a tropical rainforest, Atmos. Chem. Phys., 11(14), 7223–7233, doi:10.5194/acp-11-7223-2011, 2011.

Wolfe, G. M., Crounse, J. D., Parrish, J. D., St. Clair, J. M., Beaver, M. R., Paulot, F., Yoon, T. P., Wennberg, P. O. and Keutsch, F. N.: Photolysis, OH reactivity and ozone reactivity of a proxy for isoprene-derived hydroperoxyenals (HPALDs), Phys. Chem. Chem. Phys., 14(20), 7276–7286, doi:10.1039/c2cp40388a, 2012.

Wolfe, G. M., Marvin, M. R., Roberts, S. J., Travis, K. R. and Liao, J.: The framework for 0-D atmospheric modeling (F0AM) v3.1, Geosci. Model Dev., 9(9), 3309–3319, doi:10.5194/gmd-9-3309-2016, 2016.

Zimmerman, P. R., Greenberg, J. P. and Westberg, C. E.: Measurements of atmospheric

hydrocarbons and biogenic emission fluxes in the Amazon Boundary layer, J. Geophys. Res. Atmos., 93(D2), 1407–1416, doi:10.1029/JD093iD02p01407, 1988.

CHAPTER 4

$ClNO_2$ OBSERVATION DURING KORUS-AQ 2016

4.1 Introduction

Nitryl chloride ($ClNO_2$) is a night time radical reservoir that generates chlorine (Cl) upon sunrise (R4.1), with a lifetime (τ_{ClNO2}) of ≈ 30 minutes at midday in the northern hemisphere mid-latitude summer, under clear sky conditions ($J_{ClNO2} \approx 5.47 \times 10^{-04}\ s^{-1}$, (Madronich and Flocke, 1998)). It is produced through heterogeneous reaction of chloride (Cl^-) containing aerosols and dinitrogen pentoxide (N_2O_5(g)), which is generated from an equilibrium reaction with gas-phase nitrate radical (NO_3) and nitrogen dioxide (NO_2) (R4.2-R4.4, (Finlayson-Pitts et al., 1989)). In acidic aerosol (≈ pH 1.8), uptake of N_2O_5(g) magnitude higher than neutral pH (Roberts et al., 2008). However, this reaction has yet to be proven in ambient conditions.

During the day, N_2O_5 exists at low levels due to its thermal instability (Malko and Troe, 1982) and the short lifetime of NO_3 ($\tau_{NO3} < 5$ s) from photolysis and reaction with NO (Wayne et al., 1991). Particulate Cl^- and chlorine containing gas species can come from both natural sources such as sea salt and biomass burning (Blanchard, 1985; Woodcock, 1953), and anthropogenic sources such as steel making, incineration, bleaching processes, and coal-fired power plants (Blanchard, 1985; Fu et al., 2018; Hov, 1985; Lee et al., 2018; Reff et al., 2009; Tanaka et al., 2000). The efficiency of $ClNO_2$ production depends on heterogeneous loss of N_2O_5, which is a function of the N_2O_5 aerosol uptake coefficient (γ_{N2O5}), aerosol surface area, and N_2O_5 mean molecular speed, as well as the yield of $ClNO_2$ (ϕ_{ClNO2}) (Behnke et al., 1997; Bertram and Thornton, 2009; Hu and Abbatt, 1997; Schweitzer et al., 1998; Thornton et al., 2003). Many recent studies have reported discrepancies between field derived and laboratory parameterized γ_{N2O5}

(Brown et al., 2009; Chang et al., 2016; McDuffie et al., 2018b; Morgan et al., 2015; Phillips et al., 2016; Tham et al., 2016; Wang et al., 2017c) and ϕ_{ClNO2} (McDuffie et al., 2018a; Riedel et al., 2013; Ryder et al., 2015; Tham et al., 2018; Thornton et al., 2010; Wagner et al., 2013; Wang et al., 2017b). In a nocturnal boundary layer, $ClNO_2$ can accumulate to significant levels due to its long lifetime (τ_{ClNO2} > 30 h) with slow loss mechanisms through heterogeneous uptake (Behnke et al., 1997; Frenzel et al., 1998; George et al., 1995). At sunrise, $ClNO_2$ rapidly photolyzes to generate chlorine radicals (Cl), which can react with most volatile organic compounds (VOCs). For alkanes, Cl has up to 1 – 2 orders of magnitude large rate constants than hydroxyl radicals (e.g., $k_{OH+n\text{-}C4H10} = 2.4 \times 10^{-12}$, $k_{Cl+n\text{-}C4H10} = 2.2 \times 10^{-10}$ at 298 K) (Atkinson, 1997; Atkinson and Arey, 2003). Therefore, Cl can potentially influence the radical pool (HO_x-RO_x) and ozone (O_3) level, which can also affect the formation of secondary aerosols. This influence can be most prominent in the morning when concentrations of other oxidants are low (i.e., NO_3 and OH) (Finlayson-Pitts, 1993; Hov, 1985; Young et al., 2014).

$$ClNO_{2(g)} + h\nu \rightarrow Cl_{(g)} + NO_{2(g)} \qquad \text{R4.1}$$

$$NO_{2(g)} + O_{3(g)} \rightarrow NO_{3(g)} + O_{2(g)} \qquad \text{R4.2}$$

$$NO_{3(g)} + NO_{2(g)} \rightleftharpoons N_2O_{5(g)} \qquad \text{R4.3}$$

$$N_2O_{5(g)} \xrightarrow{\gamma(N2O5),\ Cl-(aq)} (2 - \phi) * HNO_{3(g)} + \phi * ClNO_{2(g)} \qquad \text{R4.4}$$

$$ClNO_{2(g)} + Cl^-_{(aq)} + H^+_{(aq)} \rightarrow Cl_{2(g)} + HNO_{2(aq)} \qquad \text{R4.5}$$

The first ambient measurement of $ClNO_2$ were carried out by Osthoff et al. (2008), from a ship sampling along the southeastern U.S. coast in 2006. In that study, $ClNO_2$ was observed up to ~ 1 ppbv at night time, particularly during the time period influenced by urban pollution and ship

plumes of the Houston ship channel. Since then, a growing number of measurements reported significant levels of $ClNO_2$, especially in polluted coastal regions with sources from natural and anthropogenic chloride and nitrogen oxides. Riedel et al. (2012) measured up to ~2ppbv of $ClNO_2$ off the coast of Santa Monica Bay, on board the research vessel Atlantis. Recent studies show that high levels of $ClNO_2$ are also present in mid-continental regions. Thornton et al. (2010) measured up to ~ 400 pptv in Boulder, Colorado, which is ~ 1,400 km away from the coastline. Mielke et al. (2011) reported up to ~ 250 pptv in Calgary, Alberta, Canada, during spring, which is ~ 800 km from the coastline. Back trajectory analysis results showed that the observations were most likely not influenced by marine air masses. More recently (in the past 5 years), increasing number of $ClNO_2$ observations have been conducted in Asia consistently showing significant levels of $ClNO_2$ present in the boundary layer (Liu et al., 2017; Tham et al., 2016, 2018; Wang et al., 2018, 2014, 2017b; Yun et al., 2018a). $ClNO_2$ observations at semi-rural (Wangdu and Hebei province) and urban (Hong Kong, Jinan) regions in China have measured up to 2 ppbv an d 776 pptv respectively (Tham et al., 2016; Wang et al., 2017b). At the mountain top (957 m above sea level) in Hong Kong, up to 4.7 ppbv of $ClNO_2$ was reported (Wang et al., 2016). The high levels of $ClNO_2$ in these studies were mostly correlated with continental pollution in vicinity (e.g., power plant plumes, biomass burning). A recent study by Yun et al. (2018a) reported the highest-recorded mixing ratio of $ClNO_2$ (8.3 ppb), during a severe haze event in a semi-rural site downwind of the Pearl River Delta in the winter. Overall, observations have shown that $ClNO_2$ is ubiquitous in the tropospheric boundary layer.

However, measurements are still limited, as discrepancies remain between global chemical transport models and observations. Uncertainties in model simulated $ClNO_2$ can arise from limited emission inventories, low resolution of the grid, uncertainties in γ_{N2O5} and ϕ_{ClNO2} parameterization,

complexity of the terrain, and meteorological conditions and these have been dealt in previous studies (Lowe et al., 2015; McDuffie et al., 2018b, 2018a; Sarwar et al., 2012, 2014; Sherwen et al., 2017; Zhang et al., 2017). For instance, smoothing out local $ClNO_2$ peaks by diluting local NO_x emissions, will result in limited NO_3 and N_2O_5 production. According to Sarwar et al. (2012, 2014), the Community Multiscale Air Quality (CMAQ) model with a finer grid (i.e. 12 km) simulated $ClNO_2$ that corresponded better to the observations, compared to the model runs with coarser grid size (i.e., 108 km), embedded with similar chemistry. Another modeling study by Sherwen et al. (2017) compared the $ClNO_2$ levels between the GEOS-Chem simulations and observations in inland areas (i.e., London, UK and a mountain top near Frankfurt, Germany) during the summer of 2015. Compared to observations, the simulations underestimated the $ClNO_2$ maxima levels by ~ 7 times in inland areas (Sherwen et al., 2017). Modeling studies have consistently suggested the significance of Cl initiated reactions in regional and global O_3 production and in the lifetime of VOCs in the troposphere (Knipping and Dabdub, 2003; Sarwar et al., 2014; Sherwen et al., 2016; Simon et al., 2009; Tanaka et al., 2000, 2003). Sarwar et al. (2014) explored the production of $ClNO_2$ from sea salt and biomass burning and its impact in the Northern Hemisphere by including $ClNO_2$ formation chemistry in the CMAQ model. The results showed that, compared to the simulations without $ClNO_2$ formation, monthly 8 h wintertime maximum O_3 and OH increased up to 15 % and 20 %, respectively. The impact was the largest in China and Western Europe. In the Hong Kong-Pearl River Delta (HK-PRD) region, Li et al. (2016) simulated up to ~ 1 ppbv of $ClNO_2$ originating from sea salt, biomass burning, and anthropogenic emissions (e.g., coal combustion) with the Weather Research and Forecasting coupled with Chemistry (WRF-CHEM) model. This resulted in ~ 16 % O_3 increase in the planetary boundary. Another modeling study of WRF-CHEM embedded with an updated chlorine chemistry, simulated

3-6 % of surface O_3 increase in the North China Plain and Yangtze River Delta during the summer (Zhang et al., 2017). A recent study by Wang et al. (2019) updated the standard version of the GEOS-Chem (Chen et al., 2017; Sherwen et al., 2016) to better track partitioning between aerosol chloride and gas-phase chlorine species. Comparison between their model simulations with and without $ClNO_2$ production showed enhanced O_3 up to 8 ppb during the winter season in Europe.

East Asian countries are of particular interest due to the rapid economic growth in the past decades with high anthropogenic emissions from densely populated megacities (e.g., Shanghai, Guangzhou, Beijing, Tokyo, Seoul). The majority of the world's megacities are situated in coast regions (Neumann et al., 2015) with high NO_x emissions and abundant sources of chloride from both anthropogenic and natural origin. These regional characteristics likely promote $ClNO_2$ production. Moreover, considering that nearly half the population in the world lives near the coast, defined as < 100 km from coastline (Hinrichsen, 1998), a careful evaluation of the impact of $ClNO_2$ on local tropospheric chemistry is crucial.

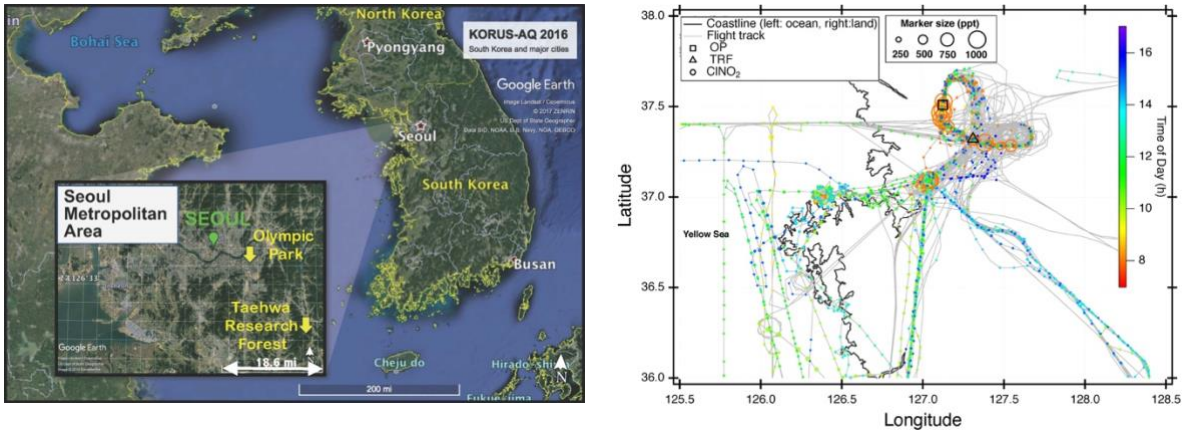

Figure 4.1 (a) Location of two ground sites (Taehwa Research Forest and Olympic Park) where the chemical ionization mass spectrometer (CIMS) was installed during the KORUS-AQ 2016 field campaign (b) Airborne measurements of $ClNO_2$ and DC-8 flight tracks during the whole campaign. The $ClNO_2$ data points are 60 sec averaged and color coded by time of day of the measurement. The marker size is proportional to the mixing ratio of $ClNO_2$.

In this study, we present $ClNO_2$ observation results from the Korean-United States Air quality (KORUS-AQ) study conducted in the Seoul Metropolitan Area (SMA), South Korea during late Spring (May 2 to June 12, 2016). The field campaign was an international collaboration between the National Institute of Environmental Research (NIER) of South Korea and the National Aeronautics and Space Administration (NASA) of the United States with the aim to better understand the impact of a megacity on regional air quality. A comprehensive suite of measurements were deployed at two super sites (Olympic Park site, OP; Taewha Research Forest, TRF) and aboard the NASA DC-8 to make airborne observations over the South Korean peninsula and the Yellow Sea. The two ground sites were within the SMA region, which is the second largest metropolitan area in the world with a population of ~ 24 million (Park et al., 2017). As shown in Figure 4.1(a). the OP site is located in the southern part of Seoul, surrounded by high rise residence buildings and close to major freeways. The TRF site is in the middle of a forested areas, ~ 26 km southeast of the OP site. Previous studies have shown that the TRF site is affected by both aged anthropogenic air masses from the city and fresh biogenic emissions from the forest (Kim et al., 2015a, 2016b). Both sites were ~ 50 km to the east of the nearest coastline. Figure 4.1(b) shows the flight tracks of the NASA DC-8, during the KORUS-AQ campaign. Spiral patterns were conducted near the TRF site to measure a vertical profile of the troposphere. Airborne observations were carried out during the daytime, between 8:00 and 17:00 local time. A summary of the analytical techniques of the measurements presented in this study are shown in Table 4.1. Meteorology during the observation period can be classified into dynamic (May 4^{th} – 16^{th}), stagnation (May 17^{th} – 22^{nd}), transport (May 25^{th} – 31^{st}), and blocking period. During the stagnant period, high pressure system was persistent in the Korean peninsula resulting in local air masses to be more dominant within the SMA compared to the dynamic and transport periods. Rex block

patterns were observed during the blocking period (June 1st – 6th). During this period, a high pressure system was adjacent to a low pressure over the Korean peninsula resulting in more local influence with occasional stagnation.

Table 4.1 Summary of the measurements carried out during the KORUS-AQ 2016 field campaign, used in this study.

Compound	Method		
	TRF	**OP**	**DC-8**
NO	[a]CL	[b]FRM	[c]CL
NO2	[d]CRDS	[e]CAPS	[c]CL
O3	[f]DIAL	[g]SL-UV	[c]CL
SO2	[h]PF	[i]UV florescence	
CO	[j]IR	[k]NDIR	
ClNO2, Cl2	[l]CIMS	[l]CIMS	[l]CIMS
VOCs	[m]PTR-ToF-MS	[o]QCL	[p]PTR-Tof-MS
	[n]TILDAS		[q]WAS
chloride (< 1 μm)			
nitrate (< 1 μm)		[r]ToF-AMS	[s]HR-ToF-AMS
sulfate (< 1 μm)			
Surface area (< 200 nm)			[t]SMPS
Surface area (200 nm – 5 μm)			[u]LAS
Jvalues			[v]CAFS

[a]Chemiluminescence with a molybdenum converter (Thermo Scientific 42i – TL), [b]Chemiluminescence detector (Federal Reference Method, Teledyne T200U), [c]NCAR 4-channel chemiluminescence (Weinheimer et al., 1994), [d]Cavity Ring Down Spectroscopy (Los Gatos Research NO2 analyzer), [d]Cavity Attenuated Phase shift spectroscopy (Teledyne T500U CAPS analyzer), [f]NASA TROPospheric Ozone Differential Absorption Lidar (Sullivan et al., 2014), [g]UV photometric method (2B 211), [h]Pulsed fluorescence method (Thermo Scientific 43i-HL), [i]UV florescence method (KENTEK), [j]Infrared CO analyzer (Thermo Scientific 48i-HL), [l]Chemical Ionization Mass Spectrometer (Slusher et al., 2004), [m]Proton-Transfer-Reaction Time-of-Flight Mass Spectrometer (IONICON), [n]Tunable Infrared Laser Direct Absorption Spectroscopy (Aerodyne), [o]Quantum Cascade Laser spectrometer (Aerodyne), [p]Universtiy of Oslo/Innsbruck Proton-Transfer-Reaction Time-Of-Flight Mass Spectrometer (Müller et al., 2014), [q] Whole Air Sampler (Colman et al., 2001), [r]Aerosol Mass Spectrometer (Aerodyne), [s] Universtiy of Colorado, Boulder, Aerosol Mass Spectrometer (Nault et al., 2018), [t]NASA, Scanning Mobility Particle Size, [u]NASA, Laser Aerosol Spectrometer, [v]NCAR, Charged-couple device Actinic Flux Spectroradiometer (Shetter and Müller, 1999)

4.2 Results and Discussion

4.2.1 $ClNO_2$ Observations

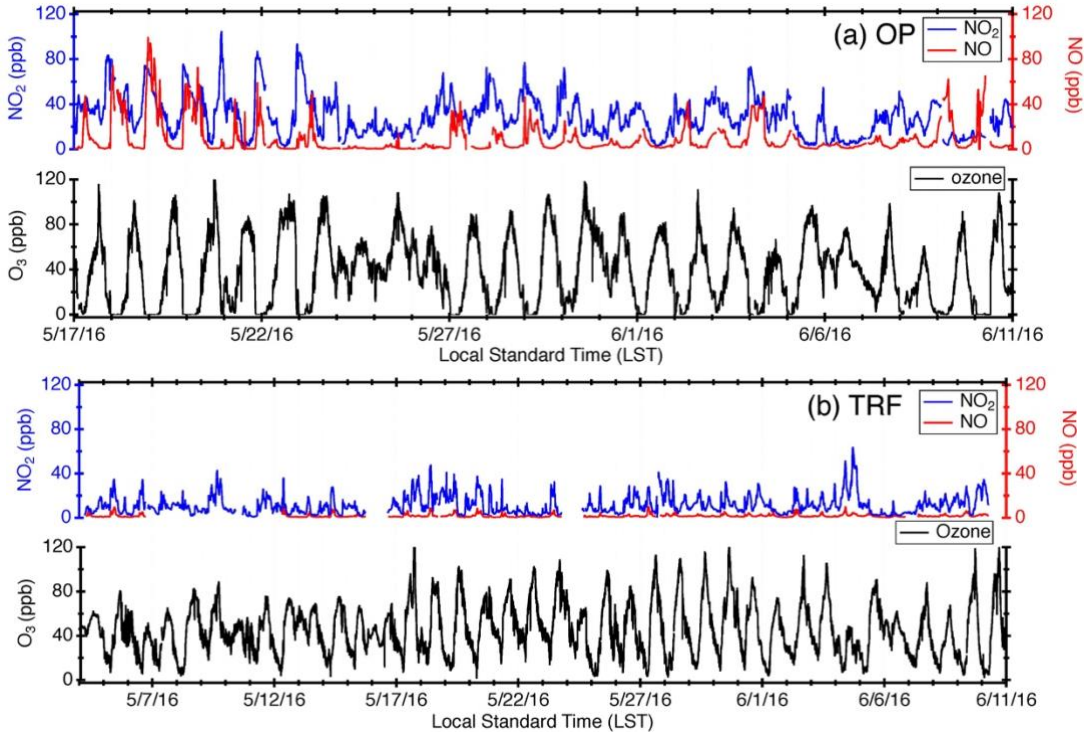

Figure 4.2 Temporal variation of trace gases measured at the (a) Olympic Park site (OP) and (b) Taehwa Research Forest (TRF). For both OP and TRF, the frequency of the averaged data is 10 min for NO_x and 1 min for O_3

Figure 4.2 shows the temporal variation of trace gases measured during the campaign at (a) the OP site (May 17th – June 11th) and (b) the TRF site (May 5th – June 11th). The OP site, which was located near heavy traffic, showed high levels of NO_x throughout the campaign. During most nights (except for May 24th – 26th, 30th – 31st, and June 6th – 7th), O3 was completely titrated by NO. On the other hand, at the TRF site, which is a forested region downwind of the urban area, O_3 remained at ~ 30 ppbv throughout the night. During the measurement period, measurable amount of $ClNO_2$ were observed at both ground sites (Figure 4.3). The maximum observed $ClNO_2$ was ~ 800 pptv (5 min averaged) and ~ 2.5 ppbv (5 min averaged) at the OP and TRF sites,

respectively. At both sites, $ClNO_2$ started accumulating at sunset and rapidly photolyzed upon sunrise, which was ~ 5:30 local standard time (LST) during the campaign. Nighttime relationship between $ClNO_2$ and Cl_2 varied day by day and did not show a clear correlation. This implies that the sources or potentially loss processes of Cl_2 and $ClNO_2$ were not consistent at night. This is similar to Riedel et al (2012), where they reported a wide range of correlation between Cl_2 and $ClNO_2$ off the coast of LA.

Daytime (11:00 – 18:00, LST) $ClNO_2$ was up to ~100 pptv at OP and ~250 pptv at TRF (Figure 4.4). The level showed a positive correlation with Cl_2, especially in relatively high O_3 conditions (> 50 ppbv). When O_3 was relatively low (< 50 ppbv), Cl_2 production was suppressed, while $ClNO_2$ was not necessarily limited. Excluding the days with low O_3 (i.e., May 26th and 29th for OP and May 6th, 29th, and June 4th for TRF), the relationship between daytime $ClNO_2$ and Cl_2 showed positive correlation with R^2 of 0.49 and 0.80 for OP and TRF, respectively. This positive correlation is consistent with the results reported by Liu et al. (2017) in the North China Plain. In their study, up to ~ 450 pptv of both Cl_2 and $ClNO_2$ was measured during the daytime (10:00 – 20:00, LST), with strong correlation of $R^2 = 0.83$. Cl_2 levels were also suppressed in low O_3 and OH conditions during low solar radiation periods. Therefore, the authors suggested that daytime Cl_2 levels could be positively related to photochemical activities. Considering the short lifetime of Cl_2 and $ClNO_2$ during the day (i.e., 11:00 – 18:00 LST in our study), the levels we observed are likely affected through local production. According to Liu et al. (2017), the air mass showed moderate correlation to SO_2 with possible influences from power plants. However, in this study, the $ClNO_2$ measured at both the OP and TRF sites was uncorrelated with SO_2 ($R^2 = 0.02$), which implies that the air masses that we sampled are not fresh emissions from power plants.

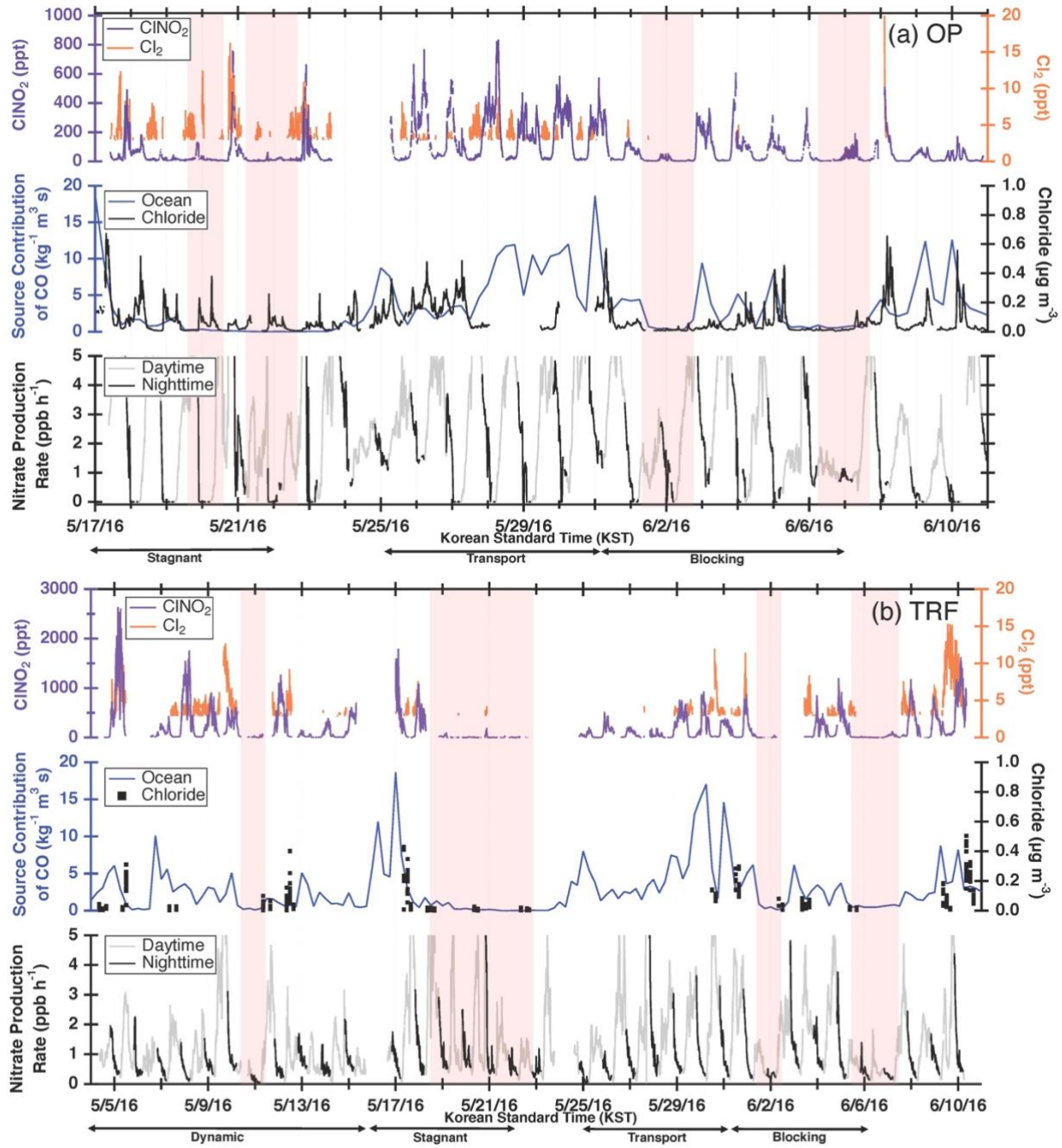

Figure 4.3 $ClNO_2$ and Cl_2 observation results at (a) OP and (b) TRF averaged over 5min. FLEXPART back trajectory analysis were made for source contribution of CO-like substance originating from the ocean, assuming inert CO. Aerosol chloride mass concentration (ambient μg m^{-3}) was measured at the ground for the OP site and on the NASA DC-8 for TRF. For airborne chloride, measurements below 1 km over the TRF site is shown. Red shades are the time frames with limited $ClNO_2$ production. The time frames for each meteorological condition that dominated during the observation period are classified in black arrows at the bottom of the Figures 4.3 (a) and (b).

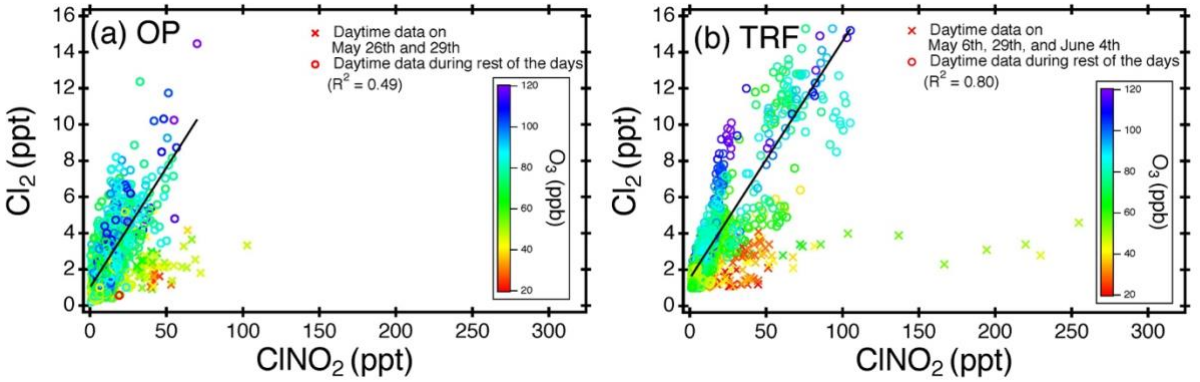

Figure 4.4 Scatter plot of daytime (11:00 – 18:00 local time) $ClNO_2$ and Cl_2 at (a) OP and (b) TRF, color coded with measured O_3. 5 min averaged data for the whole campaign were used for both sites. Data points of Cl_2 below detection limit (2.9 ppt, 2σ , over 30 min) are shown for the purpose of comparison to observed $ClNO_2$ levels.

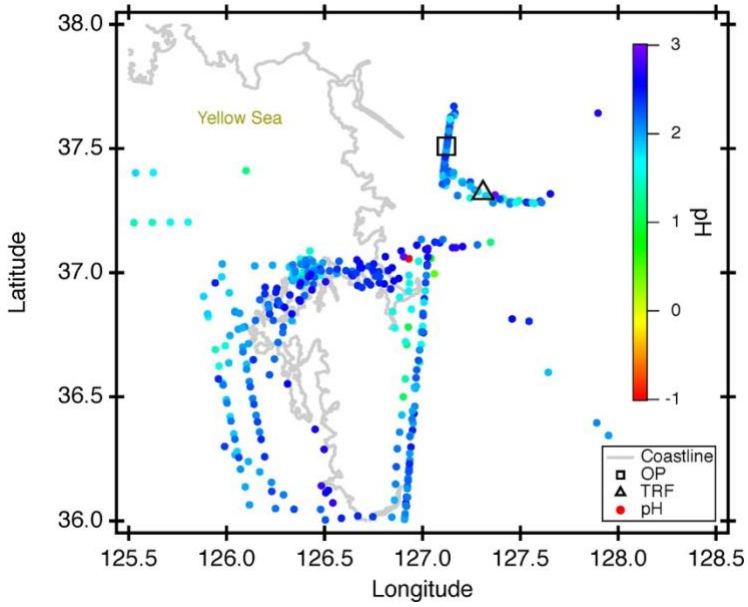

Figure 4.5 Aerosol pH calculated with E-AIM constrained with airborne measurements.

The first possibility we explored is the direct generation of Cl_2 from reactions in acidic particles. $ClNO_2$ is very insoluble ($\gamma_{ClNO2} \approx 10^{-6}$, (Rossi, 2003)) in near-neutral pH. However according to Roberts et al. (2008), γ_{ClNO2} can increase up to 3 orders of magnitude in acidic surfaces (~ pH 1.8) leading to direct production of gas-phase Cl_2. Aerosol acidity was mostly below pH 2 during the campaign, based on thermodynamic calculations, constrained with airborne observations (Figure 4.5). Therefore, the efficiency of this reaction in ambient conditions requires further investigation. Another possibility is the autocatalytic production of Cl from heterogeneous reactions of gas-phase $ClONO_2$ (i.e., $ClONO_{2(g)} + Cl^-_{(aq)} + H^+_{(aq)} \rightarrow Cl_{2(g)} + HNO_3$, (Deiber et al., 2004; Gebel and

Finlayson-Pitts, 2001)) and HOCl (i.e., $HOCl_{(g)} + Cl^-_{(aq)} + H^+_{(aq)} \rightarrow Cl_{2(g)} + H_2O$, (Vogt et al., 1996)) on particles. These reactions are also favored as particle acidity increases. In order to further investigate its possibility, daytime Cl_2 was simulated by constraining the box model with measurements of $ClNO_2$ and other trace gases corresponding to each data point in Figure 4.4. Based on the availability of parameters, we were able to simulate 1680 and 1229 runs for the OP and TRF, respectively. This corresponds to more than 96 % of the daytime data points shown in Figure 4.4. γ_{ClONO2} and γ_{HOCl} were set to 0.06 (Deiber et al., 2004; Hanson et al., 1994; Hanson and Ravishankara, 1994), which is an upper-limit of previous laboratory studies, and the yields were assumed to be unity. HCl generation from hydrogen abstraction of VOCs by Cl were included in the mechanisms used in the model runs. The end points of the 72 hour simulation results are presented in Figure 4.6. As shown in the Figure, the box model simulations were able to reproduce the positive correlation between Cl_2 and $ClNO_2$. Moreover, modeled Cl_2 was suppressed in low O_3 conditions, which corresponds to the observations. This can be explained by Cl reacting with O_3, producing ClO, leading to gas-phase $ClONO_2$ and HOCl production. These can react on acidic aerosols to generated Cl_2. Sources of Cl could be from photo-labile gas-phase chlorine compounds (e.g., Cl_2, $ClNO_2$, $ClONO_2$, HOCl) or oxidation of gas-phase HCl by OH. Although the reaction between HCl and OH is relatively slow ($k = 7.86 \times 10^{-13}$ cm^3 $molecule^{-1}s^{-1}$ at 298 K, (Atkinson et al., 2007)), it has been reported to be a significant source of Cl in the daytime (Riedel et al., 2012). A sensitivity test was carried out by comparing modeled Cl_2 between runs with and without HCl production from oxidation of VOCs by Cl (Figure 4.7 c,d). The results show that production of Cl_2 was suppressed by 40-70 % when HCl was not generated in the model. This significant contribution of gas-phase HCl as a Cl source, should be an upper-limit as the deposition of HCl was not considered in the model. Nonetheless, our analysis leads us to concluded that the

mechanisms we have explored could be the main contributors of the daytime Cl_2 production during KORUS-AQ.

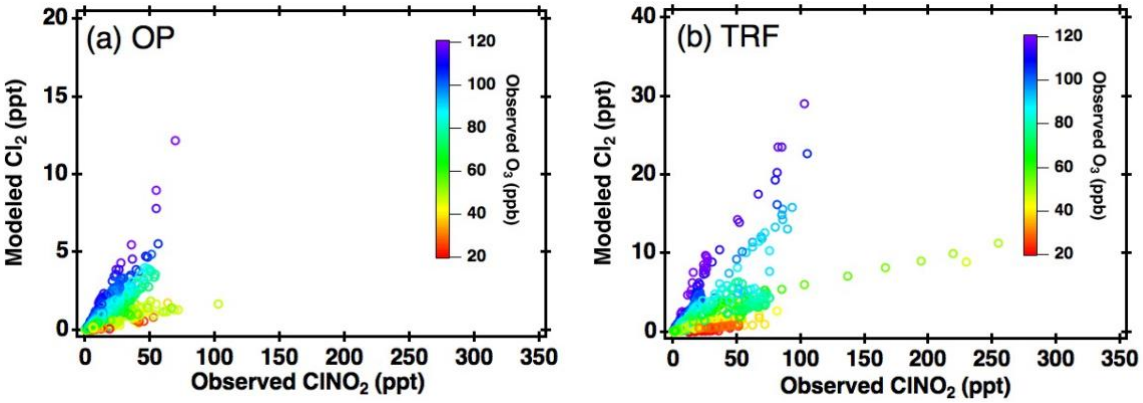

Figure 4.6 Correlation between box model simulated daytime (11:00 – 18:00 local time) Cl_2 and measured $ClNO_2$ at (a) OP and (b) TRF, color coded with measured O_3.

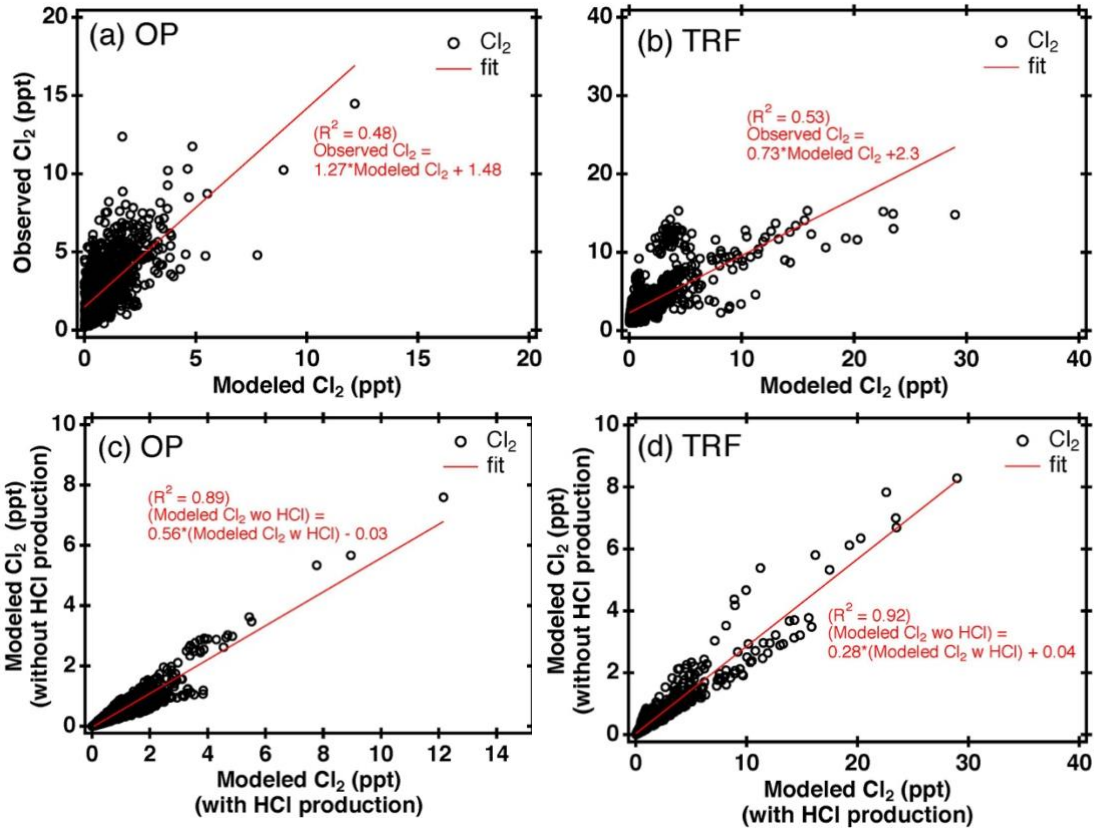

Figure 4.7 Correlation between measured Cl_2 and modeled Cl_2 at (a) OP and (b) TRF. Sensitivity tests of HCl were carried out (c and d) by switching off HCl production from chlorine radicals reacting with VOCs.

4.2.2 Sources of $ClNO_2$

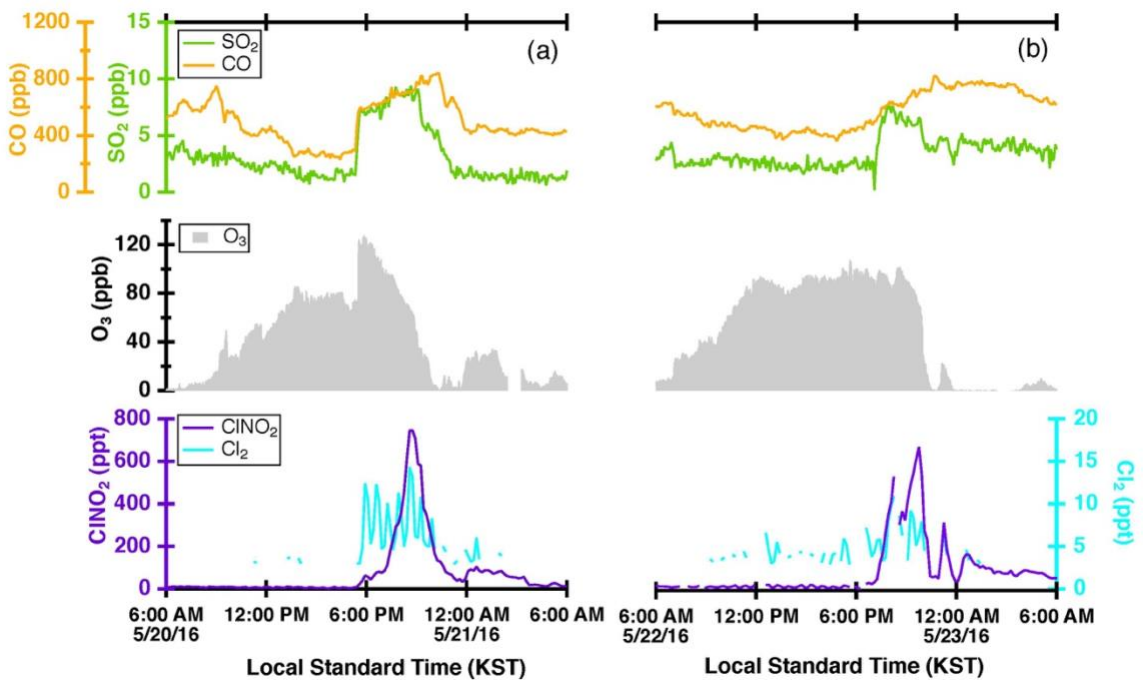

Figure 4.8 Trace gas measurements at the OP site on May 20th and 22nd

FLEXPART source contribution analysis shows that the level of $ClNO_2$ at the ground sites was highly correlated with the origin of the air mass (Figure 4.3). During the nights shaded in red in Figure 4.3 (OP: May 20th, 22nd, June 2nd, and 7th; TRF: May 11th, 19th – 22nd, June 2nd, and June 6th – 7th), there was limited production of $ClNO_2$ at the surface. These periods mostly corresponded to meteorological conditions of stagnation or blocking events, which both resulted in localized air masses to be more dominant with limited influence from the west coast. Stagnation events can be characterized by low wind speeds and increased atmospheric stability, possibly leading to enhanced levels of pollutants like NO_x. Previous studies have shown that stagnant conditions can result in enhanced levels of N_2O_5 driven by high ozone and NO_2. However, $ClNO_2$ production was limited during stagnation events in this study. This is likely due to limited availability of chloride as shown in submicron particle measurements of aerosol mass spectrometer (AMS) at the ground

site for OP and airborne over TRF (Figure 4.3). Whether the chloride is from the ocean or anthropogenic emissions is uncertain since large point sources, such as power plants or petrochemical facilities, are also present along the west coast of the SMA. On the nights of May 20th and May 22nd, rapid changes in air quality were observed with fast shifts in O_3, SO_2, and CO. This corresponded with changes in $ClNO_2$ and Cl_2 (Figure 4.8). These events suggest the importance of boundary layer advection in controlling the $ClNO_2$ levels in the region.

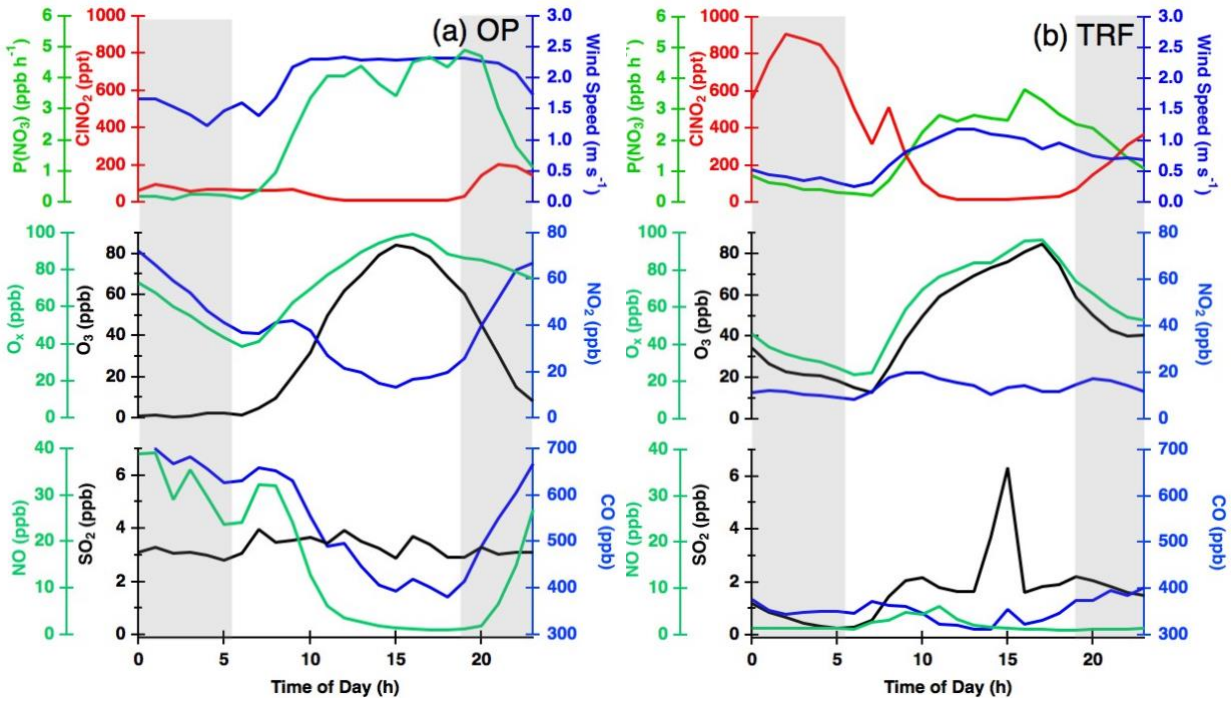

Figure 4.9 Diurnal variation of $ClNO_2$ and other trace gases measured during the campaign and averaged over selected days at (a) OP (7 days) and (b) TRF (9 days). Night time is shown as grey shades.

Different diurnal variations of $ClNO_2$ were observed between OP and TRF (Figure 4.9). The measurements were averaged over selected days (OP: May 18th – 20th, 22nd, 23rd, 29th, June 4th; TRF: May 5th, 8th, 9th, 12th, 17th, 18th, 30th, June 8th, 10th) that showed these two distinct profiles at each site. The description on these profiles are further explained in the following sentences. At

the TRF site (Figure 4.9 (b)), far from direct NO emissions, significant levels of $ClNO_2$ were sustained throughout the night during most of the observation period with rapid photolysis upon sunrise. On the other hand, at OP (Figure 4.9 (a)), $ClNO_2$ started to increase upon sunset, followed by a rapid drop at around 22:00 LST. The trend was consistent with slower nitrate radical production rate ($d[NO_3]/dt = [NO_2][O_3]k$, where $k = 3.52 \times 10^{-17}$ $cm^3molecule^{-1}s^{-1}$ at 298 K, (Atkinson et al., 2004)) as O_3 was titrated to zero by NO close to midnight. The wind direction, SO_2, and CO did not correlate. This suppressed $ClNO_2$ production in urbanized regions with high NO levels, have also been reported by Osthoff et al. (2018). However, significant levels of N_2O_5 and $ClNO_2$ could have been present in the upper part of the surface layer as shown in previous studies (Baasandorj et al., 2017; Young et al., 2012; Yun et al., 2018a). According to Baasandorj et al. (2017), O_3 was completely titrated at the surface in Salt Lake Valley, Utah, while elevated mixing ratios of N_2O_5 were observed at 155 meters above ground level, at a site along the valley wall. On the other hand, airborne measurements at the LA basin (Young et al., 2012) showed a relatively uniform $ClNO_2$ profile throughout the nocturnal boundary layer as O_3 did not change significantly within the observed altitude range (< 600 m). During the 2015 Megacity Air Pollution Study (MAPS, Seoul, 2015), a Cavity Ringdown Spectrometer (CRDS) was installed on top of the Seoul tower in May – June that measured N_2O_5, NO_x, and O_3 (Brown et al., 2017). The elevation of the measurement site was 360 m above sea level (ASL), allowing for sampling further away from direct NO emissions. In their study, the average nighttime O_3 mixing ratio was around 50 ppbv and N_2O_5 was observed most nights, with mixing ratios reaching up to 5 ppbv. Therefore, it is very likely that $ClNO_2$ levels higher than the surface measurements could have been present at higher elevation during the observation period.

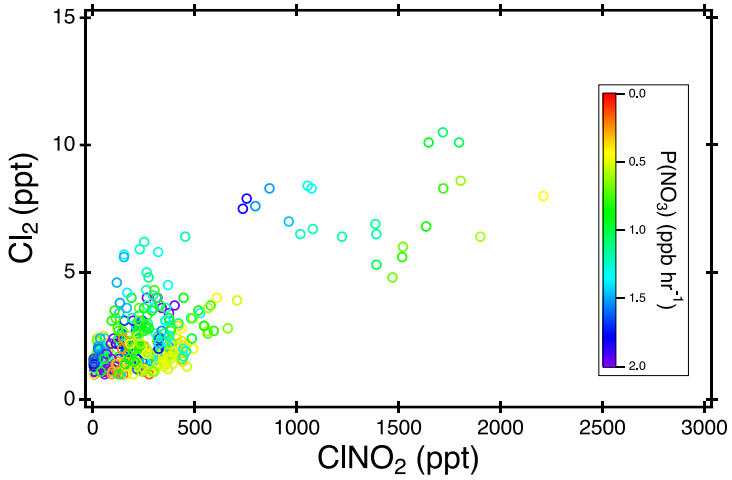

Figure 4.10 Correlation between Cl_2 and $ClNO_2$ measured at 7:00 – 9:00 am local time. Each data point is a 5 min averaged value and is color coded with the calculated production rate of the nitrate radical

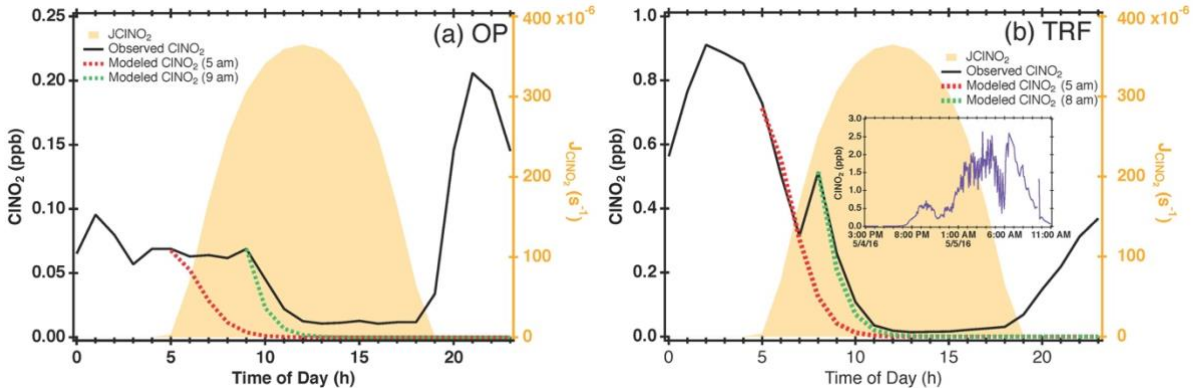

Figure 4.11 Diurnal variation of measured $ClNO_2$ (black line) and simulated $ClNO_2$ from photolytic loss (dashed line). For the red and green dashed lines, the model was constrained with measured $ClNO_2$ at sunrise and at the time when $ClNO_2$ started decreasing, respectively. J_{ClNO2} used for the photolysis was scaled with airborne measurements. The insert in (b) is the $ClNO_2$ measured on May 5th.

At both sites, $ClNO_2$ levels started to increase or sustained after the first 2-3 hours of rapid net loss upon sunrise. In the morning, $ClNO_2$ positively correlated to Cl_2 levels, but did not follow the nitrate production rate at the site (Figure 4.10). Box model simulations, initially constrained with observed $ClNO_2$ level, showed rapid photolysis upon sunrise (Figure 4.11, red dashed line). At TRF, this corresponded to the measurements until 7 – 8 am LST, when a second $ClNO_2$ peak

was observed (Figure 4.9 (b)). This $ClNO_2$ peak in the morning was observed about half the observations days during the campaign. With the net $ClNO_2$ production rate from the observation, and the loss rate from the simulated $ClNO_2$ from photolysis, a production rate of 400 pptv h^{-1} would be required to reconcile the observation. In the case of $ClNO_2$ observed on May 5th at TRF (an insert of Figure 4.11(b)), a maximum of 2.5 ppb h^{-1} of $ClNO_2$ production rate was required in the morning to reconcile the observations. At OP, 18 pptv h^{-1} was required for the 7 averaged days. The $ClNO_2$ production rate required in the morning at TRF was much higher than the previous studies that have also reported high sustained levels of $ClNO_2$ in the morning (i.e., 20 – 200 pptv h^{-1}) (Bannan et al., 2015; Faxon et al., 2015; Tham et al., 2016). In these previous studies, three possibilities have been suggested that could explain the high sustained levels of $ClNO_2$ in the early morning : 1) in-situ generation of $ClNO_2$, 2) transport of $ClNO_2$ within the boundary layer, and 3) entrainment of $ClNO_2$ from residual layer. Each possibility is explored below.

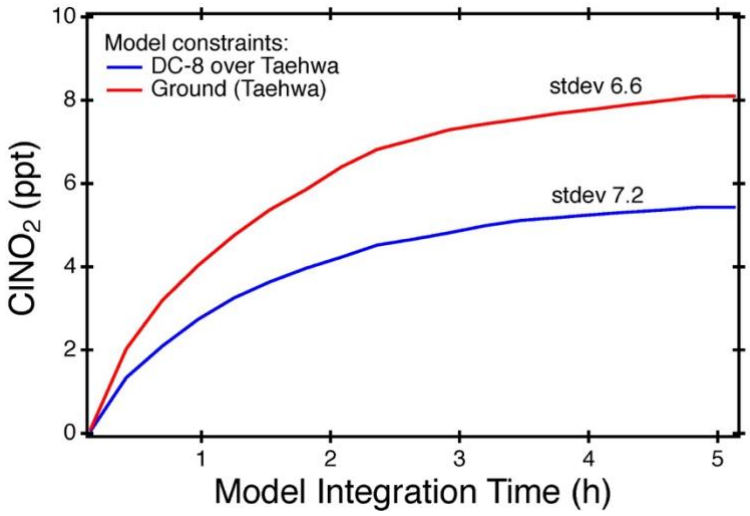

Figure 4.12 Steady state $ClNO_2$, simulated from a box model constrained with airborne measurements (blue) and ground site data form TRF (red), when there was a morning $ClNO_2$, peak. Averaged values of the model runs are shown here with standard deviations

In order to explore the possibility of in-situ formation, box model simulations of $ClNO_2$ production from heterogeneous reaction of N_2O_5 and chloride containing aerosols were conducted. N_2O_5 was calculated assuming a photo-stationary state of NO_3 (Brown et al., 2005). Aerosol surface area was taken from airborne observations over TRF. Based on the box model results in Figure 4.12, even with an assumption of 100% yield, $ClNO_2$ from heterogeneous reaction was not able to reconcile the observed level. Using the dry surface area for the first order loss of N_2O_5 on aerosols would result in an underestimation of $ClNO_2$ production in the model. According to Kim et al. (2017, 2018), hygroscopic growth factor, defined in that study as the ratio of aerosol diameter between wet aerosol at RH 88 % and dry aerosol, was less than 1.5 in the SMA region for particles below 150 nm. Therefore, the discrepancy between observed and modeled $ClNO_2$ of more than 50-fold cannot be reconciled by this underestimation. The box model simulation on gas-phase production of $ClNO_2$ (i.e., $Cl_{(g)} + NO_{2(g)} + M \rightarrow ClONO_{(g)} + M$, $Cl_{(g)} + NO_{2(g)} + M \rightarrow ClNO_{2(g)} + M$) showed at most 2 – 10 pptv of $ClNO_2$ and ClONO (Figure 4.13)

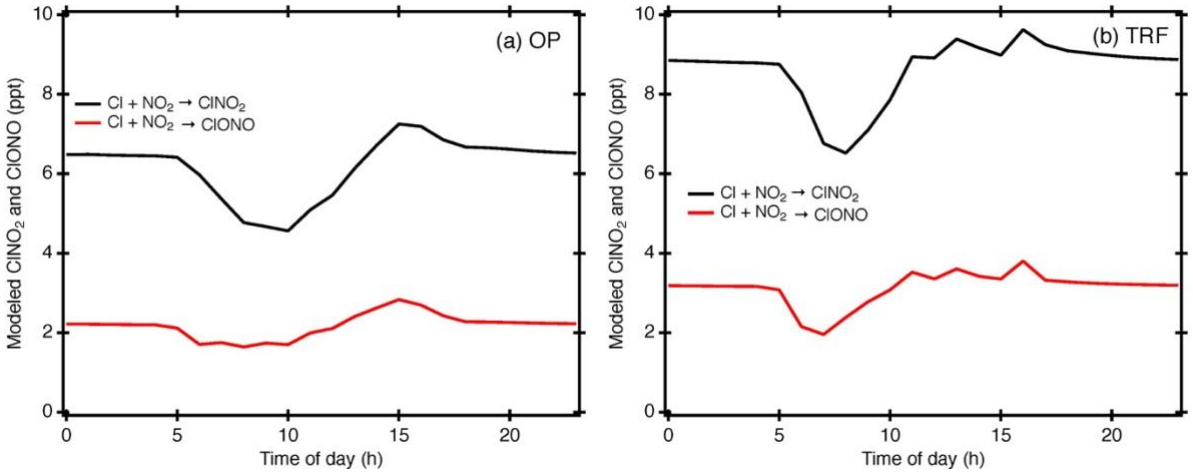

Figure 4.13 Simulated $ClNO_2$ and ClONO produced from gas phase reaction of Cl + NO_2 (i.e., $Cl_{(g)} + NO_{2(g)} + M \rightarrow ClNO_{2(g)} + M$, $k = 3.6 \times 10^{-12}$; $Cl_{(g)} + NO_{2(g)} + M \rightarrow ClONO_{(g)} + M$, $k = 1.63 \times 10^{-12}$). The model was constrained with Cl_2 and NO_2 observation with J values from the aircraft.

Therefore, horizontal or vertical transport from local sources would be the most likely explanation for the high $ClNO_2$ in the morning. Although $ClNO_2$ readily photolyzes during the day ($\tau_{ClNO2} \approx 30$ min at midday), the lifetime could be significantly long enough in the early morning to allow for transport of $ClNO_2$ to the ground sites. Based on the NCAR TUV v 5.2 model, the lifetime of $ClNO_2$, averaged between 5:30 and 8:30 LST was ~ 2 hours under clear sky conditions. Figure 4.14 shows back trajectory analysis initiated at 9 am local time at TRF. At high $ClNO_2$ days with the morning peaks, most of the air masses were from the west. During KORUS, the DC-8 did not fly to the west of the SMA in the early morning. However, there are large point sources, such as petrochemical facilities and industries, and vehicular emissions to the west and south west of the SMA region. Sullivan et al. (2019) reported that this resulted in enhanced levels of O_3 in receptor regions (i.e., Taehwa Research Forest) downwind when westerlies were prevalent. Therefore, favorable conditions such as high chloride content in aerosols from both anthropogenic and natural sources and high levels of NO_x-O_3 could have led to significant levels of $ClNO_2$ to build up and transported to TRF before being completely photolyzed. During the campaign, influence of large biomass burning was negligible as reported in Tang et al. (2018, 2019).

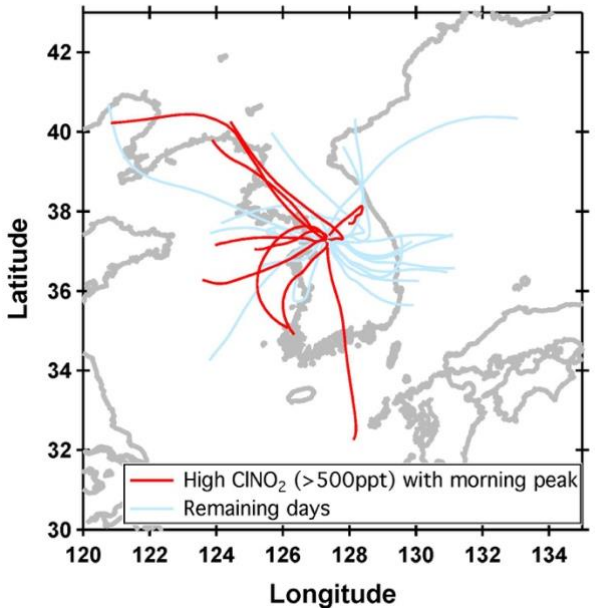

Figure 4.14 FLEXPART back trajectories from Taehwa Research Forest. Trajectories were initialized at 9 am local time and went 24 h backwards. Only the center trajectories with the highest percentage of airmasses are presented. Trajectories for days with high levels of $ClNO_2$ (> 500 pptv) at night are in red and the remaining days are shown in sky blue.

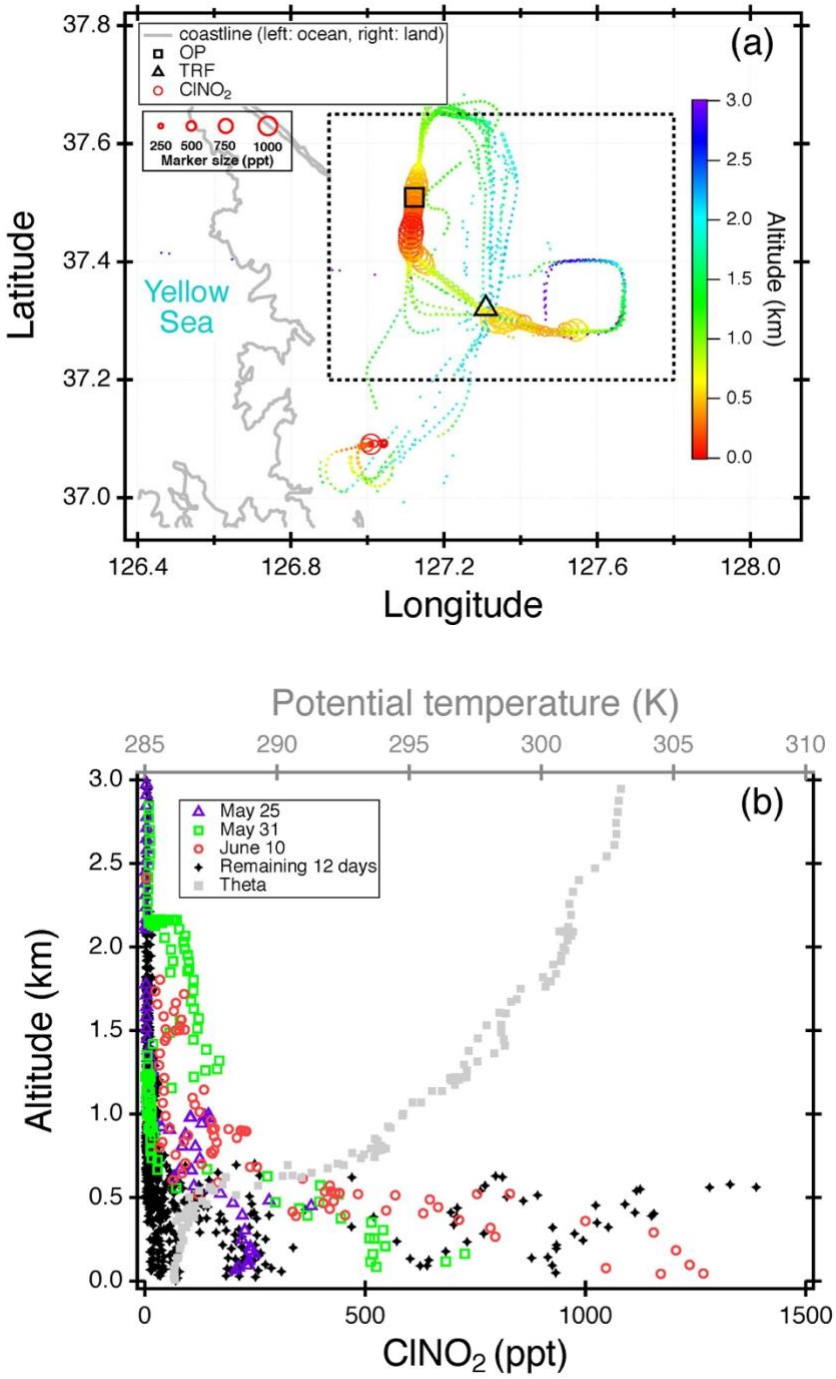

Figure 4.15 (a) Regional and (b) vertical distribution of airborne $ClNO_2$ measured over the Seoul Metropolitan Region (SMA in the morning (8:00 – 8:30 local time).

At night time, the nocturnal boundary layer is decoupled from the residual layer (Stull, 1988), where the pollution from the previous day resides. Being removed from direct NO emissions near the surface, N_2O_5 can effectively accumulate in the residual layer, with the major loss process being heterogeneous reaction on aerosols. Therefore, high levels of NO_2 and O_3 formed during the day can be trapped in the residual layer resulting in significant levels of $ClNO_2$ persisting throughout the night. Figure 4.15, shows (a) regional and (b) vertical distribution of airborne $ClNO_2$ throughout the campaign in the morning (8:00 – 8:30 LST) over the SMA region. During 3 flights (i.e., May 25th, May 31st, and June 10th), $ClNO_2$ was observed in the residual layer with a max of ~ 230pptv. However, the remaining flights observed an average of 17 ± 56 pptv of $ClNO_2$ (black circles). Even the three days (i.e., May 25th, 31st, and June 10th), that $ClNO_2$ was observed in the residual layer, the level (max 230 pptv) could not reconcile the observed levels at the TRF site, which was 342 ± 330 pptv when averaged over the corresponding 3 days at 8:00 – 8:30 LST. However, it is possible that the air mass that was measured by the DC-8 was not representative of the air mass aloft at the west side of the ground observation sites. Backtrajecotry analysis initialized at 9:00 local time showed that the TRF site was affected by both the residual layer and below (Figure 4.16). The enhancement of O_3 and SO_2 concurrent to elevation of $ClNO_2$ could be due to the transport from the residual layer where pollution from high point sources from the other day was trapped within. From the current dataset, it would be difficult to derive a clear conclusion on whether the cause of the significant $ClNO_2$ in the morning was dominantly of transport from horizontal, vertical, or both.

4.2.3 Impacts of $ClNO_2$ on O_3

Cl produced from $ClNO_2$ photolysis can influence the local air quality through reactions with VOCs followed by enhanced production of O_3. The possible impact of Cl initiated reactions on the local chemistry were investigated by running box model simulations constrained with measured $ClNO_2$. A 24 hour diurnal variation of $ClNO_2$ was averaged over the same selected days in Figure 4.9, and these were constrained throughout the model simulations. The results illustrate that when the model was constrained with $ClNO_2$ and Cl initiated chemistry, higher levels of O_3 were simulated compared to the base runs without $ClNO_2$ (Figure 4.17). The averaged net O_3 production rate was enhanced by up to 2 % and 25 % at OP and TRF in the morning and by 1 % to 2 % when averaged during the day. The OP had 7 times lower Cl than the TRF site due to low $ClNO_2$ levels (~ 60 pptv) in the morning. Since the box model simulations in our study did not take into consideration boundary layer height dynamics, emission, and deposition, this net production rate is the results of just chemical production and loss. For OH, the net production rate at TRF increased by 2 % in the morning. The results particularly from TRF are comparable with the previous study in the mountaintop site in Hong Kong, China (Wang et al., 2016). The enhancement of O_3 (max - min). was higher than their moderate $ClNO_2$ case (11 %) but lower than the high $ClNO_2$ plume case (41 %).

4.3 Conclusion

Comprehensive measurements of $ClNO_2$, Cl_2, other trace gases, and aerosol concentrations and properties have been conducted on the NASA DC-8 and at two ground sites during the KORUS-AQ 2016 field campaign. The observed averaged diurnal variations are largely consistent with the previous observations and our understanding on the photochemistry of $ClNO_2$. The

presence of ClNO2 was substantially suppressed during strong stagnation events, which could have prevented the transport of chloride near the coast. During the night, Cl_2 and $ClNO_2$ levels were not correlated while moderate to strong positive relationships were observed at daytime. Through box model simulations, we presented a quantitative analysis of the daytime observations. The results showed that heterogeneous reactions of $ClONO_2$ and HOCl in acidic aerosols may be responsible for the positive correlation between Cl2 and $ClNO_2$, as well as its dependency on O_3. The second $ClNO_2$ peak in the morning, observed 4 – 5 hours after sunrise, required a significant source of $ClNO_2$ (up to 2.5 ppbv h^{-1}). Previous studies have attributed high sustained $ClNO_2$ in the morning to transport from the residual layer (Tham et al., 2016; Wang et al., 2016). In this study, box model runs of heterogeneous and gas-phase production of $ClNO_2$ could not reconcile the observed levels. Airborne observations near the ground sites in the early morning showed negligible $ClNO_2$ levels in the residual layer in most of the days. However, there is still a possibility of the contribution of vertical transport from the residual layer. Although the current data set is limited for us to pinpoint on the vertical locations (i.e., boundary layer v.s. residual layer), back trajectories suggest that $ClNO_2$ rich air masses were mostly transported from the west, where there are significant sources of precursors. This shows that different meteorological or chemical conditions of the sites can lead to various causes of high $ClNO_2$ levels in the early morning. Finally, box model simulations constrained with observations suggest that Cl initiated chemistry can lead up to ~ 25 % increase of net chemical O_3 production rate in the morning.

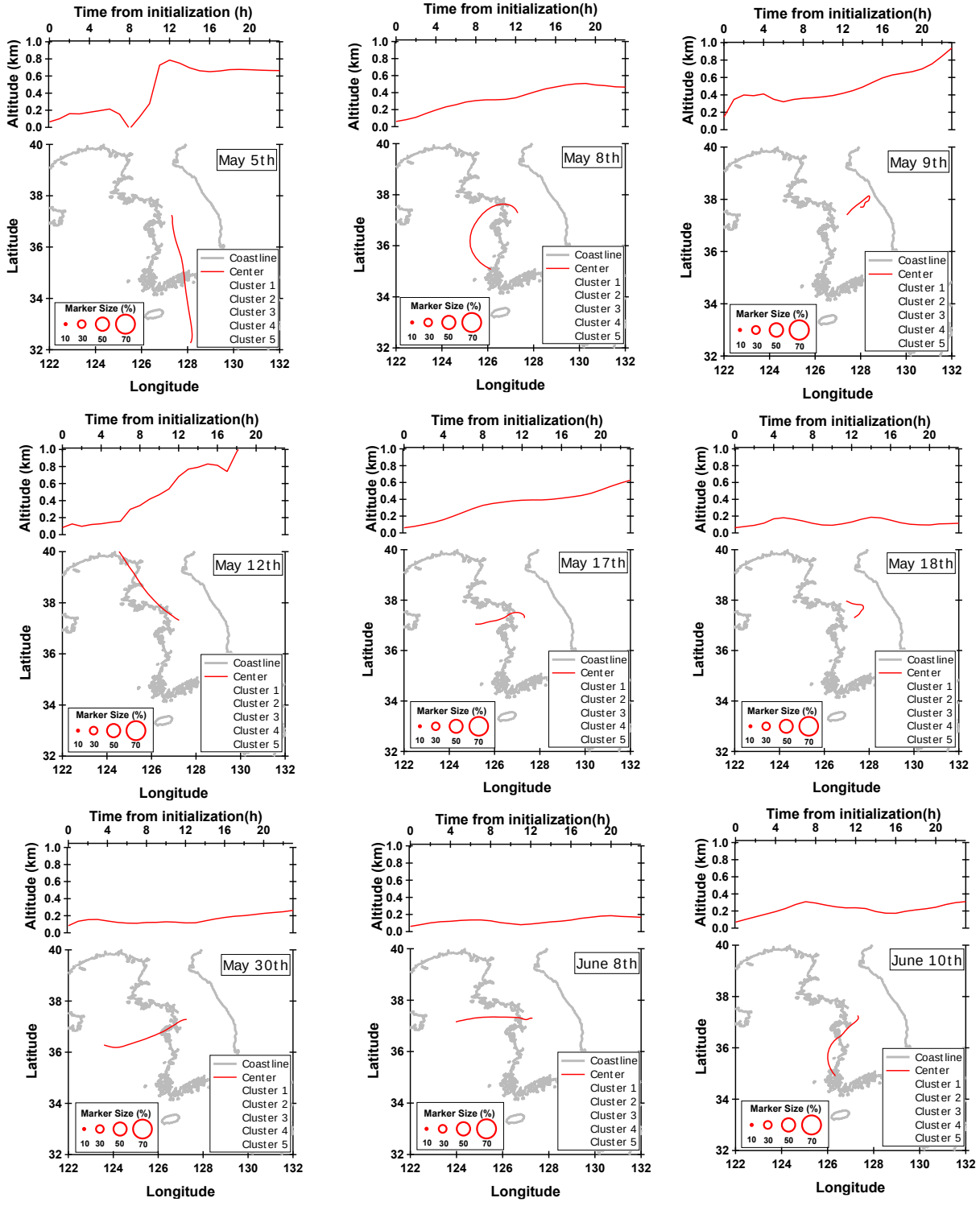

Figure 4.16 FLEXPART backtrajectories of the selected days when a second $ClNO_2$ peak was observed at TRF. Each run was initialized at 9:00 local time and each marker is an hour backward of its previous. The red line represents the center of the mass-weighted particles and the clusters are fractional contributions of airmasses in percentage.

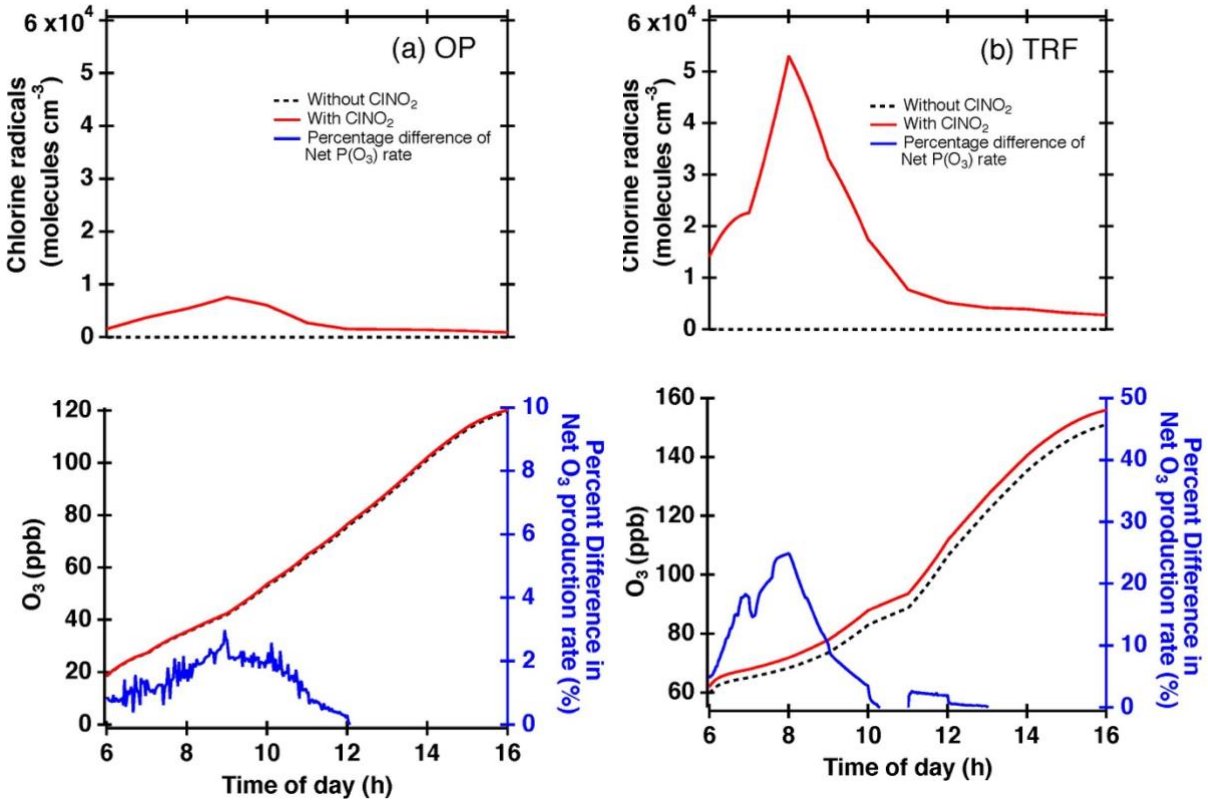

Figure 4.17 Box model simulations of chlorine radicals and O_3 at (OP) and (b) TRF, constrained with $ClNO_2$ and other trace gases observed during the field campaign. Percent difference of net O_3 production rate (NetP(O_3), blue line) was calculated from the difference of the NetP(O_3) between simulations with and without $ClNO_2$ constrained in the model (i.e., 100*(w$ClNO_2$ – wo$ClNO_2$)/wo$ClNO_2$).

4.4 References

Atkinson, R.: Gas-Phase Tropospheric Chemistry of Volatile Organic Compounds: 1. Alkanes and Alkenes, J. Phys. Chem. Ref. Data, 26(2), 215–290, doi:10.1063/1.556012, 1997.

Atkinson, R. and Arey, J.: Gas-phase tropospheric chemistry of biogenic volatile organic compounds: A review, Atmos. Environ., 37(SUPPL. 2), doi:10.1016/S1352-2310(03)00391-1, 2003.

Atkinson, R., Baulch, D. L., Cox, R. A., Crowley, J. N., Hampson, R. F., Hynes, R. G., Jenkin, M. E., Rossi, M. J. and Troe, J.: Evaluated kinetic and photochemical data for atmospheric chemistry: Volume I - gas phase reactions of O_x, HO_x, NO_x and SO_x species, Atmos. Chem.

Phys., 4(6), 1461–1738, doi:10.5194/acp-4-1461-2004, 2004.
Atkinson, R., Baulch, D. L., Cox, R. A., Crowley, J. N., Hampson, R. F., Hynes, R. G., Jenkin, M. E., Rossi, M. J. and Troe, J.: Evaluated kinetic and photochemical data for atmospheric chemistry: Volume III - Gas phase reactions of inorganic halogens, Atmos. Chem. Phys., 7(4), 981–1191, doi:10.5194/acp-7-981-2007, 2007.
Baasandorj, M., Hoch, S. W., Bares, R., Lin, J. C., Brown, S. S., Millet, D. B., Martin, R., Kelly, K., Zarzana, K. J., Whiteman, C. D., Dube, W. P., Tonnesen, G., Jaramillo, I. C. and Sohl, J.: Coupling between Chemical and Meteorological Processes under Persistent Cold-Air Pool Conditions: Evolution of Wintertime PM2.5 Pollution Events and N_2O_5 Observations in Utah's Salt Lake Valley, Environ. Sci. Technol., 51(11), 5941–5950, doi:10.1021/acs.est.6b06603, 2017.
Bannan, T. J., Booth, a M., Bacak, A., Muller, J. B. a, Leather, K. E., Breton, M. Le, Jones, B., Young, D., Coe, H., Allan, J., Visser, S., Slowik, J. G., Furger, M., Prévôt, A. S. H., Lee, J., Dunmore, R. E., Hopkins, J. R., Hamilton, J. F., Lewis, A. C., Whalley, L. K., Sharp, T., Stone, D., Heard, D. E., Fleming, Z. L., Leigh, R., Shallcross, D. E. and Percival, C. J.: Journal of Geophysical Research : Atmospheres of the role of Cl atom oxidation, J. Geophys. Res. Atmos., 120, 1–20, doi:10.1002/2014JD022629, 2015.
Behnke, W., George, C., Scheer, V. and Zetzsch, C.: Production and decay of $ClNO_2$ from the reaction of gaseous N_2O_5 with NaCl solution: Bulk and aerosol experiments, J. Geophys. Res. Atmos., 102(D3), 3795–3804, doi:10.1029/96JD03057, 1997.
Bertram, T. H. and Thornton, J. A.: Toward a general parameterization of N_2O_5 reactivity on aqueous particles: the competing effects of particle liquid water, nitrate and chloride, Atmos. Chem. Phys., 9(21), 8351–8363, doi:10.5194/acp-9-8351-2009, 2009.
Blanchard, D.: The oceanic production of atmospheric sea salt, J. Geophys. Res., 90(C1), 961–963 doi:10.1029/JC090iC01p00961, 1985.
Brown, S. S., Osthoff, H. D., Stark, H., Dubé, W. P., Ryerson, T. B., Warneke, C., de Gouw, J. A., Wollny, A. G., Parrish, D. D., Fehsenfeld, F. C. and Ravishankara, A. R.: Aircraft observations of daytime NO_3 and N_2O_5 and their implications for tropospheric chemistry, J. Photochem. Photobiol. A Chem., 176(1-3 SPEC. ISS.), 270–278, doi:10.1016/j.jphotochem.2005.10.004, 2005.
Brown, S. S., Dubé, W. P., Fuchs, H., Ryerson, T. B., Wollny, A. G., Brock, C. A., Bahreini, R., Middlebrook, A. M., Neuman, T. A., Atlas, E., Roberts, J. M., Osthoff, H. D., Trainer, M., Fehsenfeld, F. C. and Ravishankara, A. R.: Reactive uptake coefficients for N_2O_5 determined from aircraft measurements during the Second Texas Air Quality Study: Comparison to current model parameterizations, J. Geophys. Res. Atmos., 114(11), 1–16, doi:10.1029/2008JD011679, 2009.
Brown, S. S., An, H.-J., Lee, M., Park, J.-H., Lee, S.-D., Fibiger, D. L., McDuffie, E. E., Dubé, W. P., Wagner, N. L. and Min, K.-E.: Cavity enhanced spectroscopy for measurement of nitrogen oxides in the Anthropocene: results from the Seoul tower during MAPS 2015, Faraday Discuss., 1039, doi:10.1039/C7FD00001D, 2017.
Chang, W. L., Brown, S. S., Stutz, J., Middlebrook, A. M., R., B., Wagner, N. L., Dube, W. P., Pollack, I. B., Ryerson, T. B. and Riemer, N.: Evaluating N_2O_5 heterogeneous hydrolysis parameterizations for CalNex 2010, J. Geophys. Res., 121, 5051–5070, doi:10.1002/2015JD024737, 2016.
Chen, Q., Schmidt, J. A., Shah, V., Jaeglé, L., Sherwen, T. and Alexander, B.: Sulfate production by reactive bromine: Implications for the global sulfur and reactive bromine budgets,

Geophys. Res. Lett., 44(13), 7069–7078, doi:10.1002/2017GL073812, 2017.
Colman, J. J., Swanson, A. L., Meinardi, S., Sive, B. C., Blake, D. R. and Rowland, F. S.: Description of the analysis of a wide range of volatile organic compounds in whole air samples collected during PEM-Tropics A and B, Anal. Chem., 73(15), 3723–3731, doi:10.1021/ac010027g, 2001.
Deiber, G., George, C., Le Calvé, S., Schweitzer, F. and Mirabel, P.: Uptake study of $ClONO_2$ and $BrONO_2$ by Halide containing droplets, Atmos. Chem. Phys., 4(5), 1291–1299, doi:10.5194/acp-4-1291-2004, 2004.
Faxon, C., Bean, J. and Ruiz, L.: Inland Concentrations of Cl_2 and $ClNO_2$ in Southeast Texas Suggest Chlorine Chemistry Significantly Contributes to Atmospheric Reactivity, Atmosphere, 6(10), 1487–1506, doi:10.3390/atmos6101487, 2015.
Finlayson-Pitts, B. J.: Chlorine Atoms as a Potential Tropospheric Oxidant in the Marine Boundary Layer, Res. Chem. Intermed., 19(3), 235–249, doi:10.1163/156856793X00091, 1993.
Finlayson-Pitts, B. J., Ezell, M. J. and Pitts Jr., J. N.: Formation of chemically active chlorine compounds by reactions of atmospheric NaCl particles with gaseous N_2O_5 and $ClONO_2$, Nature, 337(19), 1989.
Frenzel, A., Scheer, V., Sikorski, R., George, C., Behnke, W. and Zetzsch, C.: Heterogeneous Interconversion Reactions of $BrNO_2$, $ClNO_2$, Br_2, and Cl_2, J. Phys. Chem. A, 102(8), 1329–1337, doi:10.1021/jp973044b, 1998.
Fu, X., Wang, T., Wang, S., Zhang, L., Cai, S., Xing, J. and Hao, J.: Anthropogenic Emissions of Hydrogen Chloride and Fine Particulate Chloride in China, Environ. Sci. Technol., 52(3), 1644–1654, doi:10.1021/acs.est.7b05030, 2018.
Gebel, M. E. and Finlayson-Pitts, B. J.: Uptake and reaction of $ClONO_2$ on NaCl and synthetic sea salt, J. Phys. Chem. A, 105(21), 5178–5187, doi:10.1021/jp0046290, 2001.
George, C., Behnke, W., Scheer, V., Zetzsch, C., Magi, L., Ponche, J. L. and Mirabel, P.: Fate of $ClNO_2$ Over Aqueous Solutions Containing Iodide, Geophys. Res. Lett., 22(12), 1505, doi:10.1029/95GL01417, 1995.
Hanson, D. R. and Ravishankara, A. R.: Reactive Uptake of $ClONO_2$ onto Sulfuric Acid Due to Reaction with HCl and H_2O, J. Phy. Chem., 98(22), 5728–5735, doi:10.1021/j100073a026, 1994.
Hanson, D. R., Ravishankara, a. R. and Solomon, S.: Heterogeneous reactions in sulfuric acid aerosols: A framework for model calculations, J. Geophys. Res., 99(D2), 3615, doi:10.1029/93JD02932, 1994.
Hinrichsen, D.: Costal Waters of the World: Trends, Threats, and Strategies, Island Press, Washington, DC. [online] Available from: http://arp.sagepub.com/content/30/4/473, 1998.
Hov, O.: The effect of chlorine on the formation of photochemical oxidants in Southern Telemark, Norway, Atmos. Environ., 19(3), 471–485, doi:10.1016/0004-6981(85)90168-4, 1985.
Hu, J. H. and Abbatt, J. P. D.: Reaction probabilities for N2O5 hydrolysis on sulfuric acid and ammonium sulfate aerosols at room temperature, J. Phys. Chem. A, 101(5), 871–878, doi:10.1021/jp9627436, 1997.
Kim, N., Park, M., Yum, S. S., Park, J. S., Song, I. H., Shin, H. J., Ahn, J. Y., Kwak, K. H., Kim, H., Bae, G. N. and Lee, G.: Hygroscopic properties of urban aerosols and their cloud condensation nuclei activities measured in Seoul during the MAPS-Seoul campaign, Atmos. Environ., 153, 217–232, doi:10.1016/j.atmosenv.2017.01.034, 2017.
Kim, N., Park, M., Yum, S. S., Park, J. S., Shin, H. J. and Ahn, J. Y.: Impact of urban aerosol properties on cloud condensation nuclei (CCN) activity during the KORUS-AQ field

campaign, Atmos. Environ., 185(December 2017), 221–236, doi:10.1016/j.atmosenv.2018.05.019, 2018.

Kim, S., Kim, S. Y., Lee, M., Shim, H., Wolfe, G. M., Guenther, A. B., He, A., Hong, Y. and Han, J.: Impact of isoprene and HONO chemistry on ozone and OVOC formation in a semirural South Korean forest, Atmos. Chem. Phys., 15(8), 4357–4371, doi:10.5194/acp-15-4357-2015, 2015.

Kim, S., Sanchez, D., Wang, M., Seco, R., Jeong, D., Hughes, S., Barletta, B., Blake, D. R., Jung, J., Kim, D., Lee, G., Lee, M., Ahn, J., Lee, S. D., Cho, G., Sung, M. Y., Lee, Y. H., Kim, D. B., Kim, Y., Woo, J. H., Jo, D., Park, R., Park, J. H., Hong, Y. D. and Hong, J. H.: OH reactivity in urban and suburban regions in Seoul, South Korea-an East Asian megacity in a rapid transition, Faraday Discuss., 189, 231–251, doi:10.1039/c5fd00230c, 2016.

Knipping, E. M. and Dabdub, D.: Impact of chlorine emissions from sea-salt aerosol on coastal urban ozone, Environ. Sci. Technol., 37(2), 275–284, doi:10.1021/es025793z, 2003.

Lee, B. H., Lopez-Hilfiker, F. D., Schroder, J. C., Campuzano-Jost, P., Jimenez, J. L., McDuffie, E. E., Fibiger, D. L., Veres, P. R., Brown, S. S., Campos, T. L., Weinheimer, A. J., Flocke, F. F., Norris, G., O'Mara, K., Green, J. R., Fiddler, M. N., Bililign, S., Shah, V., Jaegle, L. and Thornton, J. A.: Airborne observations of reactive inorganic chlorine and bromine species in the exhaust of coal-fired power plants, J. Geophys. Res. Atmos., 123, 11225–11237, doi:10.1029/2018JD029284, 2018.

Li, Q., Zhang, L., Wang, T., Tham, Y. J., Ahmadov, R., Xue, L., Zhang, Q. and Zheng, J.: Impacts of heterogeneous uptake of dinitrogen pentoxide and chlorine activation on ozone and reactive nitrogen partitioning: Improvement and application of the WRF-Chem model in southern China, Atmos. Chem. Phys., 16(23), 14875–14890, doi:10.5194/acp-16-14875-2016, 2016.

Liu, X., Qu, H., Huey, L. G., Wang, Y., Sjostedt, S., Zeng, L., Lu, K., Wu, Y., Hu, M., Shao, M., Zhu, T. and Zhang, Y.: High Levels of Daytime Molecular Chlorine and Nitryl Chloride at a Rural Site on the North China Plain, Environ. Sci. Technol., 51(17), 9588–9595, doi:10.1021/acs.est.7b03039, 2017.

Lowe, D., Archer-Nicholls, S., Morgan, W., Allan, J., Utembe, S., Ouyang, B., Aruffo, E., Le Breton, M., Zaveri, R. A., Di Carlo, P., Percival, C., Coe, H., Jones, R. and McFiggans, G.: WRF-Chem model predictions of the regional impacts of N_2O_5 heterogeneous processes on night-time chemistry over north-western Europe, Atmos. Chem. Phys., 15(3), 1385–1409, doi:10.5194/acp-15-1385-2015, 2015.

Madronich, S. and Flocke, S.: Handbook of Environmental Chemistry, in Handbook of Environmental Chemistry, pp. 1–26, Springer_Verlag, Heidelberg., 1998.

Malko, M. W. and Troe, J.: Analysis of the unimolecular reaction $N_2O_5 + M \rightleftharpoons NO_2 + NO_3 + M$, Int. J. Chem. Kinet., 14(4), 399–416, doi:10.1002/kin.550140407, 1982.

McDuffie, E. E., Fibiger, D. L., Dubé, W. P., Lopez Hilfiker, F., Lee, B. H., Jaeglé, L., Guo, H., Weber, R. J., Reeves, J. M., Weinheimer, A. J., Schroder, J. C., Campuzano-Jost, P., Jimenez, J. L., Dibb, J. E., Veres, P., Ebben, C., Sparks, T. L., Wooldridge, P. J., Cohen, R. C., Campos, T., Hall, S. R., Ullmann, K., Roberts, J. M., Thornton, J. A. and Brown, S. S.: $ClNO_2$ Yields From Aircraft Measurements During the 2015 WINTER Campaign and Critical Evaluation of the Current Parameterization, J. Geophys. Res. Atmos., 123(22), 12,994-13,015, doi:10.1029/2018JD029358, 2018a.

McDuffie, E. E., Fibiger, D. L., Dubé, W. P., Lopez-Hilfiker, F., Lee, B. H., Thornton, J. A., Shah, V., Jaeglé, L., Guo, H., Weber, R. J., Michael Reeves, J., Weinheimer, A. J., Schroder, J.

C., Campuzano-Jost, P., Jimenez, J. L., Dibb, J. E., Veres, P., Ebben, C., Sparks, T. L., Wooldridge, P. J., Cohen, R. C., Hornbrook, R. S., Apel, E. C., Campos, T., Hall, S. R., Ullmann, K. and Brown, S. S.: Heterogeneous N_2O_5 uptake during winter: Aircraft measurements during the 2015 WINTER campaign and critical evaluation of current parameterizations, J. Geophys. Res. Atmos., 4345–4372, doi:10.1002/2018JD028336, 2018b.

Mielke, L. H., Furgeson, A. and Osthoff, H. D.: Observation of $ClNO_2$ in a mid-continental urban environment, Environ. Sci. Technol., 45, 8889–96, doi:10.1021/es201955u, 2011.

Morgan, W. T., Ouyang, B., Allan, J. D., Aruffo, E., Di Carlo, P., Kennedy, O. J., Lowe, D., Flynn, M. J., Rosenberg, P. D., Williams, P. I., Jones, R., McFiggans, G. B. and Coe, H.: Influence of aerosol chemical composition on N_2O_5 uptake: airborne regional measurements in northwestern Europe, Atmos. Chem. Phys., 15(2), 973–990, doi:10.5194/acp-15-973-2015, 2015.

Müller, M., Mikoviny, T., Feil, S., Haidacher, S., Hanel, G., Hartungen, E., Jordan, A., Märk, L., Mutschlechner, P., Schottkowsky, R., Sulzer, P., Crawford, J. H. and Wisthaler, A.: A compact PTR-ToF-MS instrument for airborne measurements of volatile organic compounds at high spatiotemporal resolution, Atmos. Meas. Tech., 7(11), 3763–3772, doi:10.5194/amt-7-3763-2014, 2014.

Nault, B. A., Campuzano-Jost, P., Day, D. A., Schroder, J. C., Anderson, B., Beyersdorf, A. J., Blake, D. R., Brune, W. H., Choi, Y., Corr, C. A., de Gouw, J. A., Dibb, J., DiGangi, J. P., Diskin, G. S., Fried, A., Huey, L. G., Kim, M. J., Knote, C. J., Lamb, K. D., Lee, T., Park, T., Pusede, S. E., Scheuer, E., Thornhill, K. L., Woo, J.-H. and Jimenez, J. L.: Secondary organic aerosol production from local emissions dominates the organic aerosol budget over Seoul, South Korea, during KORUS-AQ, Atmos. Chem. Phys., 18(24), 17769–17800, doi:10.5194/acp-18-17769-2018, 2018.

Neumann, B., Vafeidis, A. T., Zimmermann, J. and Nicholls, R. J.: Future coastal population growth and exposure to sea-level rise and coastal flooding - A global assessment, PLoS One, 10(3), doi:10.1371/journal.pone.0118571, 2015.

Osthoff, H. D., Roberts, J. M., Ravishankara, A. R., Williams, E. J., Lerner, B. M., Sommariva, R., Bates, T. S., Coffman, D., Quinn, P. K., Dibb, J. E., Stark, H., Burkholder, J. B., Talukdar, R. K., Meagher, J., Fehsenfeld, F. C. and Brown, S. S.: High levels of nitryl chloride in the polluted subtropical marine boundary layer, Nat. Geosci., 1(5), 324–328, doi:10.1038/ngeo177, 2008.

Osthoff, H. D., Odame-ankrah, C. A., Tokarek, T. W., Taha, Y. M. and Corinne, L.: Low Levels of Nitryl Chloride in the Lower Fraser Valley of British Columbia, Atmos. Chem. Phys., 18, 6293–6315, 2018.

Park, M. S., Park, S. H., Chae, J. H., Choi, M. H., Song, Y., Kang, M. and Roh, J. W.: High-resolution urban observation network for user-specific meteorological information service in the Seoul Metropolitan Area, South Korea, Atmos. Meas. Tech., 10(4), 1575–1594, doi:10.5194/amt-10-1575-2017, 2017.

Phillips, G. J., Thieser, J., Tang, M., Sobanski, N., Schuster, G., Fachinger, J., Drewnick, F., Borrmann, S., Bingemer, H., Lelieveld, J. and Crowley, J. N.: Estimating N_2O_5 uptake coefficients using ambient measurements of NO_3, N_2O_5, $ClNO_2$ and particle-phase nitrate, Atmos. Chem. Phys., 16(20), 13231–13249, doi:10.5194/acp-16-13231-2016, 2016.

Reff, A., Bhave, P. V., Simon, H., Pace, T. G., Pouliot, G. A., Mobley, J. D. and Houyoux, M.: Emissions Inventory of PM2.5 Trace Elements across the United States, Environ. Sci.

Technol., 43(15), 5790–5796, doi:10.1021/es802930x, 2009.
Riedel, T. P., Bertram, T. H., Crisp, T. A., Williams, E. J., Lerner, B. M., Vlasenko, A., Li, S. M., Gilman, J., De Gouw, J., Bon, D. M., Wagner, N. L., Brown, S. S. and Thornton, J. A.: Nitryl chloride and molecular chlorine in the coastal marine boundary layer, Environ. Sci. Technol., 46(19), 10463–10470, doi:10.1021/es204632r, 2012.
Riedel, T. P., Wagner, N. L., Dubé, W. P., Middlebrook, A. M., Young, C. J., Öztürk, F., Bahreini, R., Vandenboer, T. C., Wolfe, D. E., Williams, E. J., Roberts, J. M., Brown, S. S. and Thornton, J. A.: Chlorine activation within urban or power plant plumes: Vertically resolved ClNO2 and Cl2 measurements from a tall tower in a polluted continental setting, J. Geophys. Res. Atmos., 118(15), 8702–8715, doi:10.1002/jgrd.50637, 2013.
Roberts, J. M., Osthoff, H. D., Brown, S. S. and Ravishankara, A. R.: N2O5 oxidizes chloride to Cl2 in acidic atmospheric aerosol, Science, 321(5892), 1059, doi:10.1126/science.1158777, 2008.
Rossi, M. J.: Heterogeneous Reactions on Salts, Chem. Rev., 103(12), 4823–4882, doi:10.1021/cr020507n, 2003.
Ryder, O. S., Campbell, N. R., Shaloski, M., Al-Mashat, H., Nathanson, G. M. and Bertram, T. H.: Role of Organics in Regulating $ClNO_2$ Production at the Air–Sea Interface, J. Phys. Chem. A, 119(31), 8519–8526, doi:10.1021/jp5129673, 2015.
Sarwar, G., Simon, H., Bhave, P. and Yarwood, G.: Examining the impact of heterogeneous nitryl chloride production on air quality across the United States, Atmos. Chem. Phys., 12(14), 6455–6473, doi:10.5194/acp-12-6455-2012, 2012.
Sarwar, G., Simon, H., Xing, J. and Mathur, R.: Importance of tropospheric $ClNO_2$ chemistry across the Northern Hemisphere, Geophys. Res. Lett., 41(11), 4050–4058, doi:10.1002/2014GL059962, 2014.
Schweitzer, F., Mirabel, P. and George, C.: Multiphase Chemistry of N_2O_5, $ClNO_2$, and $BrNO_2$, J. Phys. Chem. A, 102(22), 3942–3952, doi:10.1021/jp980748s, 1998.
Sherwen, T., Schmidt, J. A., Evans, M. J., Carpenter, L. J., Großmann, K., Eastham, S. D., Jacob, D. J., Dix, B., Koenig, T. K., Sinreich, R., Ortega, I., Volkamer, R., Saiz-Lopez, A., Prados-Roman, C., Mahajan, A. S. and Ordóñez, C.: Global impacts of tropospheric halogens (Cl, Br, I) on oxidants and composition in GEOS-Chem, Atmos. Chem. Phys., 16, 12239–12271, doi:10.5194/acp-16-12239-2016, 2016.
Sherwen, T., Evans, M. J., Sommariva, R., Hollis, L. D. J., Ball, S. M., Monks, P. S., Reed, C., Carpenter, L. J., Lee, J. D., Forster, G., Bandy, B., Reeves, C. E. and Bloss, W. J.: Effects of halogens on European air-quality, Faraday Discuss., 200, 75–100, doi:10.1039/c7fd00026j, 2017.
Shetter, R. E. and Müller, M.: Photolysis frequency measurements using actinic flux spectroradiometry during the PEM-Tropics mission: Instrumentation description and some results, J. Geophys. Res. Atmos., 104(D5), 5647–5661, doi:10.1029/98JD01381, 1999.
Simon, H., Kimura, Y., McGaughey, G., Allen, D. T., Brown, S. S., Osthoff, H. D., Roberts, J. M., Byun, D. and Lee, D.: Modeling the impact of $ClNO_2$ on ozone formation in the Houston area, J. Geophys. Res., 114, D00F03, doi:10.1029/2008JD010732, 2009.
Slusher, D. L., Huey, L. G., Tanner, D. J., Flocke, F. M. and Roberts, J. M.: A thermal dissociation - Chemical ionization mass spectrometry (TD-CIMS) technique for the simultaneous measurement of peroxyacyl nitrates and dinitrogen pentoxide, J. Geophys. Res. D Atmos., 109(19), 1–13, doi:10.1029/2004JD004670, 2004.
Stull, R. B.: An introduction to boundary layer meteorology, Dordrecht; Boston : Kluwer

Academic Publishers., 1988.
Sullivan, J. T., McGee, T. J., Sumnicht, G. K., Twigg, L. W. and Hoff, R. M.: A mobile differential absorption lidar to measure sub-hourly fluctuation of tropospheric ozone profiles in the Baltimore-Washington, D.C. region, Atmos. Meas. Tech., 7(10), 3529–3548, doi:10.5194/amt-7-3529-2014, 2014.
Sullivan, J. T., McGee, T. J., Stauffer, R. M., Thompson, A. M., Weinheimer, A., Knote, C., Janz, S., Wisthaler, A., Long, R., Szykman, J., Park, J., Lee, Y., Kim, S., Jeong, D., Sanchez, D., Twigg, L., Sumnicht, G., Knepp, T. and Schroeder, J. R.: Taehwa Research Forest: A receptor site for severe pollution events in Korea during 2016, Atmos. Chem. Phys. Discuss., (January), 1–30, doi:10.5194/acp-2018-1328, 2019.
Tanaka, P. L., Oldfield, S., Neece, J. D., Mullins, C. B. and Allen, D. T.: Anthropogenic sources of chlorine and ozone formation in urban atmospheres, Environ. Sci. Technol., 34(21), 4470–4473, doi:10.1021/es991380v, 2000.
Tanaka, P. L., Riemer, D. D., Chang, S., Yarwood, G., McDonald-Buller, E. C., Apel, E. C., Orlando, J. J., Silva, P. J., Jimenez, J. L., Canagaratna, M. R., Neece, J. D., Mullins, C. B. and Allen, D. T.: Direct evidence for chlorine-enhanced urban ozone formation in Houston, Texas, Atmos. Environ., 37(9–10), 1393–1400, doi:10.1016/S1352-2310(02)01007-5, 2003.
Tang, W., Arellano, A. F., DiGangi, J. P., Choi, Y., Diskin, G. S., Agustí-Panareda, A., Parrington, M., Massart, S., Gaubert, B., Lee, Y., Kim, D., Jung, J., Hong, J., Hong, J.-W., Kanaya, Y., Lee, M., Stauffer, R. M., Thompson, A. M., Flynn, J. H. and Woo, J.-H.: Evaluating high-resolution forecasts of atmospheric CO and CO2 from a global prediction system during KORUS-AQ field campaign, Atmos. Chem. Phys., 18(15), 11007–11030, doi:10.5194/acp-18-11007-2018, 2018.
Tang, W., Emmons, L. K., Arellano Jr., A. F., Gaubert, B., Knote, C., Tilmes, S., Buchholz, R. R., Pfister, G. G., Diskin, G. S., Blake, D. R., Blake, N. J., Meinardi, S., DiGangi, J. P., Choi, Y., Woo, J.-H., He, C., Schroeder, J. R., Suh, I., Lee, H.-J., Jo, H.-Y., Kanaya, Y., Jung, J., Lee, Y. and Kim, D.: Source contributions to carbon monoxide concentrations during KORUS-AQ based on CAM-chem model applications, J. Geophys. Res. Atmos., 1–27, doi:10.1029/2018jd029151, 2019.
Tham, Y. J., Wang, Z., Li, Q., Yun, H., Wang, W., Wang, X., Xue, L., Lu, K., Ma, N., Bohn, B., Li, X., Kecorius, S., Größ, J., Shao, M., Wiedensohler, A., Zhang, Y. and Wang, T.: Significant concentrations of nitryl chloride sustained in the morning: Investigations of the causes and impacts on ozone production in a polluted region of northern China, Atmos. Chem. Phys., 16(23), 14959–14977, doi:10.5194/acp-16-14959-2016, 2016.
Tham, Y. J., Wang, Z., Li, Q., Wang, W., Wang, X., Lu, K., Ma, N., Yan, C., Kecorius, S., Wiedensohler, A., Zhang, Y. and Wang, T.: Heterogeneous N2O5 uptake coefficient and production yield of ClNO2 in polluted northern China: roles of aerosol water content and chemical composition, Atmos. Chem. Phys., 18(17), 13155–13171, doi:10.5194/acp-18-13155-2018, 2018.
Thornton, J. A., Braban, C. F. and Abbatt, J. P. D.: N_2O_5 hydrolysis on sub-micron organic aerosols: the effect of relative humidity, particle phase, and particle size, Phys. Chem. Chem. Phys., 5(20), 4593, doi:10.1039/b307498f, 2003.
Thornton, J. A., Kercher, J. P., Riedel, T. P., Wagner, N. L., Cozic, J., Holloway, J. S., Dubé, W. P., Wolfe, G. M., Quinn, P. K., Middlebrook, A. M., Alexander, B. and Brown, S. S.: A large atomic chlorine source inferred from mid-continental reactive nitrogen chemistry,

Nature, 464(7286), 271–274, doi:10.1038/nature08905, 2010.
Vogt, R., Crutzen, P. and Sander, R.: A mechanism for halogen release from sea-salt, Nature, 383(September), 327–331, 1996.
Wagner, N. L., Riedel, T. P., Young, C. J., Bahreini, R., Brock, C. A., Dubé, W. P., Kim, S., Middlebrook, A. M., Öztürk, F., Roberts, J. M., Russo, R., Sive, B., Swarthout, R., Thornton, J. A., VandenBoer, T. C., Zhou, Y. and Brown, S. S.: N_2O_5 uptake coefficients and nocturnal NO_2 removal rates determined from ambient wintertime measurements, J. Geophys. Res. Atmos., 118(16), 9331–9350, doi:10.1002/jgrd.50653, 2013.
Wang, H., Lu, K., Guo, S., Wu, Z., Shang, D., Tan, Z., Wang, Y., Le Breton, M., Zhu, W., Lou, S., Tang, M., Wu, Y., Zheng, J., Zeng, L., Hallquist, M., Hu, M. and Zhang, Y.: Efficient N₂O₅ Uptake and NO₃ Oxidation in the Outflow of Urban Beijing, Atmos. Chem. Phys. Discuss., 3(3), 1–27, doi:10.5194/acp-2018-88, 2018.
Wang, T., Tham, Y. J., Xue, L., Li, Q., Zha, Q., Wang, Z., Poon, S. C. N., Dubé, W. P., Blake, D. R., Louie, P. K. K., Luk, C. W. Y., Tsui, W. and Brown, S. S.: Observations of nitryl chloride and modeling its source and effect on ozone in the planetary boundary layer of southern China, J. Geophys. Res. Atmos., (2), 2476–2489, doi:10.1002/2015JD024556.Received, 2016.
Wang, X., Wang, T., Yan, C., Tham, Y. J., Xue, L., Xu, Z. and Zha, Q.: Large daytime signals of N2O5 and NO3 inferred at 62 amu in a TD-CIMS: Chemical interference or a real atmospheric phenomenon, Atmos. Meas. Tech., 7(1), 1–12, doi:10.5194/amt-7-1-2014, 2014.
Wang, X., Wang, H., Xue, L., Wang, T., Wang, L., Gu, R., Wang, W., Tham, Y. J., Wang, Z., Yang, L., Chen, J. and Wang, W.: Observations of N_2O_5 and $ClNO_2$ at a polluted urban surface site in North China: High N_2O_5 uptake coefficients and low $ClNO_2$ product yields, Atmos. Environ., 156(3), 125–134, doi:10.1016/j.atmosenv.2017.02.035, 2017a.
Wang, X., Jacob, D. J., Eastham, S. D., Sulprizio, M. P., Zhu, L., Chen, Q., Alexander, B., Sherwen, T., Evans, M. J., Lee, B. H., Haskins, J. D., Lopez-Hilfiker, F. D., Thornton, J. A., Huey, G. L. and Liao, H.: The role of chlorine in global tropospheric chemistry, Atmos. Chem. Phys, 19, 3981–4003, doi:10.5194/acp-2018-1088, 2019.
Wang, Z., Wang, W., Tham, Y. J., Li, Q., Wang, H., Wen, L., Wang, X. and Wang, T.: Fast heterogeneous N_2O_5 uptake and $ClNO_2$ production in power plant and industrial plumes observed in the nocturnal residual layer over the North China Plain, Atmos. Chem. Phys, 175194(3), 12361–12378, doi:10.5194/acp-17-12361-2017, 2017b.
Wayne, R. P., Barnes, I., Biggs, P., Burrows, J. P., Canosa-Mas, C. E., Hjorth, J., Le Bras, G., Moortgat, G. K., Perner, D., Poulet, G., Restelli, G. and Sidebottom, H.: The nitrate radical: Physics, chemistry, and the atmosphere, Atmos. Environ. Part A, Gen. Top., 25(1), 1–203, doi:10.1016/0960-1686(91)90192-A, 1991.
Weinheimer, A. J., Walega, J. G., Ridley, B. A., Gary, B. L., Blake, D. R., Blake, N. J., Rowland, F. S., Sachse, G. W., Anderson, B. E. and Collins, J. E.: Meridional Distributions of NO_x, NO_y and Other Species in the Lower Stratosphere and Upper Troposphere during AASE II, Geophys. Res. Lett., 21(23), 2583–2586 [online] Available from: //a1994pt47400034, 1994.
Woodcock, A. H.: Salt Nuclei in Marine Air As a Function of Altitude and Wind Force, J. Meteorol., 10(5), 362–371, doi:10.1175/1520-0469(1953)010<0366:SNIMAA>2.0.CO;2,

1953.

Young, C. J., Washenfelder, R. A., Roberts, J. M., Mielke, L. H., Osthoff, H. D., Tsai, C., Pikelnaya, O., Stutz, J., Veres, P. R., Cochran, A. K., Vandenboer, T. C., Flynn, J., Grossberg, N., Haman, C. L., Lefer, B., Stark, H., Graus, M., De Gouw, J., Gilman, J. B., Kuster, W. C. and Brown, S. S.: Vertically resolved measurements of nighttime radical reservoirs in los angeles and their contribution to the urban radical budget, Environ. Sci. Technol., 46(20), 10965–10973, doi:10.1021/es302206a, 2012.

Young, C. J., Washenfelder, R. A., Edwards, P. M., Parrish, D. D., Gilman, J. B., Kuster, W. C., Mielke, L. H., Osthoff, H. D., Tsai, C., Pikelnaya, O., Stutz, J., Veres, P. R., Roberts, J. M., Griffith, S., Dusanter, S., Stevens, P. S., Flynn, J., Grossberg, N., Lefer, B., Holloway, J. S., Peischl, J., Ryerson, T. B., Atlas, E. L., Blake, D. R. and Brown, S. S.: Chlorine as a primary radical: Evaluation of methods to understand its role in initiation of oxidative cycles, Atmos. Chem. Phys., 14(7), 3427–3440, doi:10.5194/acp-14-3427-2014, 2014.

Yun, H., Wang, T., Wang, W., Tham, Y. J., Li, Q., Wang, Z. and Poon, S. C. N.: Nighttime NO_x loss and ClNO2 formation in the residual layer of a polluted region: Insights from field measurements and an iterative box model, Sci. Total Environ., 622–623(x), 727–734, doi:10.1016/j.scitotenv.2017.11.352, 2018.

Zhang, L., Li, Q., Wang, T., Ahmadov, R., Zhang, Q., Li, M. and Lv, M.: Combined Impacts of Nitrous Acid and Nitryl Chloride on Lower Tropospheric Ozone: New Module Development in WRF-Chem and Application to China, Atmos. Chem. Phys. Discuss., (May), 1–31, doi:10.5194/acp-2017-389, 2017.

CHAPTER 5

I_2 near the Antarctic Peninsula during Austral Fall 2018

5.1 Introduction

The relevance of halogen chemistry in the tropospheric boundary layer was first recognized in the Arctic, where depletion of ozone levels from its background conditions were regularly observed during springtime (Bottenheim and Gallant, 1986; Oltmans and Komhyr, 1986). Barrie et al. (1988, 1989) firstly confirmed from filtered bromine that these ozone depletion events (ODEs) are caused by the photocatalytic cycle of gas-phase bromine during the Arctic spring. ODEs were later observed also in the Antarctic (Kreher et al., 1996, 1997). Compared to OH, which is primarily generated from O_3 photolyzed in the UV range (< 300 nm), halogen gas species are photolyzed in near UV to visible range. Therefore, halogen initiated chemistry is less sensitive to O_3 column density and intensity of solar radiation. Studies by Foster et al. (2001) and Saiz-Lopez et al. (2007) reported that bromine and iodine chemistry were active even in twilight conditions in the Arctic and Antarctic boundary layer, respectively.

The presence of iodine gas species in the polar boundary layer can accelerate ODEs since the cross reaction between IO and BrO is up to 2 orders of magnitude faster than the self-reaction between BrO (Atkinson et al., 2007). Reactive gas-phase iodine species can also trigger new particle formation that has implications towards the radiative forcing of the atmosphere. The first evidence of correlation between iodine and ultrafine aerosols, which are particles with diameters less than 50 nm, were found in coastal regions with tidal cycles (Alicke et al., 1999; Allan et al., 2000; Carpenter et al., 1999; O'Dowd et al., 1999, 1998). Under tidal stress, macroalgae can emit iodocarbons that can be photolyzed to produce iodine oxide species that polymerize and trigger

new particle formation (O'dowd et al., 2002). Previous studies (Davison et al., 1996; O'Dowd et al., 1997) reported new particle enhancements originating from coastal Antarctic region but the cause of this increase was not clear. A following study by Atkinson et al. (2012) observed particle formation and its following growth at the Weddell sea where significant levels of I_2 (average of 5.8 ppt) and IO (average of 5.1 ppt) in air and iodocarbons in sea ice brine channels were observed.

In the past two decades, observations of gas-phase iodine have been carried out in the Arctic (Hönninger et al., 2004; Mahajan et al., 2010a; Raso et al., 2017; Tuckermann et al., 1997) and Antarctic (Atkinson et al., 2012; Frieß et al., 2001; Grilli et al., 2013; Saiz-lopez et al., 2007) boundary layer. The first direct observation of IO in the Antarctic boundary layer was made by Saiz-Lopez et al. (2007) using a long-path differential optical absorption spectroscopy (LP-DOAS). In that study, they measured up to ~ 20 ppt of both IO and BrO during springtime at the Halley station, which is located in the Brunt ice shelf, Antarctica. Based on back trajectory analysis, the significant levels of halogen oxides were found in airmasses that were mostly over sea ice. Another study by Atkinson et al. (2012) measured I_2 and HOI in the Weddell sea from late January to early March by sampling air with a coupled diffusion denuder system, which was later on analyzed with a gas chromatography mass spectrometer. I_2 was measured up to 12 ppt and 31 ppt over sea ice and surface snow near the Brunt ice shelf, respectively. IO was also detected around 7 ppt by the multiple axis-differential optical absorption spectroscopy (MAX-DOAS). While significant levels of gas-phase iodine has been measured in West Antarctica, production might be limited in the east part of the continent. Grilli et al. (2013) reported IO and BrO observations with a near-UV-Visible laser spectrometer based on mode-locked cavity-enhanced absorption spectroscopy (ML-CEAS) during Austral Summer at the Dumont d'Urville station in East Antarctica, which was close to detection limits, 0.04 ppt and 2 ppt, respectively. Therefore, they concluded that halogen chemistry

might not be as significant in East Antarctica as in the West part of the continent. Discrepancies in iodine chemistry also exist between the two polar regions. Satellite observations from 2004 to 2006 showed high levels of IO in the Spring time Antarctic, especially over the Weddell sea, while IO was not detected in the Arctic (Schonardt et al., 2008). Direct observations in the Arctic also confirm this by reporting IO levels of below detection limit (Hönninger et al., 2004; Pohler et al., 2010; Tuckermann et al., 1997). The only studies that measured over the detection limit in the Arctic boundary layer are Mahajan et al. (2010a) and Raso et al. (2017) where they measured up to 3.4 ppt of IO in Hudson Bay, Canada and 1 ppt of I_2 in Utqiagvik, Alaska. These levels in the Arctic are significantly lower than what has been observed in West Antarctica. Considering that similar levels of BrO has been observed in both the north and south polar regions, this discrepancy in iodine levels suggest that the mechanism or environment driving the chemistry remains uncertain.

Concentration of aqueous iodide in the ocean is around 1000 times less than bromide due to the uptake by marine organisms (Sugawara and Terada, 1969). Inorganic iodine gas species like I_2, IO, and HOI have a very short lifetime due to heterogeneous uptake and rapid photolysis with a photolytic lifetime of ~13sec, ~ 9sec, and ~ 4 min, respectively, at noontime during spring near the Antarctic peninsula (Madronich and Flocke, 1998). Therefore, a strong source is required to explain the observed levels in west Antarctica. Possible sources of gas-phase iodine species have been suggested such as biogenic sources from sea ice diatoms and accelerated reactions within the ice matrix compared to the aqueous phase. Diatoms, which are microalgae, have been reported to release iodocarbons (Moore et al., 1996; Tokarczyk and Moore, 1994), iodide (De La Cuesta and Manley, 2009), and HOI (Hill and Manley, 2009). Sea ice, especially in the Weddell Sea, has been reported to be rich in diatoms, living underneath or within the sea ice (Ackley et al., 2008; Gerhard

et al., 2004; Haas et al., 2001). Moreover, significant levels of iodocarbons have been observed in the sea ice water in coastal Antarctica (Carpenter et al., 2007; Fogelqvist and Tanhua, 1995). The iodocarbons emitted by sea ice diatoms can move up to the surface through brine channels of the porous Antarctic sea ice (Garrison and Buck, 1989). Atkinson et al. (2012) reported visible bands of sea ice diatoms along with enhanced chlorophyll- a and iodocarbons in the Weddell Sea. In their study, calculated iodine flux from measured iodocarbons in sea ice could not reconcile the observed levels of atmospheric I_2 and IO. For this reason, the authors suggested that the gas-phase I_2 were mainly from iodide (I^-) concentrated in brine channels by sea ice diatoms and the following multiphase reaction with gas-phase HOI. This mechanism was also supported by Saiz-Lopez et al. (2015; 2008), where they were able to reconcile the observed IO levels in the Weddell Sea through a multiphase model embedded with mechanisms of I^- and HOI released from micro-organisms. Accelerated reactions in the ice matrix have also been suggested as a mechanism producing gas-phase iodine species. Previous laboratory studies (Kim et al., 2016a; O'Driscoll et al., 2006) reported that conversion of iodide to molecular I_2 and triiodide can occur when solutions are frozen. Although these studies have not been proven in a real environmental condition, it is possible that these ice-mediated reactions can accelerate the release of gas-phase I_2 to the above atmosphere or snowpack. However, due to limited ambient observations, the sources and impact of molecular I_2 in polar regions are still uncertain.

Here, we present I_2 observation results during the ARAON2018 campaign carried out in April-May of 2018, which is the Fall season in the southern hemisphere. Year-long ground (Saiz-lopez et al., 2007) and satellite observations (Schonardt et al., 2008) in Antarctica showed IO levels peak in the Spring time and another possible smaller enhancement might exist during Austral Fall. Measurements of I_2 in Antarctica are very limited, especially in the Fall season. The main questions

addressed in this study are: 1) What are the levels of iodine gas species in the Antarctic boundary layer during Austral Fall?, 2) What are the possible sources?, 3) What are the possible impacts of the halogen chemistry?

5.2 Results and Discussion

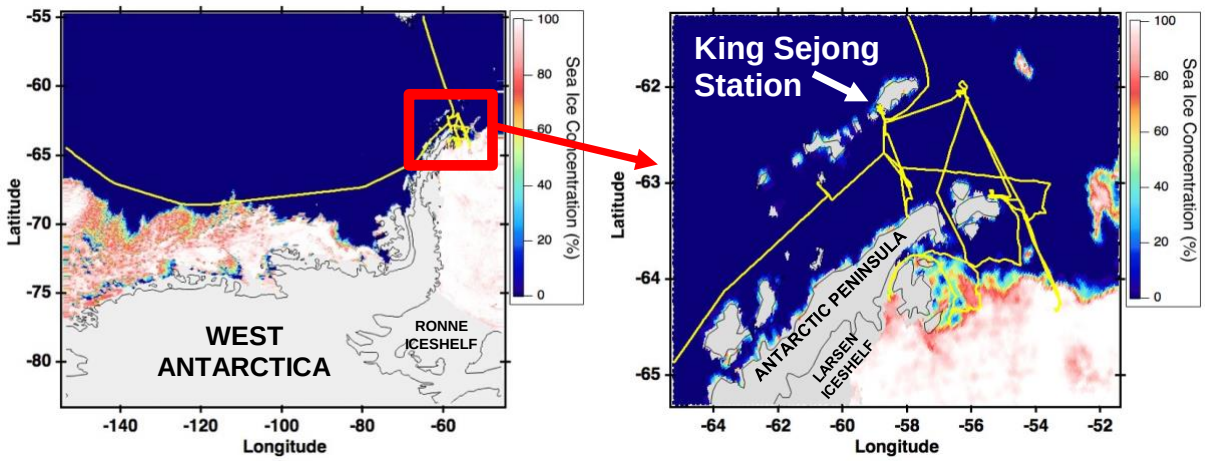

Figure 5.1 Ship track of R/V ARAON during the ARAON2018 campaign. Sea ice concentrations are from the Advance Microwave Scanning Radiometer (AMSR2 v 5.4) showing conditions in April 18th 2018. The entire track in which the observation were carried out are shown in left and the detailed route near the Antarctic peninsula is shown in right.

5.2.1 I_2 Observation Results during ARAON2018

Figure 5.1 shows the cruise path of the Korean icebreaker ARAON during the ARAON2018 campaign. The R/V ARAON started from Christchurch, New Zealand (March 27th), went through the Southern Ocean, the Antarctic peninsula, and arrived in Punta Arenas, Chile (May 3rd). VOCs were measured with a Proton Transfer Reaction-Mass Spectrometer (PTR-MS) and data was collected during most of the campaign period. For the halogen measurements with a CIMS, observations were mostly carried out near the Antarctic peninsula. Sea ice concentrations from April 18th 2019 were taken from the Advanced Microwave Scanning Radiometer (AMSR2

v 5.4) from the Bren University (Spreen et al., 2008). The CIMS measurements close to the Antarctic peninsula was from April 13th to 28th and during this period, the sea ice extent did not vary significantly from what is shown in Figure 5.1. As shown in the figure, the R/V ARAON went near the edges of the sea ice in the Weddell Sea and close to King Sejong station in King George Island.

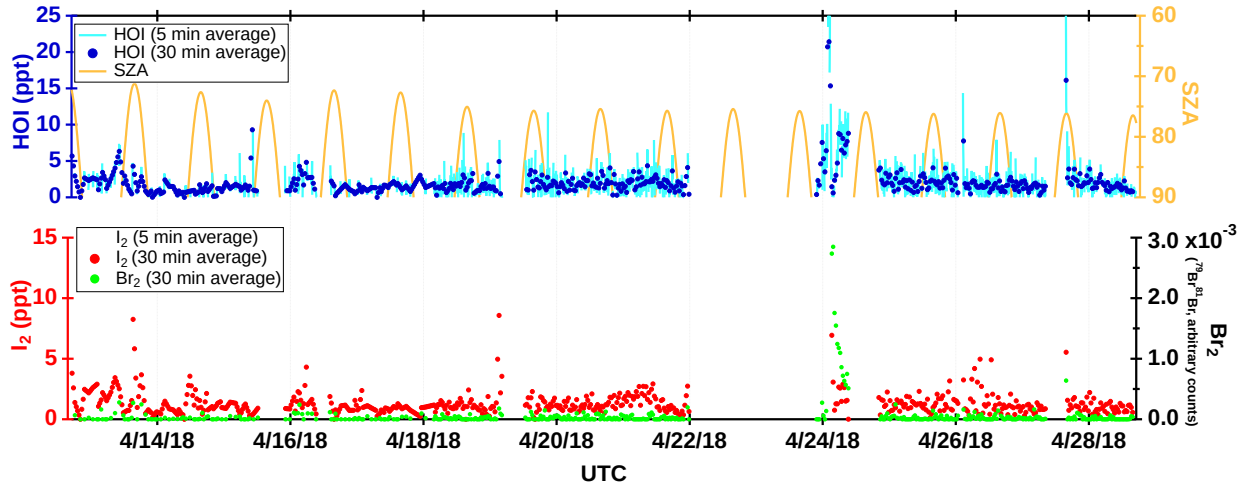

Figure 5.2 Temporal variation of the solar zenith angle (SZA), HOI, I_2, and Br_2 during ARAON2018 campaign.

Figure 5.2 shows temporal variations of the measured halogen gas species and solar zenith angle during the campaign. All the CIMS measurements presented in this figure are from near the Antarctic peninsula. 30 min averaged data show around ~ 1 ppt of background HOI and I_2 levels throughout the observation period. This background level is lower than what was reported by Atkinson et al. (2012), where they measured I_2 and HOI in the Weddell Sea from late January to early March. From sampled air, which was analyzed afterwards with a GC, Atkinson et al. (2012) observed 5 – 10 ppt of constant I_2 in the Weddell Sea and over the Brunt Ice shelf. The max levels

of ambient I_2 they measured was around 31 ppt, which is about twice of the maximum levels we observed during ARAON2018. The total of HOI and ICl reported in their study was around 2 ppt and 4 ppt for background and maximum level, respectively. Overall, lower levels of ambient iodine gas species were observed during Austral Fall, from our observations, than Austral Summer, reported by Atkinson et al. (2012). The difference can be generally explained by the differences in solar radiation intensity with limited photo-activity during Austral Fall. However, considering that episodic levels of I_2 and HOI were observed both in the presence and absence of solar radiation, various production mechanisms should be responsible for driving the chemistry during ARAON2018.

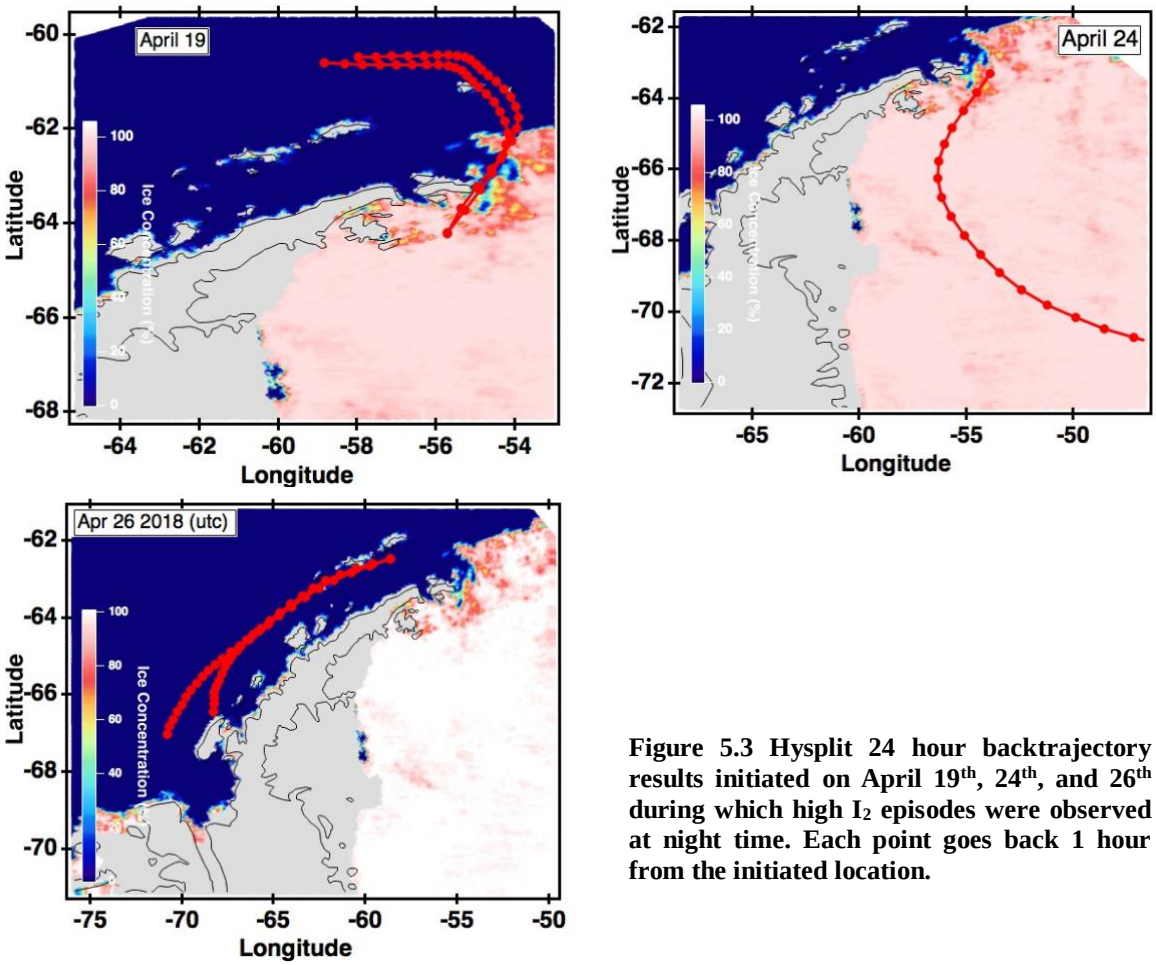

Figure 5.3 Hysplit 24 hour backtrajectory results initiated on April 19th, 24th, and 26th during which high I_2 episodes were observed at night time. Each point goes back 1 hour from the initiated location.

5.2.2 Possible Sources of I_2 during ARAON2018

Considering the short lifetime of I_2 during the day under clear sky conditions (τ_{I2} ~ 15 seconds based on TUV v 5.3), a strong source would be required to reconcile the daytime levels of I_2. Laboratory studies (Gálvez et al., 2016; Kim et al., 2016a) have shown that photolysis of iodine species in ice media can be a pathway for gas-phase I_2 release to ambient air. A field observation study by Raso et al. (2017) reported up to 35 ppt of I_2 within the Arctic snowpack under irradiation while max levels of I_2 was 1 ppt in the ambient atmosphere above the snowpack. In their study, they suggested a pathway initiated by hydroxyl radicals that lead to iodine radicals and subsequent production of triiodide and I_2. This could have been the case also in our study but further studies, such as a 1-D model simulations, are required to examine whether this route is sufficient to explain the observed levels.

During ARAON2018, significant levels of I_2 were also observed in the absence of light. Figure 5.3 shows HYSPLIT backtrajectory results initiated at the time when I_2 episodes were observed under dark conditions, going 24 hours back in time. The trajectories show that in April 19th and 26th, airmasses were mostly coming from the open ocean while on the 24th, airmasses were from over the sea ice of the Weddell sea. In the open ocean, laboratory studies (Carpenter et al., 2013; Garland et al., 1980; Garland and Curtis, 1981) have suggested that the multi-phase reaction between ambient O_3 and iodide in the ocean can produce HOI, which can further react with iodide and generate gas-phase I_2. This reaction does not require the presence of light and therefore could explain the background and episodes of I_2 at nighttime.

Another possible source of gaseous iodine is from biotic sources from sea ice. The three I_2 episodes shown in Figure 5.2 were all from when the ARAON was close to sea ices in King George Island (April 26th) and Weddell Sea (April 29th and 24th). During the cruise, near the Antarctic

peninsula, brown layers of sea ice diatoms were commonly observed on the sides of the broken sea ice as shown in Figure 5.4. These microorganisms can emit iodine species (Hill and Manley, 2009; De La Cuesta and Manley, 2009; Moore et al., 1996) that can move up through brine channels of the highly porous sea ice in the Weddell Sea and released to the surface above. Weddell sea has been reported to have high biological activity with abundant diatoms underneath the sea ice (Ackley et al., 2008; Atkinson et al., 2012; Gerhard et al., 2004; Haas et al., 2001). To further investigate, other gas-phase tracers of biological activities have been compared in Figures 5.5 and 5.6. Figure 5.5 shows I_2 (left) and dimethyl sulfide (DMS) (right) observations with the sea ice concentration map in April 26th 2018. Regions with red squares show episodes of I_2 that also showed enhanced DMS levels. On the other hand, the region within the blue square showed up to 20 ppt of I_2 but did not observe increased DMS emissions. Rather, the data in the blue square were collected when the airmass was mostly from over the sea ice based on backtrajecotry results. At this time point, however, it is difficult to draw a clear correlation and further studies are required. Another feature that was observed are the peaks of isoprene and DMS that lasted for 30 minutes to 2 hours (Figure 5.6), which also corresponded to increased I_2 concentration in the yellow shaded periods. These peaks were observed when the ARAON was breaking through sea ice. A study by Koga et al. (2014) also observed a similar trend during a cruise in Antarctica on the Shirase icebreaker from December to March in 2009. During their observation period, they measured DMS over the Southern Ocean with a PTR-MS and reported abrupt peaks of DMS while the Shirase was breaking through sea ice. These sudden enhancement of VOCs can be released from biological activities through the openings of the sea ice and therefore could be a possible source of iodine release to the ambient atmosphere.

Figure 5.4 Brown layers of sea ice diatoms underneath the sea ice observed near the Antarctic peninsula during ARAON2018

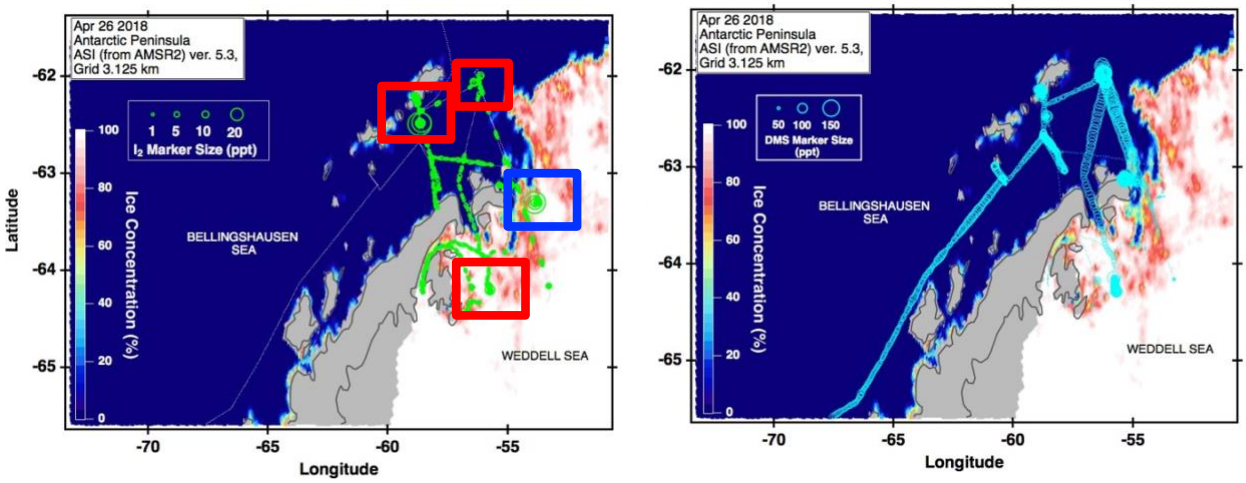

Figure 5.5 I_2 (Left) and DMS (Right) concentration during the ARAON2018 campaign. Marker sizes are proportional to the concentration. Sea ice concentration is from the April 26th data taken from AMSR2 v. 5.3

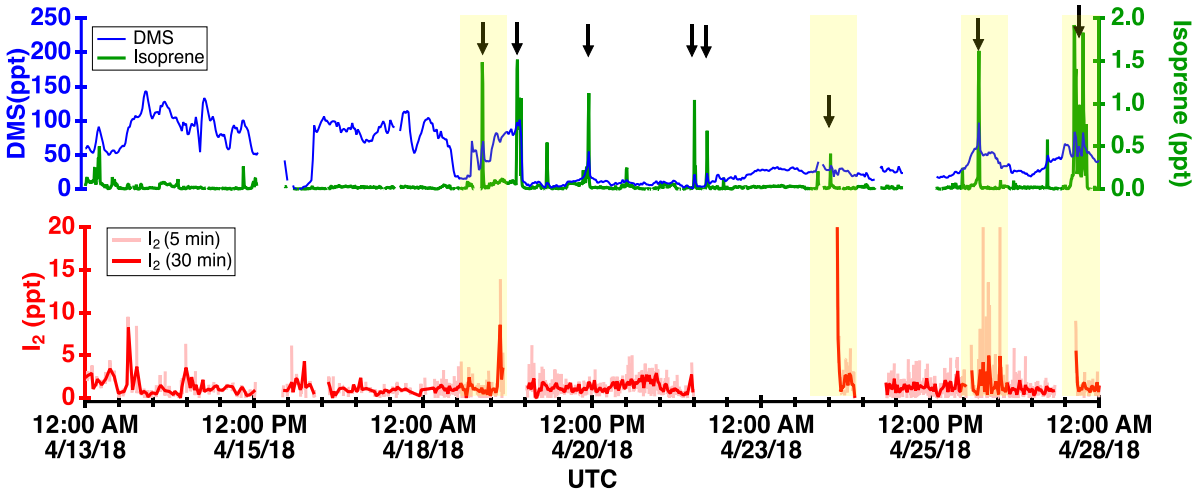

Figure 5.6 Temporal variation of I_2, DMS, and isoprene during the ARAON2018 near the Antarctic peninsula. The black arrows denote when there were abrupt peaks of DMS and the yellow shades are when these DMS peaks coincided to I_2 increase.

5.2.3 Impact of I_2 in the Antarctic Boundary Layer

Ozone depletion events in polar regions are known to be initiated by bromine species in the atmosphere (Barrie et al., 1988, 1989). The presence of iodine has long been hypothesized to accelerate this process through faster reactions of iodine oxides with bromine oxides compared to self-reactions of these halogen oxides. During ARAON2018, short ozone depletion events corresponding to enhanced levels of iodine and bromine gas species were observed (Figure 5.7). The reason for the fast restoration of the O_3 levels is probably due to the constant movement of the icebreaker and from the horizonal and vertical mixing. Even low levels of I_2 can significantly impact the level of O_3. Box model simulations by Raso et al. (2017) showed that in the presence of the observed levels of ~1 ppt of I_2 in the Arctic, the rate of ozone depletion increased by 31 % compared to when only bromine and chlorine precursors are present. Therefore, the co-existence

of significant levels of iodine and bromine gas-species observed during ARAON2018 is expected to trigger accelerated ozone depletion episodes.

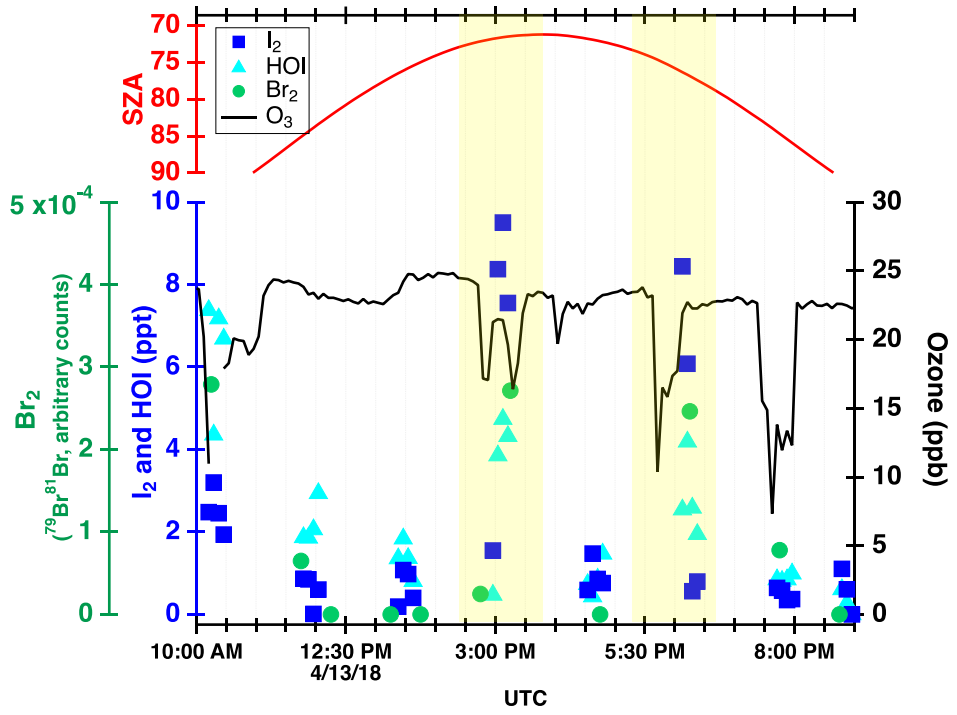

Figure 5.7 Comparison between measured ozone, gas-phase iodine and bromine species, and SZA. Yellow shades are when O_3 depletion events were observed.

5.3 Conclusion

During the ARAON2018, up to 15 ppt of I_2 and 20 ppt of HOI were observed during Austral Fall onboard the Korean icebreaker ARAON. Constant background levels of ~1 ppt of both compounds were measured throughout the cruise near the Antarctic peninsula. Significant levels of these halogen gas species were observed both in the presence and absence of light, which implies multiple mechanisms are driving the production of these compounds. The source of the iodine species are rather uncertain but shows correlation to other biological tracers, such as DMS and acetone. This could be an indication of possible sources from sea ice diatoms that are prevalent

in the Weddell Sea. However, further studies are required to clarify the sources of these halogen compounds. The presence of gas-phase iodine has long been hypothesized to trigger ODEs. Short O_3 depletion events were observed onboard the ARAON corresponding to enhanced levels of I_2 and Br_2. This significant levels of iodine gas-species have implications towards new particle formation and ODEs that will in turn influence the radiative forcing and oxidative capacity of the pristine Antarctic boundary layer.

5.4 References

Ackley, S. F., Lewis, M. J., Fritsen, C. H. and Xie, H.: Internal melting in Antarctic sea ice: Development of "gap layers," Geophys. Res. Lett., 35(11), 1–5, doi:10.1029/2008GL033644, 2008.

Alicke, B., Hebestreit, K., Stutz, J. and Platt, U.: Iodine oxide in the marine boundary layer, Nature, 397, 572–573, 1999.

Allan, B. J., Mcfiggans, G., Plane, J. M. C. and Coe, H.: Observations of iodine monoxide in the remote marine boundary layer, J. Geophys. Res., 105(Dll), 14363–14369, 2000.

Atkinson, H. M., Huang, R. J., Chance, R., Roscoe, H. K., Hughes, C., Davison, B., Schönhardt, A., Mahajan, A. S., Saiz-Lopez, A., Hoffmann, T. and Liss, P. S.: Iodine emissions from the sea ice of the Weddell Sea, Atmos. Chem. Phys., 12(22), 11229–11244, doi:10.5194/acp-12-11229-2012, 2012.

Atkinson, R., Baulch, D. L., Cox, R. A., Crowley, J. N., Hampson, R. F., Hynes, R. G., Jenkin, M. E., Rossi, M. J. and Troe, J.: Evaluated kinetic and photochemical data for atmospheric chemistry: Volume III - Gas phase reactions of inorganic halogens, Atmos. Chem. Phys., 7(4), 981–1191, doi:10.5194/acp-7-981-2007, 2007.

Barrie, L. A., Bottenheim, J. W., Schnell, R. C., Crutzen, P. J. and Rasmussen, R. A.: Ozone destruction and photochemical reactions at polar sunrise in the lower Arctic atmosphere, Nature, 334(14), 6–9, 1988.

Barrie, L. A., den Hartog, G., Bottenheim, J. W. and Landsberger, S.: Anthropogenic aerosols and gases in the lower troposphere at Alert Canada in April 1986, J. Atmos. Chem., 9(1–3), 101–127, doi:10.1007/BF00052827, 1989.

Bottenheim, J. W. and Gallant, A. G.: Measurements of NO_y species and O_3 at 82ºN Latitude, Geophys. Res. Lett., 13(1), 113–116, 1986.

Carpenter, L. J., Sturges, W. T., Penkett, S. A. and Liss, P. S.: Short-lived alkyl iodides and bromides at Mace Head, Ireland: Links to biogenic sources and halogen oxide production, J. Geophys. Res. Atmos., 104(D1), 1679–1689, doi:10.1029/98JD02746, 1999.

Carpenter, L. J., Wevill, D. J., Palmer, C. J. and Michels, J.: Depth profiles of volatile iodine and bromine-containing halocarbons in coastal Antarctic waters, Mar. Chem., 103(3–4), 227–236, doi:10.1016/j.marchem.2006.08.003, 2007.

Carpenter, L. J., MacDonald, S. M., Shaw, M. D., Kumar, R., Saunders, R. W., Parthipan, R.,

Wilson, J. and Plane, J. M. C.: Atmospheric iodine levels influenced by sea surface emissions of inorganic iodine, Nat. Geosci., 6(2), 108–111, doi:10.1038/ngeo1687, 2013.

Davison, B., Hewitt, C. N., O'Dowd, C. D., Lowe, J. A., Smith, M. H., Schwikowski, M., Baltensperger, U. and Harrison, R. M.: Dimethyl sulfide, methane sulfonic acid and physicochemical aerosol properties in Atlantic air from the United Kingdom to Halley Bay, J. Geophys. Res. Atmos., 101(D17), 22855–22867, doi:10.1029/96jd01166, 1996.

Fogelqvist, E. and Tanhua, T.: Iodinated C1-C4 hydrocarbons released from ice algae in Antarctica. In: Grimvall A., de Leer E.W.B.(eds) Naturally-Produced Organohalogens. Envrionment & Chemistry, vol 1, Springer, Dordrecht., 1995.

Foster, K. L., Plastridge, R. A., Bottenheim, J. W., Shepson, P. B., Finlayson-Pitts, B. J. and Spicer, C. W.: The role of Br2 and Brcl in surface ozone destruction at polar sunrise, Science (80-.)., 291(5503), 471–474, doi:10.1126/science.291.5503.471, 2001.

Frieß, U., Wagner, T., Pundt, I., Pfeilsticker, K. and Platt, U.: Spectroscopic measurements of tropospheric iodine oxide at Neumayer station, Antarctica, Geophys. Res. Lett., 28(10), 1941–1944, doi:10.1029/2000GL012784, 2001.

Gálvez, Ó., Teresa Baeza-Romero, M., Sanz, M. and Saiz-Lopez, A.: Photolysis of frozen iodate salts as a source of active iodine in the polar environment, Atmos. Chem. Phys., 16(19), 12703–12713, doi:10.5194/acp-16-12703-2016, 2016.

Garland, J. A. and Curtis, H.: Emission of iodine from the sea surface in the presence of ozone, J. Geophys. Res., 86(C4), 3183, doi:10.1029/jc086ic04p03183, 1981.

Garland, J. A., Elzerman, A. W. and Penkett, S. A.: The mechanism for dry deposition of ozone to seawater surfaces, J. Geophys. Res., 85, 7488–7492, 1980.

Garrison, D. L. and Buck, K. R.: The biota of Antarctic pack ice in the Weddell sea and Antarctic Peninsula regions, Polar Biol., 10(3), 211–219, doi:10.1007/BF00238497, 1989.

Gerhard, K., David, N. T., Christian, H., Hilary, K. and Gerhard, S. D.: Surface ice and gap layers in Antarctic sea ice: highly productive habitats, Mar. Ecol. Prog. Ser., 277, 1–12, doi:10.3354/meps277001, 2004.

Grilli, R., Legrand, M., Kukui, A., Méjean, G., Preunkert, S. and Romanini, D.: First investigations of IO, BrO, and NO_2 summer atmospheric levels at a coastal East Antarctic site using mode-locked cavity enhanced absorption spectroscopy, Geophys. Res. Lett., 40(4), 791–796, doi:10.1002/grl.50154, 2013.

Haas, C., Thomas, D. N. and Bareiss, J.: Surface properties and processes of perennial Antarctic sea ice in summer, J. Glaciol., 47(159), 613–625, doi:10.3189/172756501781831864, 2001.

Hill, V. L. and Manley, S. L.: Release of reactive bromine and iodine from diatoms and its possible role in halogen transfer in polar and tropical oceans, Limnol. Oceanogr., 54(3), 812–822, doi:10.4319/lo.2009.54.3.0812, 2009.

Hönninger, G., Leser, H., Sebastián, O. and Platt, U.: Ground-based measurements of halogen oxides at the Hudson Bay by active longpath DOAS and passive MAX-DOAS, Geophys. Res. Lett., 31(4), 1–5, doi:10.1029/2003GL018982, 2004.

Kim, K., Yabushita, A., Okumura, M., Saiz-Lopez, A., Cuevas, C. A., Blaszczak-Boxe, C. S., Min, D. W., Yoon, H. Il and Choi, W.: Production of Molecular Iodine and Tri-iodide in the Frozen Solution of Iodide: Implication for Polar Atmosphere, Environ. Sci. Technol., 50(3), 1280–1287, doi:10.1021/acs.est.5b05148, 2016.

Koga, S., Nomura, D. and Wada, M.: Variation of dimethylsulfide mixing ratio over the Southern Ocean from 36°S to 70°S, Polar Sci., 8(3), 306–313, doi:10.1016/j.polar.2014.04.002,

2014.
Kreher, K., Keys, J. G. and Johnston, P. V.: Ground-based measurements of OClO and HCl in austral spring 1993 at Arrival Heights, Antarctica, Geophys. Res. Lett., 23(12), 1545–1548, 1996.
Kreher, K., Johnston, P. V. and Wood, S. W.: Ground-based measurements of tropospheric and stratospheric BrO at Arrival Heights, Antarctica, Geophys. Res. Lett., 24(23), 3021–3024, doi:10.1029/97GL02997, 1997.
De La Cuesta, J. L. and Manley, S. L.: Iodine assimilation by marine diatoms and other phytoplankton in nitrate-replete conditions, Limnol. Oceanogr., 54(5), 1653–1664, doi:10.4319/lo.2009.54.5.1653, 2009.
Madronich, S. and Flocke, S.: Handbook of Environmental Chemistry, in Handbook of Environmental Chemistry, pp. 1–26, Springer_Verlag, Heidelberg., 1998.
Mahajan, A. S., Shaw, M., Oetjen, H., Hornsby, K. E., Carpenter, L. J., Kaleschke, L., Tian-Kunze, X., Lee, J. D., Moller, S. J., Edwards, P., Commane, R., Ingham, T., Heard, D. E. and Plane, J. M. C.: Evidence of reactive iodine chemistry in the Arctic boundary layer, J. Geophys. Res. Atmos., 115(20), 1–11, doi:10.1029/2009JD013665, 2010.
Moore, R. M., Webb, M., Tokarczyk, R. and Wever, R.: Bromoperoxidase and iodoperoxidase enzymes and production of halogenated methanes in marine diatom cultures, J. Geophys. Res. C Ocean., 101(C9), 20899–20908, doi:10.1029/96JC01248, 1996.
O'Dowd, C., Lowe, J. A., Smith, M. H., Davison, B., Hewitt, C. N. and Harrison, R. M.: Biogenic sulphur emissions and inferred non-sea-salt-sulphate cloud condensation nuclei in and around Antarctica, J. Geophys. Res., 102(Dll), 1997.
O'Dowd, C., Heard, D. E., McFiggans, G., Creasey, D. J., Smith, M. H., Lee, J. D., Pirjola, L., Pilling, M. J., Hoell, C., Kulmala, M., Plane, J. M. C. and Allan, B. J.: On the photochemical production of new particles in the coastal boundary layer, Geophys. Res. Lett., 26(12), 1707–1710, doi:10.1029/1999GL900335, 1999.
O'dowd, C. D., Jimenez, J. L., Bahreini, R., Flagan, R. C., Seinfeld, J. H., Hämerl, K., Pirjola, L., Kulmala, M., Jennings, S. G. and Hoffmann, T.: Marine aerosol formation from biogenic iodine emissions, Nature, 417(6889), 632–636, doi:10.1038/nature00775, 2002.
O'Dowd, C. D., Geever, M., Hill, M. K., Smith, M. H. and Jennings, S. G.: New particle formation: Nucleation rates and spatial scales in the clean marine coastal environment, Geophys. Res. Lett., 25(10), 1661–1664, 1998.
O'Driscoll, P., Lang, K., Minogue, N. and Sodeau, J.: Freezing halide ion solutions and the release of interhalogens to the atmosphere, J. Phys. Chem. A, 110(14), 4615–4618, doi:10.1021/jp060491v, 2006.
Oltmans, S. J. and Komhyr, W. D.: Surface ozone distributions and variations from 1973-1984 measurements at the NOAA geophysical monitoring for climatic change baseline observatories., J. Geophys. Res., 91(6), 5229–5236, doi:10.1029/JD091iD04p05229, 1986.
Pohler, D., Vogel, L., Friess, U. and Platt, U.: Observation of halogen species in the Amundsen Gulf, Arctic, by active long-path differential optical absorption spectroscopy, Proc. Natl. Acad. Sci., 107(15), 6582–6587, doi:10.1073/pnas.0912231107, 2010.
Raso, A. R. W., Custard, K. D., May, N. W., Tanner, D., Newburn, M. K., Walker, L., Moore, R. J., Huey, L. G., Alexander, L., Shepson, P. B. and Pratt, K. A.: Active molecular iodine photochemistry in the Arctic, Proc. Natl. Acad. Sci., 114(38), 10053–10058, doi:10.1073/pnas.1702803114, 2017.
Saiz-lopez, A., Mahajan, A. S., Salmon, R. A., Bauguitte, S. J., Jones, A. E., Roscoe, H. K. and

Plane, J. M. C.: Boundary Layer Halogens in Coastal Antarctica, Science, 348–352, doi:10.1126/science.1141408, 2007.

Saiz-Lopez, A. and Boxe, C. S.: A mechanism for biologically-induced iodine emissions from sea-ice, Atmos. Chem. Phys. Discuss., 8(1), 2953–2976, doi:10.5194/acpd-8-2953-2008, 2008.

Saiz-Lopez, A., Blaszczak-Boxe, C. S. and Carpenter, L. J.: A mechanism for biologically induced iodine emissions from sea ice, Atmos. Chem. Phys., 15(17), 9731–9746, doi:10.5194/acp-15-9731-2015, 2015.

Schonardt, A., Richter, A., Wittrock, F., Kirk, H., Oetjen, H., Roscoe, H. K. and Burrows, J. P.: Observations of iodine monoxide columns from satellite, Atmos. Chem. Phys, 8, 637–653, 2008.

Spreen, G., Kaleschke, L. and Heygster, G.: Sea ice remote sensing using AMSR-E 89-GHz channels, J. Geophys. Res. Ocean., 113(2), 1–14, doi:10.1029/2005JC003384, 2008.

Sugawara, K. and Terada, K.: Iodine assimilation by a marine Navicula sp. and the production of iodate accompanied by the growth of the algae, Inf. Bull. Planktology Japan, 213–218, 1969.

Tokarczyk, R. and Moore, R. M.: Production of volatile organohalogens by phytoplankton cultures, Geophys. Res. Lett., 21(4), 285–288, 1994.

Tuckermann, M., Ackermann, R., Golz, C., Lorenzen-Schmidt, H., Senne, T., Stutz, J., Trost, B., Unold, W. and Platt, U.: DOAS-observation of halogen radical-catalysed arctic boundary layer ozone destruction during the ARCTOC-campaigns 1995 and 1996 in Ny-Alesund, Spitsbergen, Tellus, 49B, 533–555, 1997.

CHAPTER 6

CONCLUSIONS

In this thesis, uncertainties remaining in the tropospheric oxidation capacity is explored through box model studies and observations of hydroxyl radicals (OH) and halogen radical precursors with a chemical ionization mass spectrometry (CIMS). Three field observations were carried out in a wide range of chemical regimes from pristine to polluted environments, including a pristine tropical forest frequently affected by pollution, a highly polluted Asian Megacity, and a pristine Antarctic boundary layer.

The work from the GoAmazon2014/5 confirms that, contrary to previous reports in forested environments, our understanding of the HO_x-NO_x-VOC chemistry is sufficient to reconcile the observed OH levels in the tropical rainforest environment. Box model simulations embedded with near-explicit chemical mechanism and five condensed mechanisms, used in chemical transport models, showed great agreement to OH levels measured with the CIMS.

Studies during the KORUS-AQ 2016 investigated the levels of $ClNO_2$ in the Seoul Metropolitan Area (SMA) and explored the possible implications in the regional chemistry. High levels of night time $ClNO_2$ were observed both at the city center and a forested area downwind. A second $ClNO_2$ peak early in the morning and significant daytime levels illustrate that this nighttime radical precursor is important in driving the oxidation chemistry within the boundary layer. Observation constrained box model simulations confirmed that the net chemical production of O_3 was enhanced up to 25 % in the presence of $ClNO_2$.

Finally, the first time I_2 observation with the CIMS was carried out in the Antarctic boundary layer during ARAON2018. The measurements during Austral Fall measured up to ~ 20

ppt of both I_2 and HOI near the Antarctic peninsula. This confirms that West Antarctica, specifically the Weddell Sea, is indeed rich in gas-phase iodine in the atmospheric boundary layer. Short ozone depletion events, which was long hypothesized to be accelerated by iodine, were observed on board the R/V ARAON.

The results presented in this thesis demonstrates, from field observations and box model studies, halogen radicals are crucial in understanding the tropospheric chemistry in certain environments such as polluted coastal areas or polar regions. However, observations are still very limited, especially in the polar regions, and simultaneous measurements of other halogen radical precursors in both the Arctic and Antarctic would help enhance our understanding. Moreover, a well-controlled experiment in a field environment is also needed to better examine the sources of halogen precursors.